

Tank System Integrated Model: A Cryogenic Tank Performance Prediction Program

L.G. Bolshinskiy
Jacobs ESSSA Group, Huntsville, Alabama

A. Hedayat, L.J. Hastings (retired), S.G. Sutherlin, and A.R. Schnell
Marshall Space Flight Center, Huntsville, Alabama

J.P. Moder
Glenn Research Center, Cleveland, Ohio

The NASA STI Program...in Profile

Since its founding, NASA has been dedicated to the advancement of aeronautics and space science. The NASA Scientific and Technical Information (STI) Program Office plays a key part in helping NASA maintain this important role.

The NASA STI Program Office is operated by Langley Research Center, the lead center for NASA's scientific and technical information. The NASA STI Program Office provides access to the NASA STI Database, the largest collection of aeronautical and space science STI in the world. The Program Office is also NASA's institutional mechanism for disseminating the results of its research and development activities. These results are published by NASA in the NASA STI Report Series, which includes the following report types:

- **TECHNICAL PUBLICATION.** Reports of completed research or a major significant phase of research that present the results of NASA programs and include extensive data or theoretical analysis. Includes compilations of significant scientific and technical data and information deemed to be of continuing reference value. NASA's counterpart of peer-reviewed formal professional papers but has less stringent limitations on manuscript length and extent of graphic presentations.
- **TECHNICAL MEMORANDUM.** Scientific and technical findings that are preliminary or of specialized interest, e.g., quick release reports, working papers, and bibliographies that contain minimal annotation. Does not contain extensive analysis.
- **CONTRACTOR REPORT.** Scientific and technical findings by NASA-sponsored contractors and grantees.
- **CONFERENCE PUBLICATION.** Collected papers from scientific and technical conferences, symposia, seminars, or other meetings sponsored or cosponsored by NASA.
- **SPECIAL PUBLICATION.** Scientific, technical, or historical information from NASA programs, projects, and mission, often concerned with subjects having substantial public interest.
- **TECHNICAL TRANSLATION.** English-language translations of foreign scientific and technical material pertinent to NASA's mission.

Specialized services that complement the STI Program Office's diverse offerings include creating custom thesauri, building customized databases, organizing and publishing research results...even providing videos.

For more information about the NASA STI Program Office, see the following:

- Access the NASA STI program home page at <<http://www.sti.nasa.gov>>
- E-mail your question via the Internet to <help@sti.nasa.gov>
- Phone the NASA STI Help Desk at 757-864-9658
- Write to:
NASA STI Information Desk
Mail Stop 148
NASA Langley Research Center
Hampton, VA 23681-2199, USA

NASA/TM—2017–218239



Tank System Integrated Model: A Cryogenic Tank Performance Prediction Program

L.G. Bolshinskiy
Jacobs ESSSA Group, Huntsville, Alabama

A. Hedayat, L.J. Hastings (retired), S.G. Sutherlin, and A.R. Schnell
Marshall Space Flight Center, Huntsville, Alabama

J.P. Moder
Glenn Research Center, Cleveland Ohio

National Aeronautics and
Space Administration

Marshall Space Flight Center • Huntsville, Alabama 35812

April 2017

Acknowledgments

The authors would like to extend their appreciation to Main Propulsion Branch (ER22) Management, Kathy Henkel and Jay Russell, for providing opportunity and support to complete this work. Appreciation also goes to the Jacob Technology ESSSA Group Team Leads, David Sharp, Mike Reynolds, and Sherri Spotswood for their support during all stages of the Tank System Integrated Model (TankSIM) development and completion of this Technical Memorandum. Special thanks go to Jonathan Stephens of ER24 for his excellent and very helpful technical discussions, suggestions, and reviews during different stages of TankSIM work.

Available from:

NASA STI Information Desk
Mail Stop 148
NASA Langley Research Center
Hampton, VA 23681-2199, USA
757-864-9658

This report is also available in electronic form at
<<http://www.sti.nasa.gov>>

TABLE OF CONTENTS

1. INTRODUCTION	1
2. ANALYTICAL MODEL DESCRIPTION	2
2.1 Basic Model Approaches for a Settled Liquid	2
2.2 Model Approaches for an Unsettled Liquid	5
3. MASS AND ENERGY CONSERVATION EQUATIONS	6
3.1 Ullage	6
3.2 Ullage Wall (Tank Wall Interfaced to the Ullage)	8
3.3 Bulk Liquid	9
3.4 Liquid Wall (Tank Wall Interfaced to the Liquid)	9
3.5 Wall Liquid (Liquid Film on the Ullage Wall)	10
4. HEAT AND MASS TRANSFER IN THE TANK	11
4.1 External Heat Loads	11
4.2 Ullage-Bulk Liquid Interface Heat and Mass Transfer	11
4.3 Ullage Wall Heat and Mass Transfer	13
4.4 Condensation on the Ullage Wall	14
4.5 Bulk Vapor Condensation	17
4.6 Bulk Liquid Convective Heat and Mass Transfer	17
4.7 Bulk Liquid Boiling	19
4.8 Conductive Heat Transfer Through the Wall Between the Ullage and Liquid Regions	21
4.9 Fluid Thermodynamic Properties	21
5. TANK PRESSURIZATION AND ULLAGE VENTING PRESSURE CONTROL	22
5.1 Ullage Pressurization	22
5.2 Ullage Venting Methods	24
6. TANK THERMODYNAMIC VENTING PRESSURE CONTROL SYSTEMS	28
6.1 Thermodynamic Venting System Pressure Control Logic	28
6.2 Spray Bar Thermodynamic Venting System	29
6.3 Ullage Droplets Heat and Mass Transfer	39

TABLE OF CONTENTS (Continued)

7. TANK AXIAL JET THERMODYNAMIC VENTING PRESSURE CONTROL SYSTEMS	47
7.1 Axial Jet Thermodynamic Venting System	47
7.2 Heat and Mass Transfer at the Ullage-Liquid Interface	47
7.3 Helicoidally Coiled Tube-in-Shell Heat Exchanger Transfer	50
7.4 Heat Transfer at Low Acceleration Conditions	52
8. COMPUTER MODEL DESCRIPTION	55
8.1 TankSIM Program Base	55
8.2 Program Possibilities	55
8.3 Program Error Handling	56
8.4 TankSIM Functionality	57
9. PROGRAM VALIDATION AND MULTIPHASE MISSION EXAMPLE	63
9.1 Multipurpose Hydrogen Test Bed Data Validation	63
9.2 Multiphase Mission Example With Ullage Venting	73
10. SUMMARY AND FUTURE PROGRAM IMPROVEMENT	75
10.1 Summary	75
10.2 Future TankSIM Improvements	75
APPENDIX A—CONSERVATION EQUATIONS FOR MULTINODE ANALYSIS OF CRYOGENIC STORAGE TANKS	76
A.1 Leibnitz’s Theorem	76
A.2 Conservation of Mass	76
A.3 Conservation of Thermal Energy	78
APPENDIX B—HEAT AND MASS TRANSFER INSIDE THE TANK	82
B.1 Ullage-Bulk Liquid Interface Temperature	82
B.2 Requirements for Using Flat Plate Correlations to the Cylindrical Segment of the Tank	83
B.3 Free Convection Heat Transfer From the Tank Wall Inside the Tank	85
B.4 Ullage Wall Condensation Model	88

TABLE OF CONTENTS (Continued)

APPENDIX C—TANK THERMODYNAMIC VENTING PRESSURE CONTROL SYSTEMS	97
C.1 Liquid Film Heat Transfer	97
APPENDIX D—TANK AXIAL JET THERMODYNAMIC VENTING PRESSURE CONTROL SYSTEMS	99
D.1 Heat and Mass Transfer on the Ullage-Liquid Interface During Axial Jet Mixing	99
D.2 Helicoidally Coiled Tube-in-Shell Heat Exchanger Transfer	101
D.3 Heat Transfer at Low Acceleration Conditions	103
APPENDIX E—COMPUTER MODEL DESCRIPTION	105
E.1 Input Files Description	105
E.2 Variables Description for Input and Output Files	112
REFERENCES	119

LIST OF FIGURES

1.	TankSIM nodes	2
2.	Diagram of control volumes	3
3.	Tank geometry transformation for unsettled liquid (no mixing)	5
4.	Tank fluids transformation for unsettled liquid during mixing	5
5.	Diagram of mass flows	6
6.	Diagram of heat flows, not associated with mass transfer	7
7.	Horizontal heated downward-facing plate model	12
8.	Liquid-ullage interface in finite volume tank	12
9.	Calculation schematic for condensation on the upper dome	15
10.	Calculation schematic for condensation on the lower dome	16
11.	Definition sketch for lower dome convective model	18
12.	Calculation schematic for convection in the liquid on the upper dome wall	18
13.	Pressurization devices schematic: (a) Critical Venturi and (b) critical orifice	22
14.	Ullage venting pressure control logic	25
15.	Thermodynamic venting system pressure control logic	29
16.	Spray bar TVS schematic	30
17.	Spray bar heat exchanger pressure drop calculation schematic	31
18.	Spray bar heat exchanger transfer calculation schematic	34
19.	Spray injection tube schematic	36
20.	Resistance coefficient versus ratio of the injection tube to orifice velocities	38

LIST OF FIGURES (Continued)

21.	Droplet motion in the ullage	41
22.	Droplet impingement model schematic	43
23.	Droplet behavior after impingement: (a) Spreading and (b) rebounding	45
24.	Axial jet TVS schematic	47
25.	Axial jet TVS submergence cases schematic: (a) High submergence and (b) low submergence	48
26.	Helicoidally coiled tube-in-shell heat exchanger: (a) Exchanger measurements and (b) calculation schematic	51
27.	Liquid-ullage interface in MHTB tank with 90% fill level	52
28.	Interface and dry wall areas for hydrogen in MHTB tank: (a) 25% fill level and (b) 90% fill level	53
29.	Error message example	56
30.	Custom error handling code segment	56
31.	Standard error handling code segment	57
32.	Program flowchart for regular mission phase	58
33.	Initialization subroutine flowchart	59
34.	Heat exchanger transfer subroutine flowchart	60
35.	TankSIM file structure	61
36.	Ullage pressure, 25% fill level	63
37.	Liquid saturation pressure, 25% fill level	64
38.	Ullage temperature, 25% fill level	64
39.	Liquid temperature, 25% fill level	64
40.	Ullage wall temperature, 25% fill level	65

LIST OF FIGURES (Continued)

41.	Ullage pressure, 50% fill level	66
42.	Liquid saturation pressure, 50% fill level	66
43.	Ullage temperature, 50% fill level	66
44.	Liquid temperature, 50% fill level	67
45.	Ullage wall temperature, 50% fill level	67
46.	Ullage pressure, 90% fill level	68
47.	Liquid saturation pressure, 90% fill level	69
48.	Ullage temperature, 90% fill level	69
49.	Liquid temperature, 90% fill level	70
50.	Ullage pressure, adjusted heat loads, 25% fill level	71
51.	Liquid saturation pressure, adjusted heat loads, 25% fill level.....	71
52.	Ullage temperature, adjusted heat loads, 25% fill level.....	72
53.	Liquid temperature, adjusted heat loads, 25% fill level	72
54.	Ullage wall temperature, adjusted heat loads, 25% fill level	72
55.	Ullage and liquid saturation pressures (cycling ullage venting)	73
56.	Ullage and liquid temperatures (cycling ullage venting)	74
57.	Ullage and liquid temperatures (cycling ullage venting, large scale)	74
58.	Cylindrical to flat tank wall transformation	84
59.	Relative difference between heat flow rates through circular and flat tank walls	85
60.	Minimal radius-to-height ratio value allows using the flat wall convective heat flow model for cylindrical walls	87
61.	Relative Nusselt numbers difference versus radius-to-height ratio for different Rayleigh numbers	88

LIST OF FIGURES (Continued)

62.	Condensation on the internal side of cylindrical wall segment	89
63.	Condensation on the upper dome	92
64.	Angle α calculation schematic	94
65.	Condensation on the lower dome	96
66.	Heat and mass transfer in the liquid film	97
67.	Geometrical parameters of axial jet	100
68.	Geometrical parameters of helicoidally coiled tube-in-shell heat exchanger	101
69.	TankSIM address input file	105
70.	TankSIM input file	106
71.	TankSIM mission profile input file	106
72.	TankSIM tank input file	108
73.	TankSIM spray bar input file	109
74.	TankSIM axial jet input file	110
75.	TankSIM external venting line input file	111
76.	TankSIM main output file	111

LIST OF TABLES

1.	Recommended values for constant C in Lockhart-Martinelli parameter	32
2.	Heat leaks in 25% fill level test, adjusted heat loads	70
3.	Coefficient K from equation (165)	83
4.	Variables description for input and output files	112

LIST OF ACRONYMS

CFD	computational fluid dynamics
J-T	Joule-Thomson
MHTB	multipurpose hydrogen test bed
NIST	National Institute of Standards and Technology
PCS	pressure control system
RefProp	NIST reference fluid thermodynamic and transport properties database
TankSIM	tank system integrated model
TM	Technical Memorandum
TVS	thermodynamic venting system

NOMENCLATURE

Areas, m²

A_{cw}	tank wall cross area on the ullage-liquid interface level
A_{lw}	wall-liquid interface
A_u	ullage surface area for low gravity cases
A_{uw}	wall-ullage interface
A_{wl}	wall liquid-ullage interface
Bo	Bond number, dimensionless
C_p	constant pressure specific heat, J/(kg·K)
C_v	constant volume specific heat, J/(kg·K)
D_c	average diameter of coil, m
D_{cr}	critical bubbles diameter, m
D_d	bubble departure diameter, m
D_{dr}	ullage droplets diameter, m
D_{hex}	heat exchanger hydraulic diameter, m
D_{jnz}	axial jet nozzle internal diameter, m
D_{mi}	spray manifold internal diameter, m
D_{sh}	internal diameter of coiled heat exchanger shell, m
\bar{e}	average internal energy, J/kg
G	mass flux through cross-section of the heat exchanger, kg/(m ² ·s)
gr	system acceleration ratio, dimensionless
\bar{h}	average enthalpy, J/kg

Heat Transfer Coefficients, W/(m²·K)

h_{boil}	boiling heat transfer coefficient inside heat exchanger
h_{cond}	ullage wall condensation heat transfer coefficient
h_{conv}	two-phase flow forced convection heat transfer coefficient inside heat exchanger
h_{drimp}	heat transfer coefficient from a tank wall to impinging droplets
h_{exm}	two-phase flow heat transfer coefficient inside the heat exchanger
h_{mex}	forced convection heat transfer coefficient inside spray manifold
h_{mext}	total heat transfer coefficient from spray manifold to heat exchanger

NOMENCLATURE (Continued)

Enthalpies, J/kg

h_{drv}	vapor by liquid droplets temperature and pressure
h_{intv}	vapor by interface temperature and pressure
h_{lv}	vapor by liquid temperature and pressure
h_{sthe}	pressurization non-condensable gas from pressurization system
h_{stv}	pressurization vapor from pressurization system
h_{uhe}	non-condensable gas in ullage by ullage pressure and partial pressure
h_{uv}	vapor in ullage by ullage temperature and vapor partial pressure
h_{wlw}	vapor by wall liquid temperature and pressure
h_{fg}	latent heat on the liquid-ullage interface, J/kg

Others

Ja	Jacobs number, dimensionless
k	thermal conductivity, W/(m·K)
k_{mex}	spray manifold wall thermal conductivity heat transfer coefficient, W/(m ² ·K)
l^*	linear length scale for wall conduction heat transfer, m
M, m	mass, kg

Mass Flow Rates, kg/s

\dot{m}	mass flow rate
\dot{m}_{chill}	liquid taking from the tank for pipe system chilldown
\dot{m}_{cnj}	condensation initiated by axial jet
\dot{m}_{drboil}	droplets boil-off to ullage
\dot{m}_{drl}	unevaporated droplets falling to liquid
\dot{m}_{drwl}	unevaporated droplets move to wall liquid
\dot{m}_{evap}	evaporation from liquid interface to ullage
\dot{m}_{fir}	liquid taking from the tank for engine firing
$\dot{m}_{hepress}$	noncondensable pressurant to the ullage
\dot{m}_{hevent}	noncondensable gas vented from the ullage
\dot{m}_{lboil}	bulk liquid boil-off

NOMENCLATURE (Continued)

\dot{m}_{lvent}	vented liquid
\dot{m}_{mixl}	total from injection pipe to bulk liquid
\dot{m}_{mixu}	total from injection pipe to ullage (droplets)
\dot{m}_{orif}	through spray bar orifice
\dot{m}_{pump}	liquid pumped from tank to thermodynamic venting system
\dot{m}_{ucndr}	bulk vapor condensation on the droplet
\dot{m}_{ucnl}	vapor condensation on the ullage bulk liquid interface
\dot{m}_{ucnwl}	vapor condensation on the wall liquid interface
\dot{m}_{uvent}	total ullage venting
\dot{m}_{vpress}	autogenous pressurant mass flow rate
\dot{m}_{vvent}	vapor vented from the ullage
\dot{m}_{wboil}	bulk liquid boiling on the wall boil-off
\dot{m}_{wlboil}	wall liquid boil-off
\dot{m}_{wll}	from wall liquid to bulk liquid
mf_{he}	noncondensable gas mass fraction in ullage, dimensionless
mf_v	liquid vapor mass fraction in ullage, dimensionless
P	pressure, Pa
P_{sat}	saturation pressure, Pa
Pr	Prandtl number, dimensionless
Pr_l	liquid Prandtl number, dimensionless
Pr_{tp}	two-phase flow Prandtl number, dimensionless

Heat Flow Rates, W

q_{addl}	additional heat flow from feed, pressurization, and venting lines to the liquid
q_{addu}	additional heat flow from feed, pressurization, and venting lines to the ullage
q_{elw}	from environment to the liquid wall
q_{enl}	from environment to the liquid
q_{enu}	from environment to the ullage
q_{euw}	from environment to the ullage wall
q_{intl}	from ullage-liquid interface to bulk liquid

NOMENCLATURE (Continued)

q_j	axial jet volumetric flow rate, m ³ /s
q_{jcnl}	condensation mass flow through gas-liquid interface, initiated by axial jet
q_{lhex}	from liquid to the heat exchanger
q_{lit}	from liquid to the injection pipe
q_{ltot}	total heat flow to the liquid from all sources
q_{lwct}	constant heat flow from construction elements to the liquid wall
q_{lwl}	from liquid wall to bulk liquid
q_{mg}	from the wall to the ullage in microgravity
q_{mhex}	from spray manifold to heat exchanger
q_{udr}	from ullage to droplets
q_{uhex}	from ullage to the heat exchanger
q_{uint}	from the ullage to the ullage-liquid interface
q_{uit}	from ullage to the injection pipe
q_{utot}	total heat flow to the ullage from all sources
q_{uwct}	constant heat flow from construction elements to the ullage wall
q_{uwl}	ullage to wall liquid
q_{uwu}	from ullage wall to ullage
q_{uwlw}	conduction from the ullage wall to the liquid wall
q_{uwwl}	from the ullage wall to the wall liquid
q'_{unif}	heat flux from the environment, uniformly distributed on the tank surface, W/m ²
Re_{tp}	two-phase flow Reynolds number, dimensionless
S^*	conduction shape factor, dimensionless
S_{dr}	speed of droplets created by spray bar jets in ullage, m/s
s	axial jet nozzle submergence, m
T	temperature, K
T_{env}	environmental temperature, K
T_{sat}	saturation temperature, K
U	bubbles terminal velocity, m/s
V	volume, m ³
V_f	volume available for the flow of fluid in the annulus, m ³
V_{tot}	total internal tank volume, m ³
V_u	ullage volume, m
X	vapors quality inside heat exchanger, dimensionless

NOMENCLATURE (Continued)

X_{lm}	two-phase flow Martinelli-Nelson parameter, dimensionless
γ	coiled tube pitch, dimensionless
ΔT_o	axial jet nozzle outflow liquid subcooling, K
μ	viscosity, kg/(m·s)
μ_w	liquid viscosity at wall temperature, kg/(m·s)
ρ	density, kg/m ³
ρ_{ave}	average density for homogeneous fluid in macrogravity, kg/m ³
σ	Stefan-Boltzmann constant, W/(m ² ·K ⁴)
σ_l	surface tension, kg/s ²
χ_{lw}	liquid wall heat experimental absorption coefficient for multilayer MLI, dimensionless
χ_{uw}	ullage wall heat absorption experimental coefficient for multilayer MLI, dimensionless

Subscripts

<i>ave</i>	average value
<i>b</i>	bulk liquid
<i>dr</i>	droplet in the ullage
<i>drimp</i>	impinged droplet
<i>he</i>	noncondensable gas
<i>hest</i>	noncondensable gas storage
<i>int</i>	bulk liquid-ullage interface
<i>it</i>	injection tube
<i>j</i>	axial jet
<i>l</i>	liquid
<i>lw</i>	liquid wall
<i>orif</i>	spray bar orifice
<i>tp</i>	two-phase
<i>u</i>	ullage
<i>uhe</i>	ullage noncondensable gas
<i>uv</i>	ullage vapor
<i>uw</i>	ullage wall
<i>v</i>	vapor
<i>w</i>	tank wall
<i>wl</i>	wall liquid

TECHNICAL MEMORANDUM

TANK SYSTEM INTEGRATED MODEL: A CRYOGENIC TANK PERFORMANCE PREDICTION PROGRAM

1. INTRODUCTION

Accurate prediction of the thermodynamic state of the cryogenic propellants in launch vehicle tanks is necessary for mission planning and successful execution. Cryogenic propellant storage and transfer in space environments require that tank pressure be controlled. The pressure rise rate is determined by the complex interaction of external heat leak, fluid temperature stratification, and interfacial heat and mass transfer. If the required storage duration of a space mission is longer than the period in which the tank pressure reaches its allowable maximum, an appropriate pressure control method must be applied. Therefore, predictions of the pressurization rate and performance of pressure control techniques in cryogenic tanks are required for development of cryogenic fluid long-duration storage technology and planning of future space exploration missions.

This Technical Memorandum (TM) describes an analytical tool, Tank System Integrated Model (TankSIM), which can be used for modeling pressure control and predicting the behavior of cryogenic propellant for long-term storage for future space missions. TankSIM is written in Fortran 90 language and can be compiled with any Visual Fortran compiler. A thermodynamic vent system (TVS) or ullage venting is used to achieve tank pressure control. Utilizing TankSIM, the following processes can be modeled: tank self-pressurization, boiloff, ullage venting, and mixing.

The intended application of TankSIM is for performance prediction for cryogenic propellant storage systems during in-space missions such as Mars and Lunar exploration and rendezvous with asteroids and near-Earth objects, as well as ground-based thermal vacuum testing, under different levels of system accelerations, external heat loads, and various thermal initial conditions. Each mission profile can consist of several different phases including coast periods, propellant transfer system chilldown, propellant tank pressurization, propellant settling, and main engine operation. Each of these phases can have different accelerations, external heat loads, and durations, and they can be repeated as many times as necessary in any sequence to create a full mission timeline.

The TankSIM analytical model is described in section 2. Section 3 covers the basic mass and energy conservation equations used in this program. The mass and heat transfer in a locked-up tank during nonmixing regimes is presented in section 4. In section 5, the tank pressurization and ullage venting pressure control are described. Section 6 introduces the spray bar TVS. An axial jet TVS pressure control system is presented in section 7. In section 8, the computer model for TankSIM is described. Section 9 covers comparison between TankSIM predictions and test data as well as examples of full mission calculations. Discussions of results and plans for future improvements of TankSIM are provided in section 10.

2. ANALYTICAL MODEL DESCRIPTION

TankSIM is a lumped, multinode transient model based on mass and energy conservation equations and correlation equations for mass and heat transfer calculations.

2.1 Basic Model Approaches for a Settled Liquid

2.1.1 Model Nodes

The TankSIM network with heat and mass transfer between the nodes is depicted in figure 1 with the following 13 nodes:

- (1) Ullage.
- (2) Ullage wall—upper head part (upper dome) of the tank wall interfaced to the ullage.
- (3) Ullage wall—cylindrical part of the tank wall interfaced to the ullage; appears at low and intermediate liquid level.
- (4) Ullage wall—segment of the lower dome of the tank wall interfaced to the ullage at level, lower than dome maximum height.
- (5) Bulk liquid.

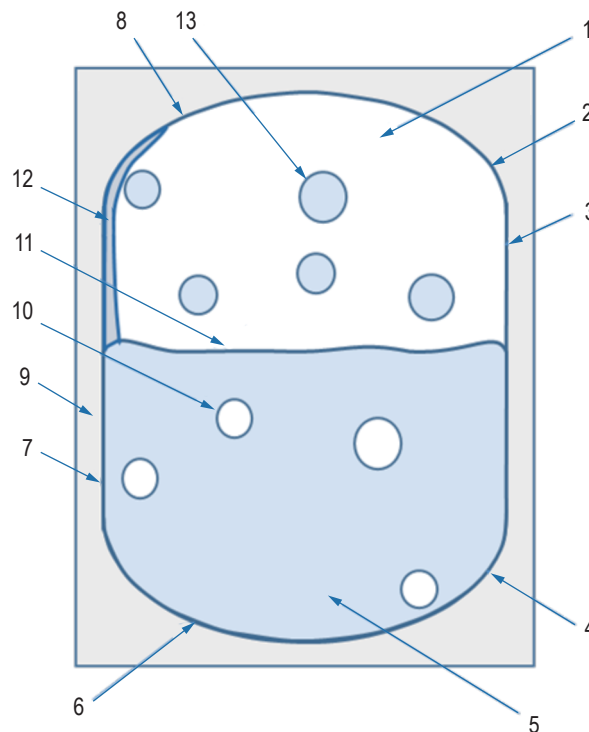


Figure 1. TankSIM nodes.

- (6) Liquid wall—bottom head part (lower dome) of the tank wall. interfaced to the liquid.
- (7) Liquid wall—cylindrical part of the tank wall interfaced to the liquid.
- (8) Liquid wall—segment of upper dome of the tank wall interfaced to the liquid when filling is above the cylindrical part of the tank.
- (9) Environment.
- (10) Bubble in bulk liquid during boiling of the bulk liquid on the wall and in volume.
- (11) Ullage—liquid interface.
- (12) Wall liquid—liquid film on the ullage tank wall.
- (13) Droplet in ullage during spray bar operation.

2.1.2 Control Volumes and Main Parameters

There are seven control volumes in the TankSIM model as shown in figure 2:

- (1) Ullage—mixture of propellant vapors and noncondensable pressurization gas. Special assumptions for the ullage were made:
 - Temperature and volume of vapor and noncondensable gas are the same and equal to the overall tank temperature and volume.
 - Total ullage pressure is a sum of vapor and noncondensable gas pressures (Dalton’s law).
 - Total ullage mass is a sum of vapor and noncondensable gas masses.
- (2) Liquid—liquid propellant in the tank.
- (3) Ullage-liquid interface—infinitely thin layer with its own temperature, containing no mass and used for the heat and mass transfer between liquid and ullage (evaporation-condensation processes) at the interface.

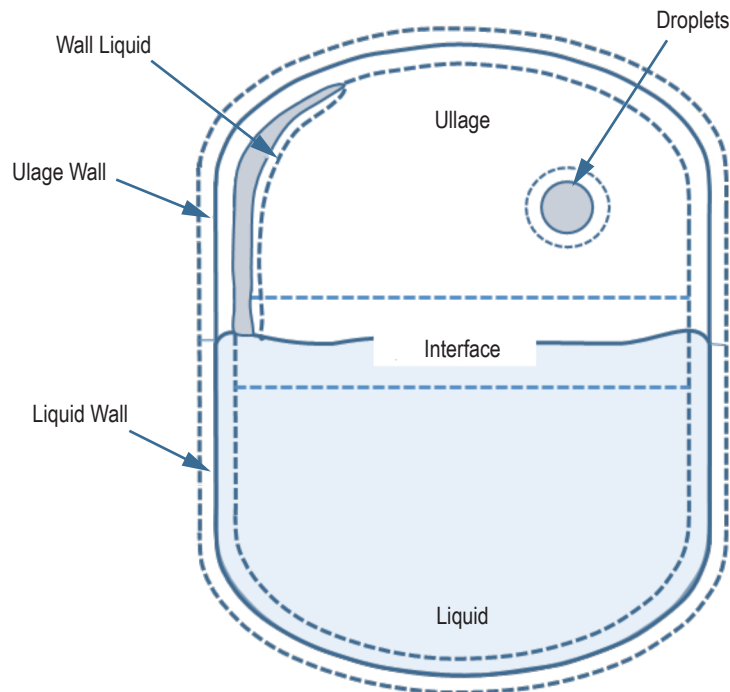


Figure 2. Diagram of control volumes.

- (4) Ullage wall—part of the tank wall interfaced to the ullage.
- (5) Liquid wall—part of the tank wall interfaced to the liquid.
- (6) Wall liquid—liquid film on the ullage wall.
- (7) Droplets in the ullage during operation of the spray bar TVS.

2.1.3 Mass Conservation Equations

As shown in appendix A, the mass conservation equations can be written as

$$\frac{dm}{dt} = \sum_k \dot{m}_k, \quad (1)$$

where m is mass of control volume or node, kg, and \dot{m}_k is mass inflow and outflow rates, positive for inflow and neagative for outflow, kg/s.

2.1.4 Energy Conservation Equations

As shown in appendix A, the internal energy and enthalpy equations for the control volume without dissipation can be written as:

$$m \frac{d(\bar{e})}{dt} = \sum_k q_k + \sum_k \dot{m}_k (h_k - \bar{e}) - P \frac{dV}{dt} \quad (2)$$

and

$$m \frac{d(\bar{h})}{dt} = \sum_k q_k + \sum_k \dot{m}_k (h_k - \bar{h}) + V \frac{dP}{dt}, \quad (3)$$

where

- m – mass of control volume, kg
- \bar{e} – average internal energy of the control volume, J/kg
- q_k – heat flow rate, not associated with in and out mass flows, W
- \dot{m}_k – in and out mass flow rates, positive for inflow and negative for outflow, kg/s
- \bar{h} – average enthalpy of the control volume, J/kg.

Detailed equations for each control volume and node will be presented in section 3.

2.2 Model Approaches for an Unsettled Liquid

2.2.1 Nonmixing Cases

For calculating heat-mass transfer in unsettled liquids during nonmixing phases, a concentric spherical enclosure model is used. In this model, the outside and inside spheres represents the tank shell and ullage, respectively, and the space between these spheres is a liquid layer. The volumes of the outer and inner spheres are equal to tank and ullage volumes, and the volume of the liquid layer is equal to the bulk liquid volume, as depicted in figure 3.

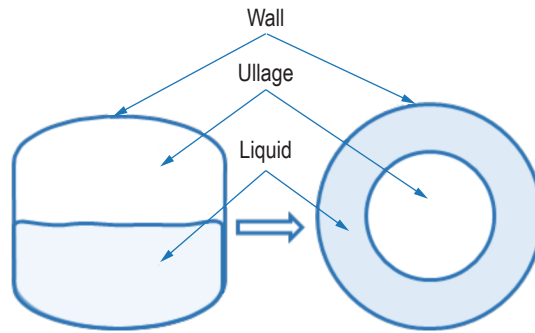


Figure 3. Tank geometry transformation for unsettled liquid (no mixing).

2.2.2 Mixing Cases

For an unsettled liquid in a mixing case, a homogeneous fluid filling the entire tank volume was assumed (fig. 4). Thermodynamic properties such as density, thermal conductivity coefficient, specific heat capacity, and others were calculated as mass weighted values by the following equation:

$$C_{p_{mix}} = \frac{C_{p_{he}}m_{he} + C_{p_v}m_v + C_{p_l}m_l}{m_{he} + m_v + m_l} . \quad (4)$$

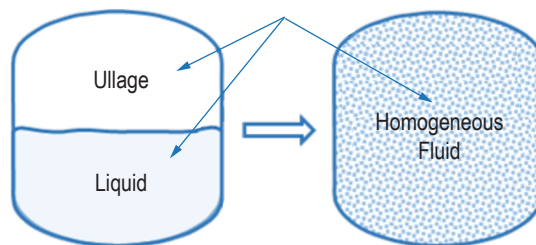


Figure 4. Tank fluids transformation for unsettled liquid during mixing.

3. MASS AND ENERGY CONSERVATION EQUATIONS

3.1 Ullage

To determine the ullage mass, temperature, and pressure, conservation of mass and energy equations (5) and (6) are utilized.

3.1.1 Ullage Mass Conservation

The ullage mass conservation equation with respect to figure 5 can be written as:

$$\frac{dm_u}{dt} = \dot{m}_{evap} + \dot{m}_{lboil} + \dot{m}_{wboil} + \dot{m}_{wlboil} - \dot{m}_{ucnwl} + \dot{m}_{drboil} - \dot{m}_{ucndr} - \dot{m}_{cnj} - (\dot{m}_{vvent} + \dot{m}_{hevent}) + (\dot{m}_{vpress} + \dot{m}_{hepress}). \quad (5)$$

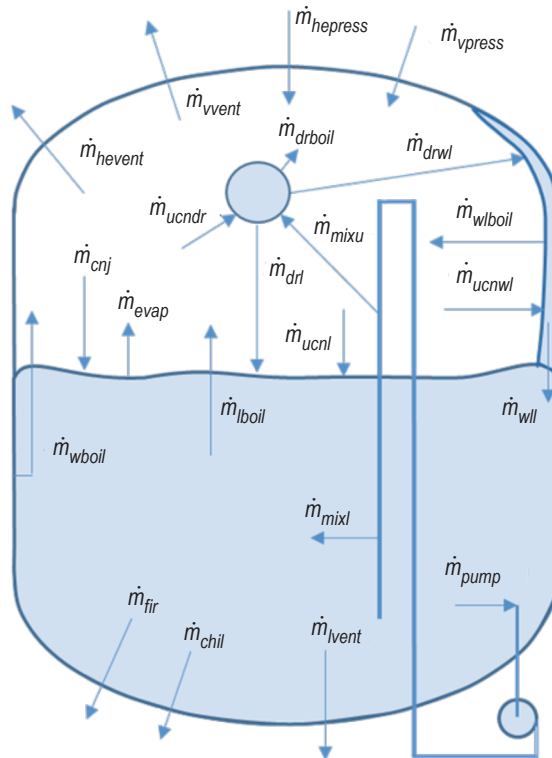


Figure 5. Diagram of mass flows.

In equation (7), $\sum_k \dot{m}_k = \dot{m}_u$ is total ullage mass change rate and

$$\begin{aligned} \sum_k \dot{m}_k h_k = & \dot{m}_{evap} h_{intv} + \dot{m}_{wboil} h_{lv} + \dot{m}_{lboil} h_{lv} + \dot{m}_{wlboil} h_{wlv} + \dot{m}_{drboil} h_{drv} \\ & + \dot{m}_{hepress} h_{sthe} + \dot{m}_{vpress} h_{stv} - \dot{m}_{ucnwl} h_{uv} - \dot{m}_{ucndr} h_{uv} - \dot{m}_{cnj} h_{uv} \\ & - (\dot{m}_{vvent} h_{uv} + \dot{m}_{hevent} h_{uhe}) . \end{aligned} \quad (8)$$

All terms described by equation (8) are not shown in figure 6.

Assuming vented gas has the same composition as the ullage (uniformly distributed species within the ullage), defining mass fractions for the vapor, mf_v , and noncondensable gas, mf_{he} , can be written as

$$mf_{he} = m_{he} / m_u = \dot{m}_{hevent} / \dot{m}_{vent} , \text{ then } mf_v = m_v / m_u = \dot{m}_{vvent} / \dot{m}_{vent} . \quad (9)$$

Rewriting the energy balance for the venting gas gives the following:

$$\dot{m}_{vvent} h_{uv} + \dot{m}_{hevent} h_{uhe} = \dot{m}_{uvent} \frac{\dot{m}_{vvent} h_{uv} + \dot{m}_{hevent} h_{uhe}}{\dot{m}_{uvent}} = \dot{m}_{uvent} (mf_v h_{uv} + mf_{he} h_{uhe}) . \quad (10)$$

Note, that $mf_v + mf_{he} = 1$.

Similarly, average ullage internal energy, \bar{e}_u , can be written as:

$$\bar{e}_u = \frac{m_v e_{uv} + m_{uhe} e_{uhe}}{m_u} = (mf_v e_{uv} + mf_{he} e_{uhe}) . \quad (11)$$

3.2 Ullage Wall (Tank Wall Interfaced to the Ullage)

3.2.1 Ullage Wall Energy Conservation

For the tank wall interfacing to the ullage, the following can be written from the energy conservation equation (see fig. 6):

$$m_{uw} \frac{d(\bar{e}_{uw})}{dt} = \sum_n q_n \quad (12)$$

or

$$m_{uw} \frac{d(\bar{e}_{uw})}{dt} = q_{euw} - q_{uwwl} - q_{uww} - q_{uwlw} . \quad (13)$$

3.3 Bulk Liquid

3.3.1 Bulk Liquid Mass Conservation Equation

The mass conservation equation for a bulk liquid is as follows (see fig. 5):

$$\frac{dm_l}{dt} = -\dot{m}_{evap} - \dot{m}_{lboil} - \dot{m}_{wboil} + \dot{m}_{wll} + \dot{m}_{drl} + \dot{m}_{mixl} - \dot{m}_{pump} - \dot{m}_{fir} - \dot{m}_{chill} - \dot{m}_{lvent} . \quad (14)$$

3.3.2 Bulk Liquid Energy Conservation Equation

For a bulk liquid, the energy equation can be written as:

$$m_l \frac{d(\bar{e}_l)}{dt} = q_{enl} + q_{lwl} + q_{intl} - q_{lit} - q_{lhex} + \sum_i \dot{m}_i h_i - \bar{e}_l \sum_i \dot{m}_i - P_l \frac{dV_l}{dt} , \quad (15)$$

where $\sum_i \dot{m}_i = \dot{m}_l$.

From figure 5,

$$\begin{aligned} \sum_i \dot{m}_i h_i &= -\dot{m}_{evap} h_{intl} - \dot{m}_{lboil} h_l - \dot{m}_{wboil} h_l + \dot{m}_{wll} h_{wl} + \dot{m}_{drl} h_{drl} \\ &+ \dot{m}_{mixl} h_{mixl} + \dot{m}_{cnj} h_{cnj} - \dot{m}_{fir} h_l - \dot{m}_{chil} h_l - \dot{m}_{vent} h_l - \dot{m}_{pump} h_l . \end{aligned} \quad (16)$$

3.4 Liquid Wall (Tank Wall Interfaced to the Liquid)

3.4.1 Liquid Wall Energy Conservation

From figure 6, the energy conservation equation for the tank wall interfacing to the liquid can be written as:

$$m_{lw} \frac{d(\bar{e}_{lw})}{dt} = \sum_n q_n \quad (17)$$

or

$$m_{lw} \frac{d(\bar{e}_{lw})}{dt} = q_{elw} + q_{uwlw} - q_{lwl} . \quad (18)$$

3.5 Wall Liquid (Liquid Film on the Ullage Wall)

3.5.1 Wall Liquid Mass Conservation

The wall liquid mass conservation equation follows:

$$\frac{dm_{wl}}{dt} = \dot{m}_{drwl} + \dot{m}_{ucnwl} - \dot{m}_{wlboil} - \dot{m}_{wll} . \quad (19)$$

3.5.2 Wall Liquid Energy Conservation

In accordance with figures 5 and 6, the energy conservation equation can be written as follows:

$$m_{wl} \frac{d(\bar{e}_{wl})}{dt} = q_{uwwl} + q_{uwl} + \dot{m}_{ucnwl} h_{ul} + \dot{m}_{drwl} h_{dr} - \dot{m}_{wlboil} h_{wl} - \bar{e}_{wl} \sum_i \dot{m}_i - P_{wl} \frac{dV_{wl}}{dt}, \quad (20)$$

where $\sum_i \dot{m}_i$ is equal to the right side of equation (19).

4. HEAT AND MASS TRANSFER INSIDE THE TANK

4.1 External Heat Loads

External heat loads are heat flows from the environment to the tank. The following five external heat load mechanisms are incorporated into the TankSIM:

- (1) Radiation to tank walls, calculated by the Stefan-Boltzmann law and corrected by the average heat absorption coefficient, used for the tank thermal insulation.
- (2) Heat flux uniformly distributed on the external surface of the tank wall.
- (3) Constant heat flows to the ullage and to the liquid from supporting elements.
- (4) Constant heat flows to the ullage wall and liquid wall from supporting elements.
- (5) Heat flows to the tank walls from venting, filling, and pressurization lines. Heat flow from the environment to the ullage wall (wall interfaced to the ullage) calculates by:

$$q_{euw} = \left[\sigma \chi_{uw} (T_{env}^4 - T_{uw}^4) + q'_{unif} \right] A_{uw} + q_{uwct} + q_{addu} \cdot \quad (21)$$

Similarly, heat flow from the environment to the liquid wall (tank wall interfaced to the liquid) is as follows:

$$q_{elw} = \left[\sigma \chi_{lw} (T_{env}^4 - T_{lw}^4) + q'_{unif} \right] A_{lw} + q_{lwct} + q_{addl} \cdot \quad (22)$$

4.2 Ullage-Bulk Liquid Interface Heat and Mass Transfer

4.2.1 Interface Temperature

Control volume representing ullage—liquid interface with no mass has only temperature, which is used for calculating heat and mass transfer across the interface. Temperature of the interface is calculated by the modified Alabovskii's¹ equation (detailed description is provided in app. B):

$$T_{int} = \frac{KT_l + T_u}{K + 1} = \frac{T_l + T_u/K}{1 + 1/K}, \quad (23)$$

where

$$K = \frac{k_l}{k_u} \left(\frac{\mu_u \rho_l}{\mu_l \rho_u} \text{Pr}_l \right)^{0.5} (1 + m)$$

$m = \frac{q_{evap}}{q_{intl}}$ is the ratio of evaporation heat to total heat flows through interface.

4.2.2 Heat and Mass Transfer at the Liquid-Ullage Interface

Mass of evaporated/condensed liquid/vapor from the ullage—liquid interface is calculated using the energy jumping boundary condition suggested by Delhaye² and Meserole et al.³:

$$\dot{m}_{evap} = \frac{q_{uint} - q_{intl}}{h_v(T_{int}, P_u) - h_l(T_{int}, P_u)}. \quad (24)$$

In this equation, positive/negative mass flow rate corresponds to the evaporation/condensation from/to the interface. Both q_{uint} and q_{intl} flow rates are calculated by the heat conduction model with assumptions that temperatures of the ullage and bulk liquid are linearly depend on the height:

$$q_{uint} = 2 A_{int} \frac{k_u (T_u - T_{int})}{h_u}, \quad q_{intl} = 2 A_{int} \frac{k_l (T_{int} - T_l)}{h_l}. \quad (25)$$

The conduction model was chosen because there are no correlations for liquid-gas interface heat flow rates in a finite volume. Usually, the Horizontal Heated Downward-Facing Plate model is used (see ref. 4). It is based on the finite flat plate, heated from the bottom, in infinite space (fig. 7), which is far from real conditions (fig. 8).

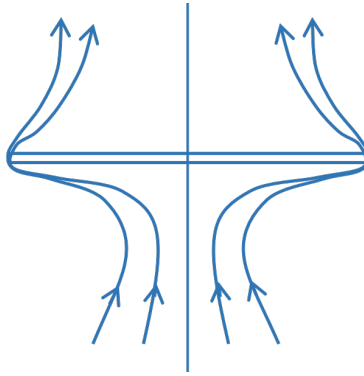


Figure 7. Horizontal heated downward-facing plate model.

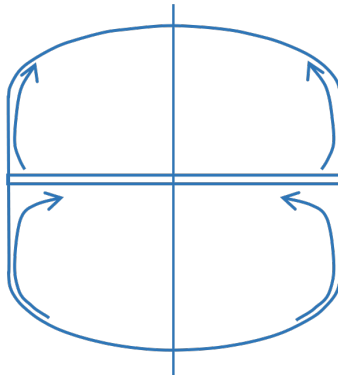


Figure 8. Liquid-ullage interface in finite volume tank.

4.3 Ullage Wall Heat and Mass Transfer

The ullage wall is divided into three segments—the cylindrical segment and the upper and lower domes.

4.3.1 Ullage Wall Convection for the Cylindrical Segment

The heat transfer coefficient for the cylindrical part is calculated using the Churchill and Usagi⁵ blending equation, applied to both laminar and turbulent convection regimes. Assuming the tank wall is a flat plate model (see app. B.3),

$$Nu = \left[(Nu_l)^6 + (Nu_t)^6 \right]^{1/6}, \quad (26)$$

where

$$Nu_l = \frac{2}{\ln \left[1 + 2 / \left(\bar{C}_l Ra^{1/4} \right) \right]} \quad (\text{Nusselt number for laminar convection})$$

$$\bar{C}_l = \frac{0.671}{\left[1 + (0.492 / Pr)^{9/16} \right]^{4/9}} \quad (\text{Correction coefficient for laminar Nusselt number})$$

$$Nu_t = \frac{f(T_{uw}/T_u) C_t^y Ra^{1/3}}{\left(1 + 1.4 \times 10^9 Pr / Ra \right)} \quad (\text{Nusselt number for turbulent convection})$$

$$C_t^y = \frac{0.13 Pr^{0.22}}{\left(1 + 0.61 Pr^{0.81} \right)^{0.42}} \quad (\text{Correction coefficient for turbulent } Nu_t)$$

$$f\left(\frac{T_{uw}}{T_u}\right) = 1 + 0.078 \left(\frac{T_{uw}}{T_u} - 1 \right) \quad (\text{Correction coefficient for high wall-ullage temperature difference}).$$

4.3.2 Upper and Lower Domes (Endcaps)—Ullage Heat Transfer

Due to the lack of appropriate correlations, a heat conduction mode was used to calculate heat flow between the upper and lower domes and the ullage:

$$q_{du} = \frac{2 A_{du} k_u}{h_u} (T_{uw} - T_u). \quad (27)$$

4.4 Condensation on the Ullage Wall

The condensation calculation for the ullage wall is based on the Gerstmann and Griffith^{6,7} model, and two different modifications of the Nusselt vertical flat plate condensation model. Details of the calculations are provided in appendix B.

4.4.1 Cylindrical (Barrel) Segment of the Tank

The condensation heat flow rate on the vertical cylindrical ullage wall calculates using the Nusselt model with a Rohsenow modification⁴, reintegrated for nonzero initial liquid film thickness. With this modification, the average Nusselt number, $\bar{N}u$, is as follows:

$$\bar{N}u = 0.9428 \left[\frac{g\rho_l(\rho_l - \rho_v)h'_{fg}L^3}{k_l\mu_l(T_{sat} - T_w)} \right]^{1/4} \left[(\sqrt{b+1} - 2\sqrt{b})(\sqrt{b} + \sqrt{b+1})^{1/2} + \sqrt{2}b^{3/4} \right]. \quad (28)$$

The liquid film thickness, δ , can be calculated as:

$$\delta = \left(\frac{4\mu_l k_l (T_{sat} - T_w) L}{\rho_l (\rho_l - \rho_v) g h'_{fg}} \right)^{1/4} \left(\sqrt{b} + \sqrt{b + \frac{x}{L}} \right)^{1/2}, \quad (29)$$

where x is a coordinate along the vertical surface as shown in figure 62 in appendix B, and L is a height of the cylindrical segment

In equations (28) and (29), the dimensionless parameter, b , as a function of initial liquid film thickness, δ_0 , is as follows:

$$b = \frac{\delta_0^4}{16} \frac{\rho_l (\rho_l - \rho_v) g h'_{fg}}{\mu_l k_l (T_{sat} - T_w) L}. \quad (30)$$

4.4.2 Upper Dome (Endcup) Segment Interfaced to the Ullage

For the mass and heat transfer on the upper dome, the Gerstmann and Griffith^{6,7} condensation model on the bottom side of the inclined flat plate was used. Applying their model, the upper dome is divided into two regions with respect to angle α : $0^\circ \leq \alpha \leq 20^\circ$ and $20^\circ < \alpha \leq 90^\circ$.

For $0^\circ \leq \alpha \leq 20^\circ$, the Nusselt number is:

$$\bar{N}u = \frac{0.90}{Ra^{1/6} (1 + 1.1Ra^{1/6})}, \quad (31)$$

where $Ra = \frac{\rho_l \sigma h_{fg}}{k_l \mu_l (T_{sat} - T_w)} \left[\frac{\sigma}{g(\rho_l - \rho_v) \cos(\alpha)} \right]^{1/2}$ is a modified Rayleigh number.

For $20^\circ < \alpha \leq 90^\circ$, a modified Nusselt model was recommended⁶. In this model, the free-falling acceleration, g , should be replaced by $g \sin(\alpha)$ as shown in the following equation:

$$\bar{Nu}_l = 0.9428 \left[\frac{g \sin(\alpha) \rho_l (\rho_l - \rho_v) h'_{fg} L^3}{k_l \mu_l (T_{sat} - T_w)} \right]^{1/4} \left[(\sqrt{b+1} - 2\sqrt{b})(\sqrt{b} + \sqrt{b+1})^{1/2} + \sqrt{2b}^{3/4} \right], \quad (32)$$

$$\delta = \left(\frac{4\mu_l k_l (T_{sat} - T_w) L}{\rho_l (\rho_l - \rho_v) g \sin(\alpha) h'_{fg}} \right)^{1/4} \left(\sqrt{b} + \sqrt{b + \frac{x}{L}} \right)^{1/2}, \quad (33)$$

and

$$b = \frac{\delta_0^4 \rho_l (\rho_l - \rho_v) g \sin(\alpha) h'_{fg}}{16 \mu_l k_l (T_{sat} - T_w) L}. \quad (34)$$

For the heat and mass transfer rates calculation, the upper dome is divided into layers as depicted in figure 9. Each layer (for example, ABCD) has its own angle α , side area, Rayleigh number, and liquid film thickness. The final liquid film thickness from the previous layer is used as an initial thickness for the next one.

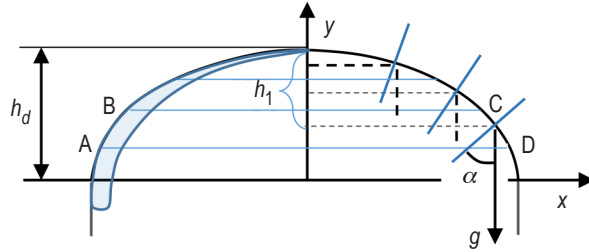


Figure 9. Calculation schematic for condensation on the upper dome.

Angle α can be found as follows:

$$\text{tg}(\alpha) = \frac{h_d}{r} \sqrt{\frac{\bar{h}_1(2 - \bar{h}_1)}{(1 - \bar{h}_1)^2}}, \quad (35)$$

where

$$\bar{h}_1 = \frac{h_1}{h_d}$$

4.4.3 Lower Dome (Endcup)—Ullage Interface

As shown by Oosthuizen⁸, the condensation on the upper side of the inclined plate can be described by modified Nusselt equations, where the free-falling acceleration is replaced by $g \sin(\beta)$. As depicted in figure 10, the angle β is an angle between a tangent line and free-fall acceleration. The condensation on the lower dome can be calculated as follows:

$$\bar{N}u_l = 0.9428 \left[\frac{g \sin(\beta) \rho_l (\rho_l - \rho_v) h'_{fg} L^3}{k_l \mu_l (T_{sat} - T_w)} \right]^{1/4} \left[(\sqrt{b+1} - 2\sqrt{b})(\sqrt{b} + \sqrt{b+1})^{1/2} + \sqrt{2b}^{3/4} \right] \quad (36)$$

and

$$\delta = \left(\frac{4\mu_l k_l (T_{sat} - T_w) L}{\rho_l (\rho_l - \rho_v) g \sin(\beta) h'_{fg}} \right)^{1/4} \left(\sqrt{b} + \sqrt{b + \frac{x}{L}} \right)^{1/2} \quad (37)$$

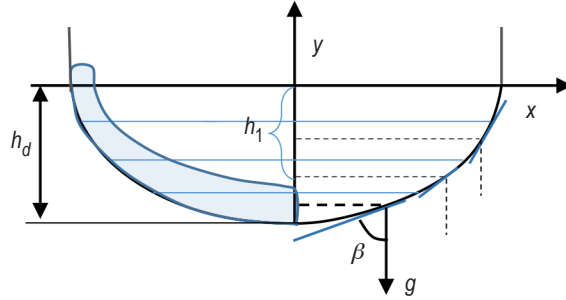


Figure 10. Calculation schematic for condensation on the lower dome.

In equations (36) and (37), parameter b is:

$$b = \frac{\delta_0^4 \rho_l (\rho_l - \rho_v) g \sin(\beta) h'_{fg}}{16 \mu_l k_l (T_{sat} - T_w) L}, \quad h'_{fg} = h_{fg} + 0.68Ja, \quad \text{and} \quad Ja = \frac{C_{p_l} (T_{sat} - T_w)}{h_{fg}}, \quad (38)$$

where L is a height of the liquid inside the lower dome.

The calculation for the lower dome is similar to that for the upper dome, as described earlier.

Angle β is described as follows:

$$\operatorname{tg}(\beta) = \frac{r}{h_d} \sqrt{\frac{(1 - \bar{h}_1)^2}{\bar{h}_1(2 - \bar{h}_1)}}, \quad (39)$$

where $\bar{h}_1 = \frac{h_1}{h_d}$.

4.5 Bulk Vapor Condensation

Bulk vapor condensation occurs when the ullage temperature is lower than the vapor saturation temperature that corresponds to the vapor partial pressure, $T_u < T_{sat}(P_v)$. For this case, the condensation mass flow rate is:

$$\dot{m}_{cond} = \frac{q_{utot}}{h_v(T_u, P_v) - h_l(T_u, P_v)}. \quad (40)$$

4.6 Bulk Liquid Convective Heat and Mass Transfer

For wall-liquid heat transfer modeling, the wall is divided into three segments—the cylindrical segment and upper and lower domes.

4.6.1 Convection on the Cylindrical Segment of the Liquid Wall

The heat transfer coefficient for the cylindrical part of the liquid wall is calculated using the same Churchill and Usagi⁵ blending equation as was applied for ullage-ullage wall (eq. (26)). In this case, the Rayleigh and Prandtl numbers and correction coefficients are calculated using liquid properties and liquid and wall temperatures.

4.6.2 Heat Transfer on the Lower Dome (Endcup) Interfaced to the Liquid

For heat transfer between the lower dome and bulk liquid, the horizontal heated upward-facing plate with uniform wall and liquid temperatures model, described by Rohsenow⁴, is used:

$$Nu = \left[(Nu_l)^{10} + (Nu_l)^{10} \right]^{1/10}, \quad (41)$$

where

$$Nu_l = \frac{1.4}{\ln \left[1 + 1.4 / \left(0.835 \bar{C}_l Ra^{1/4} \right) \right]} - \text{laminar } Nu,$$

$$Nu_t = 0.14 \left(\frac{1 + 0.0107 Pr}{1 + 0.01 Pr} \right) Ra^{1/3} - \text{turbulent } Nu ,$$

and

$$\bar{C}_l = \frac{0.671}{\left[1 + (0.492/Pr)^{9/16} \right]^{4/9}} - \text{correction coefficient} .$$

As suggested by Goldstein et al.⁹, the length scale accepted in that model is the ratio A_{wet}/p , where A_{wet} is a lower dome wetted area and p is a perimeter of a wetted segment (see fig. 11).

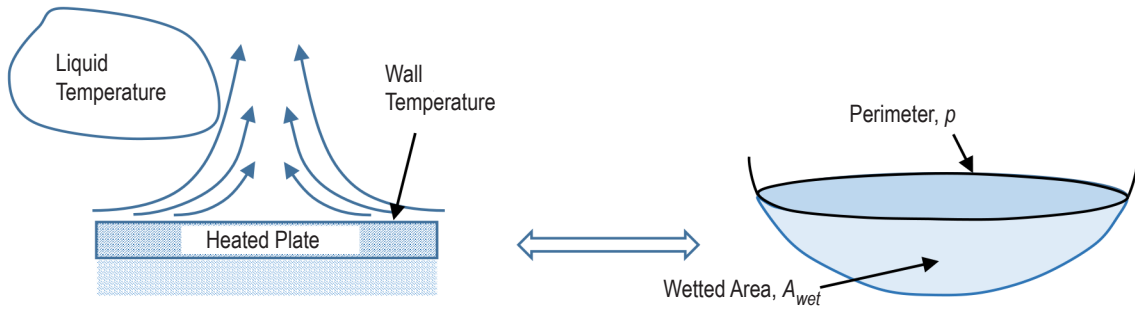


Figure 11. Definition sketch for lower dome convective model.

4.6.3 Upper Dome (Endcup)—Liquid Heat Transfer

For the upper dome wetted segment, the modified Churchill and Usagi model (eq. (26)) can be used. In this model, as suggested by Rich¹⁰, free-fall acceleration g is replaced by $g \cos(\varphi)$, where angle φ is the angle between the direction of acceleration and the upper dome tangent line as depicted in figure 12. After replacing the free-fall acceleration, the Rayleigh number is:

$$Ra = \frac{g \cos(\varphi) \beta_l \rho_l^2 C_{p_l} (T_{lw} - T_l) L^3}{k_l \mu_l} , \quad (42)$$

where L is a height at liquid in the upper dome.

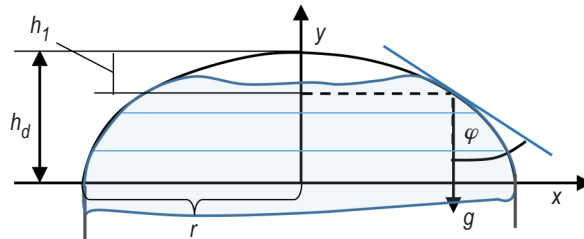


Figure 12. Calculation schematic for convection in the liquid on the upper dome wall.

Angle φ can be found as follows:

$$tg(\varphi) = \frac{r}{h_d} \sqrt{\frac{(1-\bar{h}_1)^2}{\bar{h}_1(2-\bar{h}_1)}} \text{ and } \cos(\varphi) = \frac{1}{\sqrt{1+tg^2(\varphi)}}, \quad (43)$$

where $\bar{h}_1 = \frac{h_1}{h_d}$.

4.7 Bulk Liquid Boiling

The liquid starts to boil when its saturation pressure is higher than the liquid pressure, $P_{sat} > P_l$.

4.7.1 Bulk Liquid Boiling on the Tank Wall (Heterogeneous Boiling)

The liquid is boiling on the wall when the temperature of the wall is higher than the liquid saturation temperature, $T_{lw} > T_{sat}(P_l)$. To describe this process, a correlation containing the heat flux from the wall to the liquid, including the dependency of the wall material properties, was accepted. As reported by Grigoryev et al.¹¹, there are two correlations that depend on thermal properties of the liquid and the wall. The first correlation is used for nitrogen, oxygen, methane, and other cryogenic liquids (excluding hydrogen, neon, and helium). In this case,

$$\frac{Q_{boil}}{A_{lw}} = \frac{A_1^3}{A_1 + 2m} \left(\frac{h_{fg}\rho_v\Delta T_0}{\sigma T_{sat}} \right) \left(C_1 \frac{k_l\rho_l\Delta T}{\mu_l} + C_2 h_{fg}\rho_v \right), \quad (44)$$

where

Q_{boil}/A_{lw} = heat flux from the wall to the liquid

$$A_1 = -m + \sqrt{m^2 + \gamma M}$$

$$C_1 = 8.010^{-5}$$

$$C_2 = 10^{-4}.$$

The second correlation is suggested for low point boiling cryogens, such as hydrogen, parahydrogen, neon, and helium, where $\sqrt{k_l C p_l \rho_l} \approx \sqrt{k_w C p_w \rho_w}$:

$$\frac{Q_{boil}}{A_{lw}} = A_2^2 \left(\frac{h_{fg}\rho_v\Delta T_0}{\sigma T_{sat}} \right) \left(C_3 \frac{k_l\rho_l\Delta T}{\mu_l} + C_4 h_{fg}\rho_v \right) \quad (45)$$

and

$$A_2 = -0.25(m - 2\phi D) + \sqrt{[0.25(m - 2\phi D)]^2 + 0.5(\gamma M + m\phi D)}, \quad (46)$$

where $C_3 = 3 \times 10^{-2}$ and $C_4 = 3 \times 10^{-3}$. All other parameters are the same for both of the heat fluxes¹¹:

$$D = \frac{\Delta T \sqrt{k_w C_w \rho_w}}{h_{fg} \rho_v},$$

$$m = 178.884 \frac{k_l}{\sqrt{k_w C_w \rho_w}},$$

$$M = 2 \frac{k_l \Delta T}{\alpha' h_{fg} \rho_v},$$

$$\Delta T_0 = 0.01 \text{ K},$$

$$\alpha' = 0.01,$$

$$\gamma = 0.45447,$$

$$\phi = 0.44597.$$

4.7.2 Bulk Liquid Pool Boiling (Homogeneous Boiling)

Liquid boils in a large volume when its saturation pressure is higher than the internal pressure, $P_{sat} > P_l$. In this case, the boiling mass flow rate can be calculated as:

$$\dot{m}_{boil} = \frac{q_{l,tot}}{h_v(T_l, P_u) - h_l(T_l, P_u)}. \quad (47)$$

4.8 Conductive Heat Transfer Through the Wall Between the Ullage and Liquid Regions

Conduction heat transfers between the wall interfaced to the ullage and the wall interfaced to the liquid are calculated assuming temperature distribution inside both ullage and liquid wall segments are linear:

$$q_{cond} = \frac{A_{cw} k_w}{l^*} (T_{uw} - T_{lw}), \quad (48)$$

where $l^* = 0.5h_{tank}$ is a length scale and A_{cw} is a cross-sectional area of the tank wall at the liquid level.

4.9 Fluid Thermodynamic Properties

To calculate thermodynamic properties as functions of pressure and temperature, the NIST RefProp FORTRAN subroutines are used¹². Using these procedures significantly decreases calculation speed (several times) compared to the interpolation from property tables without significantly increasing calculation precision. They are used inside the TankSIM code to ensure greater accuracy in conservation of mass and energy only. In all other cases, the property tables are accepted. This combination of procedures and property tables allows saving calculation time and having high precision of energy and mass conservation.

For creating property tables, two FORTRAN programs were used—one for building propellant tables and the other for pressurization (noncondensable) gas tables. Pressurization gas tables includes superheated gas properties only, but propellant tables include three parts—saturation line, superheated vapor, and subcooled liquid. During a table creation, the user can choose the pressure and temperature ranges and their changing steps using precisions calculated for each part of the table. It should be noted that, for superheated vapor and subcooled liquid, instead of temperature itself, the normalized temperatures $t_{nmv} = (t_u - t_{vsat})/dt_v$ for vapor and $t_{nml} = (t_{lsat} - t_l)/dt_l$ for liquid are used.

In these equations, t_{nmv} and t_{nml} are normalized temperatures, t_u and t_l are ullage and bulk liquid temperatures, respectively, t_{vsat} is the vapor saturation temperature by vapor partial pressure, t_{lsat} is the liquid saturation temperature by total ullage pressure, dt_v is the vapor temperature range which automatically begins from the vapor saturated temperature, t_{vsat} , and ends with maximal temperature decided by the user, and dt_l is the liquid temperature range, which automatically begins from the triple point and ends at the liquid saturation temperature. As one can see, both ranges change from 0 to 1.

The TankSIM package includes folder ‘NIST_For’ that contains all needed programs for building property tables. The NIST_For program also gives a possibility to use an input file or manually put the required information into the program.

5. TANK PRESSURIZATION AND ULLAGE VENTING PRESSURE CONTROL

5.1 Ullage Pressurization

There are two types of pressurization procedures: (1) Using noncondensable gas and (2) autogenous (using propellant hot vapor). The use of each procedure depends on the propellant and specific requirements for that particular system.

5.1.1 Pressurization With Noncondensable Gas

The model of the noncondensable gas pressurization is based on critical (choked) gas flow through orifice or Venturi between the storage of the gas and pressurized tank. In this case, the mass flow rate can be calculated as described in the Miller's Handbook¹³, as shown in figure 13.

$$\dot{m}_{press} = C_d A \sqrt{k \rho_1 P_1 \left(\frac{2}{k+1} \right)^{\frac{k+1}{k-1}}} = \frac{\pi d^2}{4} C_d \sqrt{k \rho_1 P_1 \left(\frac{2}{k+1} \right)^{\frac{k+1}{k-1}}}, \quad (49)$$

where

- $k = C_p/C_v$ – heat capacity ratio on the gas storage side, dimensionless
- C_d – discharge coefficient, dimensionless
- A – orifice hole or Venturi throat cross-sectional area; other parameters can be seen in figure 13, m²
- d – orifice hole or Venturi throat diameter, m
- l – thickness of the orifice or length of Venturi cylindrical part, m
- P_1 – gas pressure on the gas storage side, Pa
- ρ_1 – gas density on the gas storage side, kg/m³
- V_1 – volume of the noncondensable gas storage, m³.

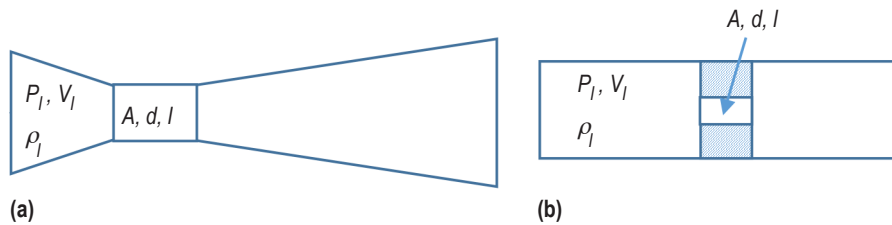


Figure 13. Pressurization devices schematic: (a) Critical Venturi and (b) critical orifice.

Assuming that the process is to be isentropic, and because noncondensable gas is far from the saturation state, the downstream pressure, density, and temperature can be found by the following equations for perfect gas¹³.

$$P_2 = P_1 \left(\frac{2}{k+1} \right)^{\frac{k}{k-1}}, \quad \rho_2 = \rho_1 \left(\frac{2}{k+1} \right)^{\frac{1}{k-1}}, \quad \text{and} \quad T_2 = T_1 \frac{2}{k+1}. \quad (50)$$

With the same assumptions, the final (after pressurization) parameters of the noncondensable gas in storage in accordance to Spalding and Cole¹⁴ can be found:

$$P_{fin} = P_{beg} \left(\frac{\rho_{fin}}{\rho_{beg}} \right)^k, \quad T_{fin} = T_{beg} \left(\frac{\rho_{fin}}{\rho_{beg}} \right)^{k-1}. \quad (51)$$

The final density of the noncondensable gas in storage can be found using the mass flow rate from the storage to the tank, calculated by equation (49):

$$\rho_{fin} = \rho_{beg} - \left(\frac{\dot{m}_{hepress} \Delta t}{V_1} \right), \quad (52)$$

where

- Δt = pressurization time
- $P_{beg}, T_{beg}, \rho_{beg}$ = initial values
- $P_{fin}, T_{fin}, \rho_{fin}$ = final values
- $\dot{m}_{hepress}$ = noncondensable pressurization gas mass flow rate, kg/s.

The discharge coefficient calculates differently for critical orifice and critical Venturi. For orifice with $1 < l/d < 6$, the discharge coefficient is $C_d = 0.83932$ according to Ward-Smith¹⁵. For critical Venturi, the discharge coefficient, as suggested by Simmons¹⁶, depends on the Reynolds number which is calculated using Venturi throat diameter.

$$C_d = 1 - \frac{7.9139}{\sqrt{Re}}, \quad (53)$$

where $Re = \frac{4\dot{m}}{\pi\mu d}$.

5.1.2 Autogenous Pressurization

Autogenous pressurization usually is used during the engine firing. In this case, changing of the ullage volume is determined by the propellant flow rate needed for the engine. Pressurization mass flow rate is calculated using partial pressures of the vapor and noncondensable gas as follows:

$$P_{he} = \frac{m_{he} R_{he} T_u}{V_{u fin}}, \quad (54)$$

where

V_{ubeg} is an initial ullage volume, m³.

$V_{u\text{fin}} = V_{ubeg} + \frac{\dot{m}_{fir}}{\rho_l} \Delta t$ is a final ullage volume, m³.

Partial pressure of the vapor calculates as $P_v = P_u - P_{he}$; then, vapor density under new pressure, $\rho_{v\text{fin}}$, can be found. Finally, the mass flow rate for pressurization vapors is calculated as:

$$\dot{m}_{v\text{press}} = \frac{\rho_{v\text{fin}} V_{u\text{fin}} - m_{v\text{beg}}}{\Delta t} . \quad (55)$$

5.2 Ullage Venting Methods

Ullage venting is used for pressure control operation during long-term propellant storage. The venting system operates between a prescribed pressure interval, namely P_{min} and P_{max} . P_{min} and P_{max} represent minimum and maximum ullage pressures prescribed during the venting operation for ullage and/or saturated liquid. Ullage venting is modeled for the following cases:

- (1) Cycling venting.
- (2) Continuous venting through a constant orifice.
- (3) Continuous venting through an adjustable orifice while keeping ullage pressure at a prescribed constant value.

5.2.1 Cycling Venting

Ullage cycling venting is modeled for the following cases:

- Ullage venting if ullage and/or liquid saturation pressures reach/reaches prescribed P_{max} .
- Ullage venting if ullage pressure reaches prescribed P_{max} .
- Ullage venting if liquid saturation pressure reaches prescribed P_{max} .

Details of cycling venting operation logic for the three cases is shown in figure 14. The input flag allows the user to choose one of the control logic needed to be used in each particular case.

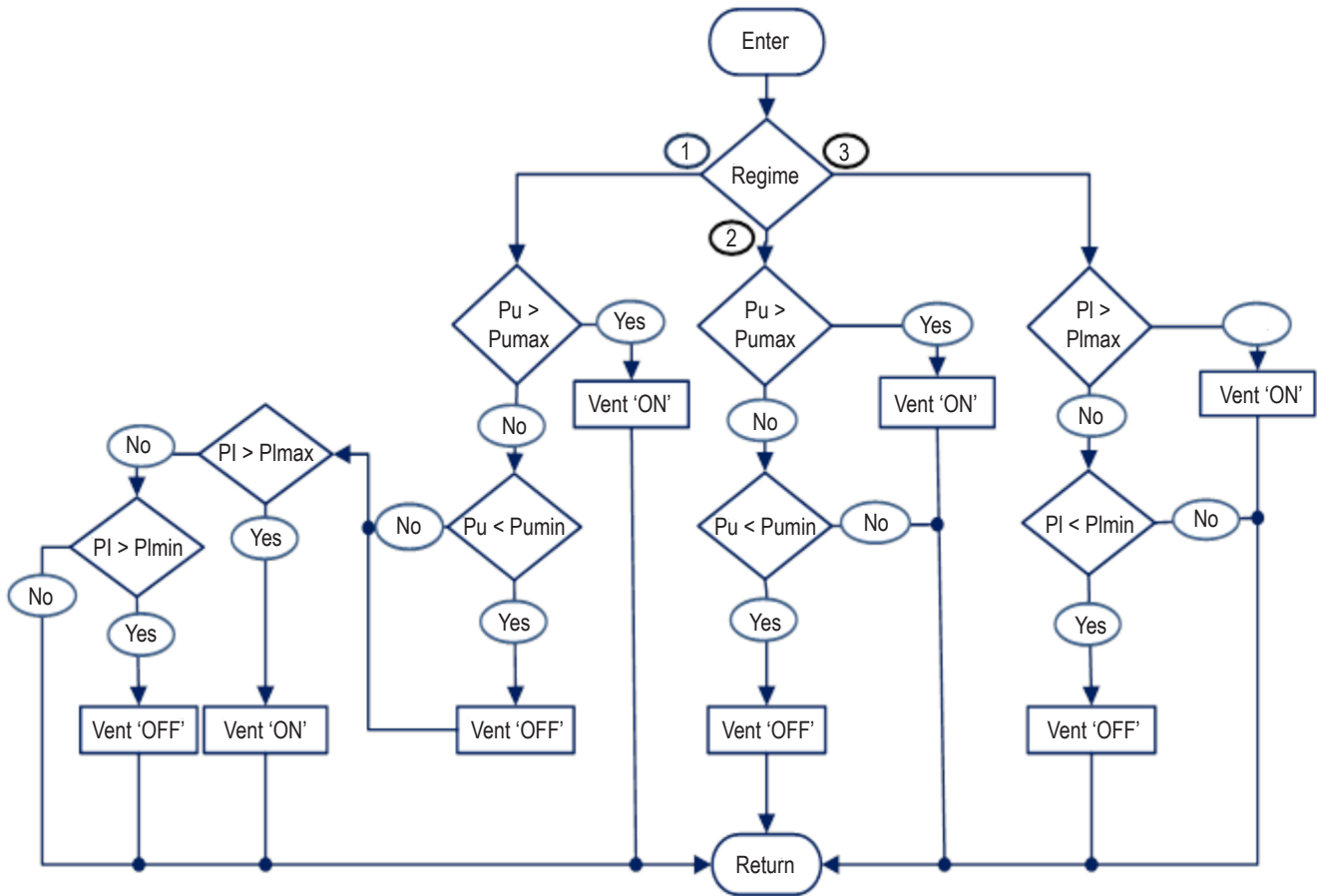


Figure 14. Ullage venting pressure control logic.

5.2.2 Liquid Boiling and Liquid Level Swell During Ullage Venting

During the ullage venting process, ullage pressure drops below liquid saturation pressure and may lead to the following conditions:

- Homogenous boiling—when ullage pressure becomes lower than the liquid saturation pressure.
- Heterogeneous boiling—when the liquid saturation temperature drops lower than the tank wall temperature, due to homogenous boiling, which leads to boiling on the wall.

In a settled liquid, vapor bubbles increase the liquid volume and liquid level (liquid level swell) until they reach the liquid surface and join the ullage. The time that a bubble leaves the liquid and becomes a part of the ullage region depends on several factors, most importantly, bubble size and system acceleration.

Basic assumptions used for the liquid level swell model follow:

- Heat transfer coefficient between the wall and bulk liquid is high, so the temperature difference between the wall and bulk liquid is small.
- The nucleate boiling takes place on the wall.
- The terminal distance for the bubbles is assumed to be equal to the liquid level.

To determine the diameter of departure bubbles, an additional assumption for the departure bubble diameter was made. If bubbles with wall departure diameter cover an area less than the wall area, the terminal time for bubbles is calculated using the wall departure diameter. If the covered area is higher or equal to the wetted wall area, bubbles merge to each other and the terminal time is calculated using the maximum bubble diameter allowed by the Bond number. This critical diameter is calculated by equation (64). To calculate the bubble-covered area, the bubbles on the surface are assumed to have hemispherical shapes.

The bubbles departure diameter calculates using the correlation, suggested by Cole and Rohsenow¹⁷:

$$Bo^{1/2} = 4.65 \times 10^{-4} (Ja^*)^{5/4} \quad (56)$$

and

$$D_d = 4.65 \times 10^{-4} \left[\frac{\sigma}{g(\rho_l - \rho_v)} \right]^{1/2} (Ja^*)^{5/4}, \quad (57)$$

where $Ja^* = \frac{T_{sat} C_{pl} \rho_l}{\rho_v h_{dg}}$ is a modified Jacobs number

D_d is a bubble departure diameter, m.

According to Levich¹⁸, the terminal velocity of rising bubbles is dependent on the bubble diameter and divided into three regions:

(1) Small bubbles. These bubbles have nondeformed spherical shapes and rise by straight lines. Their diameters correspond to Reynolds numbers, $Re < 1$, which leads to the following:

$$D < 2 \left(\frac{3\mu_l^2}{2g(\rho_l - \rho_v)\rho_l \bar{\mu}} \right)^{1/3}, \quad (58)$$

where $\bar{\mu} = \frac{\mu_l + \mu_v}{2\mu_l + 3\mu_v}$.

Velocity is calculated by the Rybczynski-Hadamard equation:

$$U = \frac{(\rho_l - \rho_v)gD^2}{6\mu_l} \bar{\mu}. \quad (59)$$

For $\mu_v \ll \mu_l$, inequality equation (58) and equation (59) become:

$$D < 2 \left(\frac{3\mu_l^2}{g(\rho_l - \rho_v)\rho_l} \right)^{1/3} \text{ and } U = \frac{(\rho_l - \rho_g)gD^2}{12\mu_l}. \quad (60)$$

(2) Intermediate size bubbles, for which $1 < Re < 700$. These bubbles have only a slightly deformed spherical shape, and at Reynolds numbers close to 700, they begin to vibrate and rise by a spiral motion instead of a straight line. Diameters of these bubbles are in the range:

$$2 \left(\frac{3\mu_l^2}{g(\rho_l - \rho_v)\rho_l} \right)^{1/3} \leq D \leq 2 \left[\frac{324\mu_l^2\sigma}{g^2\rho_l^3} \right]^{1/5}. \quad (61)$$

Velocity is calculated as:

$$U = \frac{(\rho_l - \rho_v)gD^2}{36\mu_l}. \quad (62)$$

(3) Large bubbles—fully deformed bubbles with $Re > 700$. Their terminal velocity does not depend on size:

$$U = \left[\frac{4\sigma^2 g \rho_v}{30\mu_l \rho_l^2} \right]^{1/5}. \quad (63)$$

Increasing their Re number by increasing size only can lead to bubble instability and bubble breakup. The critical diameter of the bubbles, a diameter at which breakup of large bubbles begins, can be calculated by the Levich equation (see ref. 18):

$$D_{cr} \approx \sqrt[3]{96} \frac{\sigma}{U^2 (\rho_v \rho_l^2)^{1/3}} \approx 4.4589 \frac{\sigma}{U^2 (\rho_v \rho_l^2)^{1/3}}, \quad (64)$$

where velocity, U , is calculated by equation (63).

6. TANK THERMODYNAMIC VENTING PRESSURE CONTROL SYSTEMS

The TVS typically includes a Joule-Thomson (J-T) expansion device, a two-phase heat exchanger, and a mixing pump to destratify and extract thermal energy from the tank without significant liquid losses. When tank pressure control cannot be achieved by mixing alone (bulk liquid becomes saturated at the ullage pressure), a small amount of liquid extracted from the recirculation flow is passed through a J-T valve where it is expanded to a lower pressure and temperature. The cold two-phase mixture is then passed through the cold side of the heat exchanger, which extracts thermal energy from the recirculation flow, and subsequently is vented out.

6.1 Thermodynamic Vent System Pressure Control Logic

The pressure control system (PCS) has two operational modes—mixing with and without venting. Depending on mission requirements, modes can be combined in three different pressure control logics:

- (1) Mixing mode is released by switching recirculation pump ‘ON’ when ullage pressure reaches the allowed maximum, $Pu \geq Pu_{max}$, and switching ‘OFF’ when ullage pressure becomes lower than the allowed minimum, $Pu < Pu_{min}$. After liquid saturation pressure reaches the allowed maximum Pl_{max} , it holds liquid saturation pressure in the range of Pl_{min} to Pl_{max} independently by switching the pump and venting ‘ON’ and ‘OFF’ at the same time.
- (2) The PCS holds ullage pressure in the range of Pu_{min} to Pu_{max} with mechanical mixing (no venting) by switching recirculation pump ‘ON’ and ‘OFF’. After liquid saturation pressure reaches Pu_{min} , hold ullage pressure in the required range by switching the pump and TVS ‘ON’ and ‘OFF’ at the same time.
- (3) The PCS holds ullage pressure in the range $Pu_{min} - Pu_{max}$ with mechanical mixing (no venting) by switching recirculation pump ‘ON’ and ‘OFF’. If ullage pressure exceeds Pu_{max} and liquid saturation pressure is higher than Pu_{min} , switch pump and the TVS ‘ON’ – ‘OFF’ at the same time. Switching between these cases is made by an input flag in the code.

A flowchart of the subroutine, which releases these logics, is presented in figure 15.

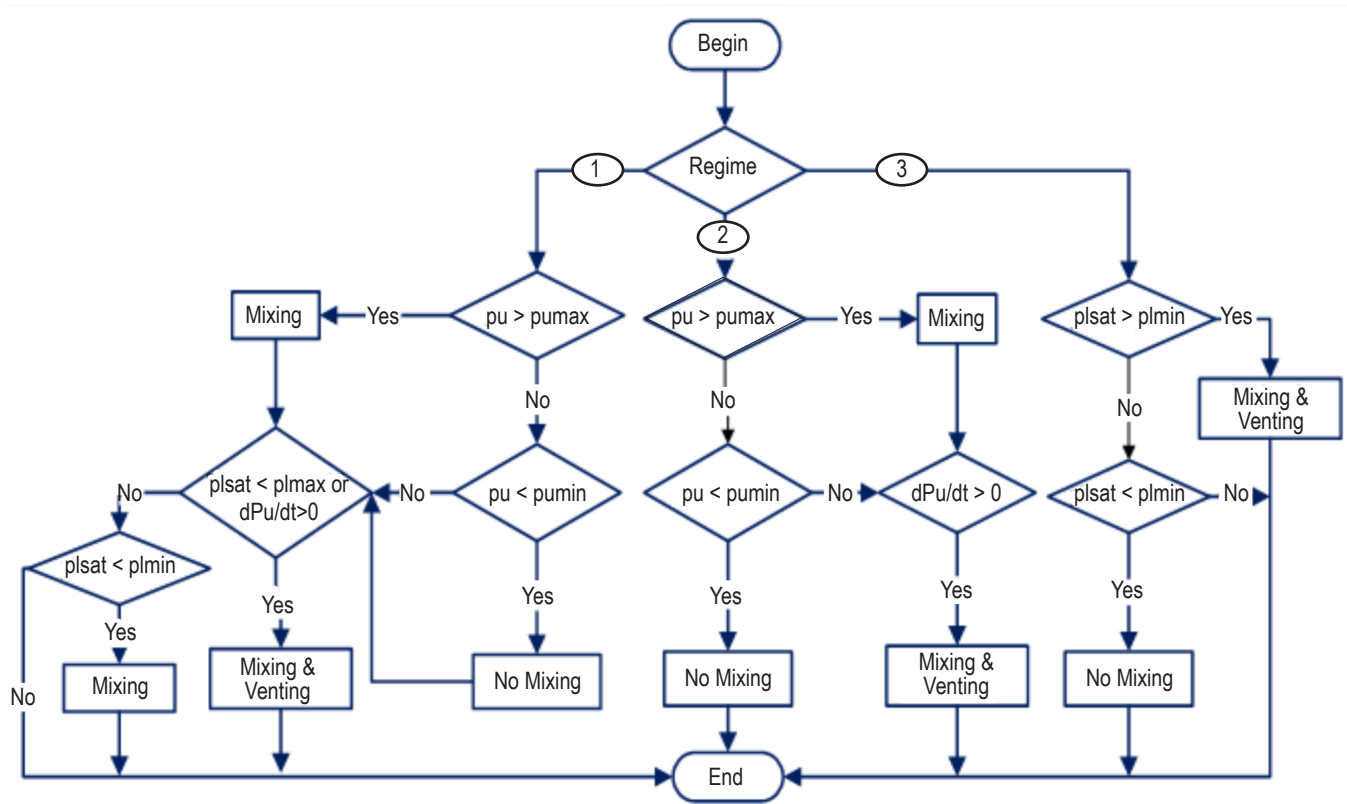


Figure 15. Thermodynamic venting system pressure control logic.

6.2 Spray Bar Thermodynamic Venting System

Spray bar TVS is used for pressure control in long-term storage cryogenic tanks under different acceleration conditions. As depicted in figure 16, it includes a recirculation pump, a TVS venting valve, a liquid cooling device, a J-T valve, a spray manifold, a heat exchanger, an injection tube manifold, injection tubes, and an external venting line with a backpressure device (orifice or critical Venturi).

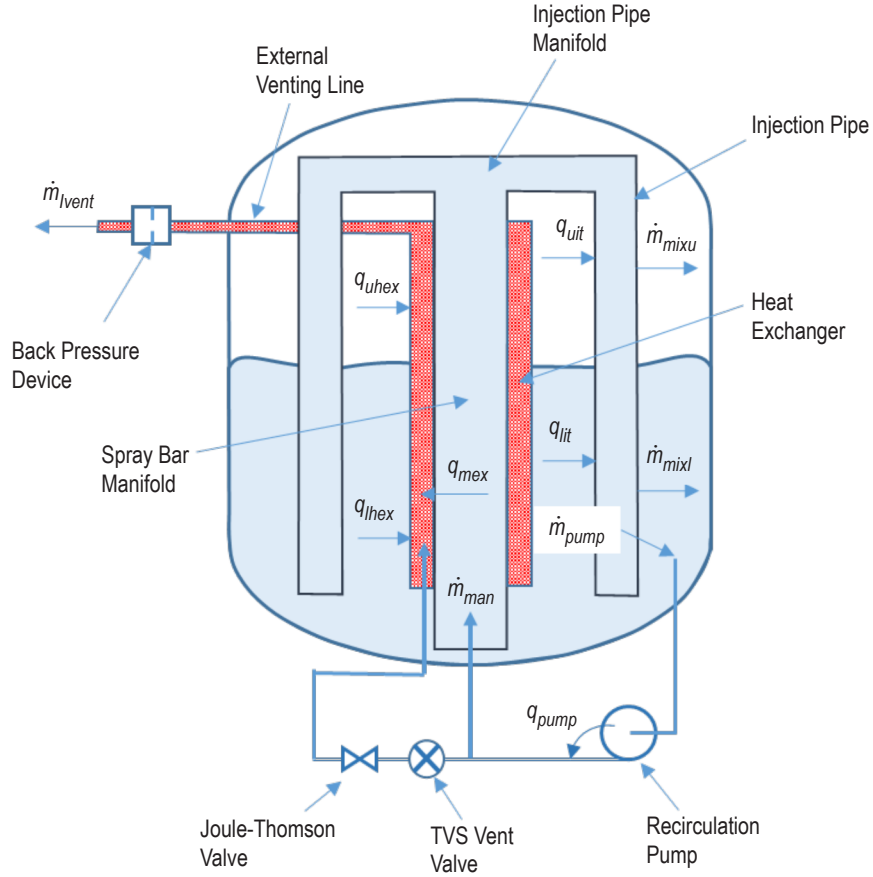


Figure 16. Spray bar TVS schematic.

6.2.1 Heat Exchanger Pressure Loss

The heat exchanger pressure loss model is based on the Lockhart-Martinelli¹⁹ two-phase flow correlations.

To calculate the total pressure change inside the heat exchanger, the momentum conservation equation is applied. In accordance with figure 17, with constant cross-sectional areas, this equation is:

$$\frac{dP}{dz} = -\left(\frac{dP}{dz}\right)_{fr} - \left(\frac{dP}{dz}\right)_g - \left(\frac{dP}{dz}\right)_{mom}, \quad (65)$$

where

$$\left(\frac{dP}{dz}\right)_g = [\alpha\rho_v + (1-\alpha)\rho_l]g \cos\omega \text{ is the gravitational hydrostatic pressure loss}$$

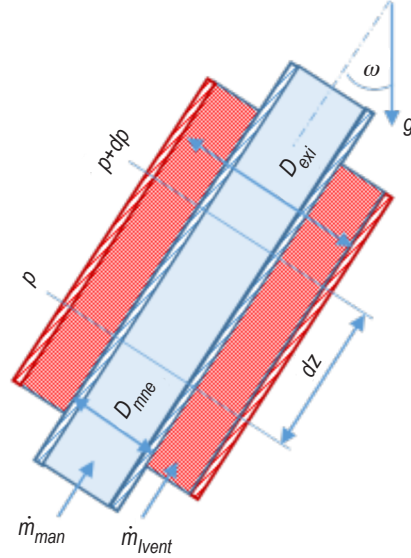


Figure 17. Spray bar heat exchanger pressure drop calculation schematic.

$$\left(\frac{dP}{dz}\right)_{mom} = \frac{d}{dz} \left\{ G^2 \left[\frac{X^2}{\rho_v \alpha} + \frac{(1-X)^2}{\rho_v (1-\alpha)} \right] \right\} \text{ is the momentum pressure loss,}$$

and

$$\left(\frac{dP}{dz}\right)_{fr} \text{ is the frictional pressure loss.}$$

In these equations,

G = two-phase mass flux through cross section of the heat exchanger, $\text{kg}/(\text{m}^2\text{s})$

X = vapor quality inside heat exchanger

$\alpha = A_v/A$ – void fraction – ratio of the gas flow cross-sectional area to the total cross-sectional area.

According to reference 19, void fraction is calculated by:

$$\alpha = \left[1 + 0.28 \left(\frac{\rho_v}{\rho_l} \right)^{0.36} \left(\frac{\mu_l}{\mu_v} \right)^{0.07} \left(\frac{1-X}{X} \right)^{0.64} \right]^{-1}. \quad (66)$$

Using Lockhart-Martinelli¹⁹ and Martinelli-Nelson²⁰ two-phase multiplier techniques, the friction pressure loss gradient can be written as:

$$\left(\frac{dP}{dz}\right)_{fr} = \Phi_{lo}^2 \left(\frac{dP}{dz}\right)_{lo} \quad (67)$$

In these equations $(dP/dz)_{lo}$ is a pressure gradient that would result if the liquid flowed alone through the channel with the total mass flux, G .

Multiplier Φ_{lo} can be found from another multiplier Φ_l by equation (68):

$$\Phi_{lo}^2 = \Phi_l^2 (1 - X)^{1.75} \quad (68)$$

As defined by Lockhart and Martinelli¹⁹, multiplier Φ_l^2 is:

$$\Phi_l^2 = \left(1 + \frac{C}{X_{lm}} + \frac{1}{X_{lm}^2}\right), \quad (69)$$

where X_{lm} is a Lockhart-Martinelli parameter, modified for boiling flow inside the pipe²⁰:

$$X_{lm} = \left(\frac{\rho_v}{\rho_l}\right)^{0.571} \left(\frac{\mu_l}{\mu_v}\right)^{0.143} \left(\frac{1-X}{X}\right) \quad (70)$$

The value of constant C in equation (69) depends on the liquid and gas flow regimes, which can be found using Reynolds numbers for two-phase flow:

$$Re_l = \frac{G(1-X)D_{hex}}{\mu_l}, \quad Re_v = \frac{GX D_{hex}}{\mu_v} \quad (71)$$

The flow is laminar if liquid or gas $Re < 2,000$ and turbulent if $Re \geq 2,000$. Recommended values of the constant C are presented in table 1.

Table 1. Recommended values for constant C in Lockhart-Martinelli parameter.

Liquid	Gas	C
Turbulent	Turbulent	20
Laminar	Turbulent	12
Turbulent	Laminar	10
Laminar	Laminar	5

As suggested by Changhong et al.²¹, the constant C for narrow annuli depends on the annuli hydraulic diameter, and can be calculated as:

$$C^* = 21 \left(1 - e^{-0.319 D_{hex}} \right). \quad (72)$$

In equation (72), D_{hex} is an annuli hydraulic diameter and $D_{hex} = D_{exi} - D_{mne}$, where D_{exi} is the internal diameter of the heat exchanger external pipe and D_{mne} is the external diameter of the heat exchanger internal pipe or a spray bar manifold tube (see fig. 17).

With assumption that the two-phase flow in a heat exchanger is homogeneous, the pressure gradient $(dP/dz)_{lo}$ can be written as reported by Carey²²:

$$\left(\frac{dP}{dz} \right)_{lo} = \frac{2 f_{lo} G^2}{\rho_l D_{hex}}, \quad (73)$$

where $f_{lo} = 0.079 \left(\frac{GD_{hex}}{\mu_l} \right)^{-0.25}$.

For the one-phase flow (liquid or gas) inside the heat exchanger, the pressure loss is calculated by modification of equation (65) without the momentum term, which can be neglected for this kind of flow:

$$\frac{dP}{dz} = -f \frac{G^2}{2\rho D_{hex}} - \rho g \cos \omega, \quad (74)$$

where ρ is a density of liquid or gas, depending of what kind of fluid is flowing in the calculated segment, and f is a friction factor, which calculates by the Ghabari-Farshad-Rieke correlation²³:

$$f = \left\{ 1.52 \log_{10} \left[\left(\frac{\varepsilon/D_{hex}}{7.21} \right)^{1.042} + \left(\frac{2.731}{Re} \right)^{0.9152} \right] \right\}^{-2.169}, \quad (75)$$

where ε is the roughness of the internal surface of the spray manifold, m , and $Re = \frac{GD_{hex}}{\mu}$ is a Reynolds number, calculated using liquid or gas viscosity.

This equation is applicable for a wide range of Reynolds numbers and relative roughness. In addition, equations (74) and (75) are used for calculating pressure drop inside the spray bar manifold, but in that case, hydraulic diameter is replaced by the manifold diameter.

6.2.2 Heat Exchanger Heat Transfer

The heat exchanger is a critical element since its function is to ensure optimal heat transfer between the vented and recirculating fluids. The exchanger design must be capable of rejecting the

maximum environmental heat leak rate anticipated as well as simultaneously reducing the liquid bulk temperature within a reasonable timeframe.

The model of heat exchanger is a multinode finite difference model that simulates two-phase flow in a quasi-steady-state mode (see fig. 18). It is based on two-phase, fluid-forced convection and nucleate boiling heat transfer inside narrow annuli, surrounded by two concentric pipe as shown in figure 18.

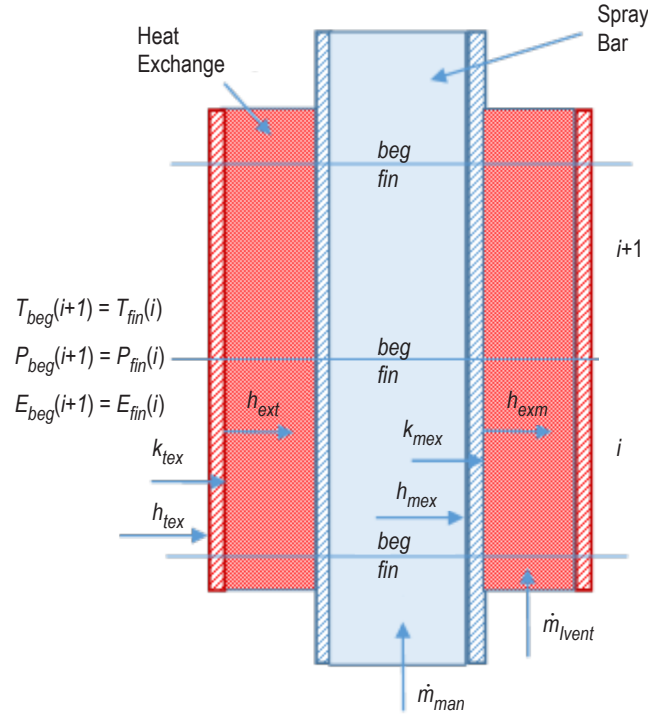


Figure 18. Spray bar heat exchanger transfer calculation schematic.

The total heat transfer coefficient from the spray manifold to the heat exchanger for each node is calculated by a standard procedure⁴:

$$h_{mext} = \frac{1}{\frac{1}{h_{mex}} + \frac{1}{h_{exm}} + \frac{\delta_{man}}{k_{mex}}}, \quad (76)$$

where h_{mex} is the forced convection heat transfer coefficient inside the spray manifold, $W/m^2 K$; it calculates by the Dittus-Boelter correlation⁴:

$$h_{mex} = 0.023 \frac{k_l}{D_{man}} Re_l^{0.8} Pr_l^{0.4}, \quad Re_l = \frac{\dot{m}_{man}}{D_{man} \mu_l}, \quad Pr_l = \frac{\mu_l C p_l}{k_l}, \quad (77)$$

where

- k_{mex} – thermal conductivity coefficient of the spray bar manifold pipe metal wall, W/m·K
- δ_{man} – manifold wall thickness, m
- D_{man} – spray bar manifold pipe internal diameter, m
- \dot{m}_{man} – spray bar manifold mass flow rate, kg/s
- h_{exm} – two-phase flow heat transfer coefficient inside the heat exchanger, W/(m²·K), calculated by the Chen correlation²⁴, $h_{exm} = h_{conv} + h_{boil}$.

In this equation, h_{conv} is a heat transfer coefficient for a forced convection calculated by the Dittus-Boelter equation and modified for two-phase flow inside a narrow annuli:

$$h_{conv} = 0.023 \frac{k_l}{D_{hex}} Re_{tp}^{0.8} Pr_l^{0.4}, \quad (78)$$

where

- Re_{tp} – Reynolds number modified for two-phase flow, $Re_{tp} = Re_l [F(X_{lm})]^{1.25}$
- X_{lm} – two-phase flow Martinelli-Nelson parameter, calculated by equation (70)
- Re_l – liquid Reynolds number for a heat exchanger two-phase flow, calculated by equation (71)
- h_{boil} – boiling contribution, calculated by the Forster-Zuber correlation corrected with a suppression factor $S(Re_{tp})$ ²²:

$$h_{boil} = 0.00122 S(Re_{tp}) \times \left[\frac{k_l^{0.79} C_{pl}^{0.45} \rho_l^{0.49}}{\sigma^{0.5} \mu_l^{0.29} h_{lv}^{0.24} \rho_v^{0.24}} \right] [T_w - T_{sat}(P_l)]^{0.24} [P_{sat}(T_w) - P_l]^{0.75}. \quad (79)$$

The suppression factor $S(Re_{tp})$ corrects the fully developed nucleate boiling prediction to account for the fact that, as the convection effect increases in strength, nucleation is more strongly suppressed. Both $F(X_{lm})$ and $S(Re_{tp})$ functions are calculated by Collier approximations²⁵ as:

$$F(X_{lm}) = \begin{cases} 1, & X_{lm}^{-1} \leq 0.1 \\ 2.35 \left(0.213 + \frac{1}{X_{lm}} \right), & X_{lm}^{-1} > 0.1 \end{cases} \quad (80)$$

and

$$S(Re_{tp}) = \frac{1}{1 + 2.56 \times 10^{-6} Re_{tp}^{1.17}}. \quad (81)$$

6.2.3 Spray Injection Tube Model

The spray injection tube is used for delivering the sprayed liquid to the ullage and bulk liquid. Its model is multinode, which assigns a node to each orifice (fig. 19).

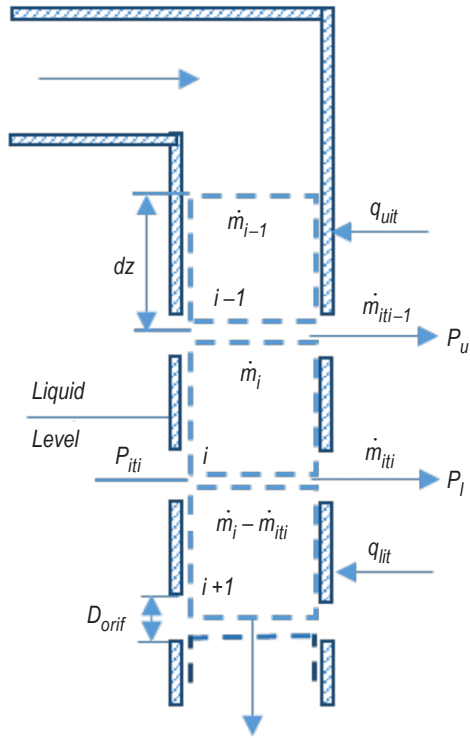


Figure 19. Spray injection tube schematic.

Pressure loss for each node calculates by the following equation:

$$\frac{dP}{dz} = -f \left(\frac{\dot{m}_{it}}{A_{it}} \right)^2 \frac{1}{2\rho_l D_{it}} + \rho_l g \cos \omega, \quad (82)$$

where

- f – friction factor, calculated by Ghabari-Farshad-Rieke correlation (eq. (75))
- \dot{m}_{it} – initial mass flow rate for each node, kg/s
- A_{it} – cross-sectional area of an injection tube, m²
- D_{it} – injection tube internal diameter, m.

In equation (82), the Reynolds number is $Re = \frac{\dot{m}_{it} D_{it}}{A_{it} \mu_l}$, with ω being the same angle as shown in figure 17.

The mass flow rate through orifices on each level is calculated by the following equation:

$$\dot{m}_{it_i} = A_{orif} \left[\frac{2\rho_{lit}(P_{it_i} - P_t)}{K_r} \right]^{1/2}, \quad (83)$$

where

A_{orif} – cross-sectional area of the orifice, m²
 ρ_{lit} – density of liquid in the injection tube, kg/m³
 P_{it_i} – pressure inside injection tube, Pa
 P_t – pressure outside the injection line (tank pressure), Pa
 K_r – resistance coefficient, which can be found in figure 20. This dependency was approximated using Idelchik's Handbook²⁶.

The above parameters are specific for different orifices.

The maximum value of the velocities ratio can be found as:

$$\frac{V_{it}}{V_{orif}} = \frac{\dot{m}_{it}}{\rho_{lit} A_{it}} \frac{\rho_{lit} A_{orif}}{\dot{m}_{orif}} = \frac{\dot{m}_{it}}{\dot{m}_{orif}} \frac{A_{orif}}{A_{it}}. \quad (84)$$

At the the first orifice, where the mass flow rate in the injection tube is the highest, it can be noted that $A_{it} = n_{orif} A_{orif}$. In other words, if there is no pressure loss in the injection pipe, $\dot{m}_{it} = n_{orif} \dot{m}_{orif}$. Equation (84) then becomes equal to unity.

For other than the first orifice level, the flow rate in the injection tube becomes lower because of liquid outflowing from the tube. In addition, if there is the pressure loss, the cross-sectional area of the tube should be higher to increase pressure inside the injection tube, so the velocities ratio will be less than the unity. In the multipurpose hydrogen test bed (MHTB), for example, the spray bar injection tube maximum velocities ratio is equal to 0.77. From figure 20, the resistance coefficient in this case is equal to 2.76.

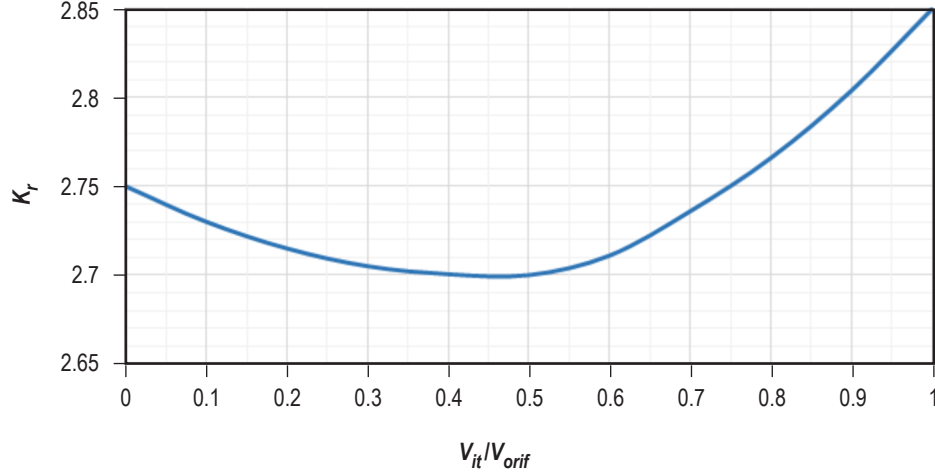


Figure 20. Resistance coefficient versus ratio of the injection tube to orifice velocities.

It is very important to note that, in TankSIM, all pressure loss calculations (heat exchanger, spray bar manifold, injection tube manifolds, injection tube, and so on) are made for straight wall segments of lines. Curved and other restriction segments have to be modeled independently in the form:

$$K_r = \left(\frac{\dot{m}_{line}}{A_{line}} \right)^2 \frac{1}{2\rho\Delta P_{line}}, \quad (85)$$

and then K_r is used in TankSIM for calculations as input.

6.2.4 Recirculation Pump

As depicted in figure 16, the recirculation pump is operated to circulate liquid in the TVS. Usually, several types of pumps are used for the TVS. They are different by their parameters and dependencies between used energy, pressure raised, and mass flow rate. To avoid modeling the particular pumps and to generalize calculations, in TankSIM, only flow rate—pressure rise and flow rate—energy functions are used in the form of fifth order equations:

$$\Delta P_{pump} = a_0 + a_1\dot{V} + a_2\dot{V}^2 + a_3\dot{V}^3 + a_4\dot{V}^4 + a_5\dot{V}^5 \quad (86)$$

and

$$W_{pump} = b_0 + b_1\dot{V} + b_2\dot{V}^2 + b_3\dot{V}^3 + b_4\dot{V}^4 + b_5\dot{V}^5, \quad (87)$$

where

ΔP_{pump} = pressure rise inside pump, kPa

W_{pump} = energy used by pump, W

\dot{V} = volumetric flow rate through the pump, m³/s.

Coefficients a_0 – a_5 and b_0 – b_5 are input numbers, which should be found before using TankSIM.

6.2.5 Joule-Thomson Cooling Device

A J-T device is used to cool a small quantity of bulk liquid, which is then used for conditioning propellant tanks during the long-duration missions. The modified Lee equation is used for a J-T modeling. This equation is applied especially for the Visco Jet—multiple orifice devices, for which the standard equation for a single orifice cannot be used, and is then modified by Pappel²⁷ for two-phase cryogenic fluids. For the metric system, the equation is:

$$\dot{m} = K_f \frac{4.6736 \times 10^{-4}}{Lohm} \sqrt{\rho \Delta P} (1 - X_{out}), \quad (88)$$

where

\dot{m}	– mass flow rate through the J-T device, kg/s
K_f	– coefficient, depended of the fluid: for hydrogen, is equal to 0.9, for methane and nitrogen, 1 (refs. 27–29)
$Lohm$	– hydraulic resistance of the J-T devices, given by a vendor ³⁰
$\rho = X_{in} \rho_v + (1 - X_{in}) \rho_l$	– inlet two-phase fluid density, kg/m ³
X_{in}	– an inlet two-phase fluid quality
ΔP	– pressure drop across the J-T device, Pa
$X_{out} = (h_{tot} - h_l) / (h_v - h_l)$	– outlet two-phase fluid quality; this value is calculated assuming isenthalpic fluid expansion through the J-T device
h_{tot}	– total enthalpy at J-T inlet temperature and pressure, J/kg
h_l and h_v	– enthalpies of the liquid and vapor, respectively; they are calculated at the outlet temperature and pressure, J/kg.

6.3 Ullage Droplets Heat and Mass Transfer

Droplets of a subcooled liquid appear in ullage during the spray bar mixing or TVS working. To calculate the heat and mass transfer to ullage droplets from the ullage and ullage wall, the follow assumptions were made:

- All droplets created by the equivalent orifices have the same size and velocity.
- Horizontal velocity of droplet does not change during its motion in the ullage.

The process of ullage droplets heat and mass transfer includes several stages:

- Jet atomization creates droplets that move towards tank walls.
- Moving droplets warm up to saturation conditions.
- Droplets boiling in the ullage.
- Droplets not boiled off in the ullage impinge ullage wall.
- Droplets warm up to saturation conditions on the wall (if not warmed up in ullage).
- Droplets boiling on the wall and adding mass to the ullage.

- Droplets not boiled off on the wall rebounding back to the ullage or adding to the wall liquid film.
- All droplets remained in the ullage, rebounded from the wall to the ullage, fall down to the liquid, or continue to interact with the ullage.

6.3.1 Generation of Droplets and Motion Parameters

The velocity of the droplet generated by an orifice can be calculated by the following equation:

$$v_{dr} = \frac{\dot{m}_{orif}}{\rho_l c_{orif} A_{orif}}, \quad (89)$$

where c_{orif} is the discharge coefficient of an orifice and \dot{m}_{orif} is the mass flow rate through the orifice, calculated by equation (83).

The droplet diameter can be found using the Lyshevskiy³¹ correlation for atomization of a liquid jet moving through gas:

$$D_{dr} = 3.01 d_{orif} \left(\frac{\rho_u We}{\rho_l} \right)^{-0.266} M^{0.0733}, \quad (90)$$

where $We = \frac{\rho_l d_{orif} v_{dr}^2}{\sigma_l}$ and $M = \frac{\mu_l^2}{\rho_l \sigma_l d_{orif}}$.

The number of droplets created by each orifice per second can be calculated as:

$$\dot{n}_{orif} = \frac{\dot{m}_{orif}}{\rho_l} \frac{6}{\pi D_{dr}^3}. \quad (91)$$

In equations (89) through (91), subscript 'l' refers to the liquid at the injection tube temperature and pressure.

During traveling in ullage, droplets can reach the wall or fall down to the liquid depending on acceleration conditions, initial droplet velocity, and distance from the injection tube to the tank wall as shown in figure 21.

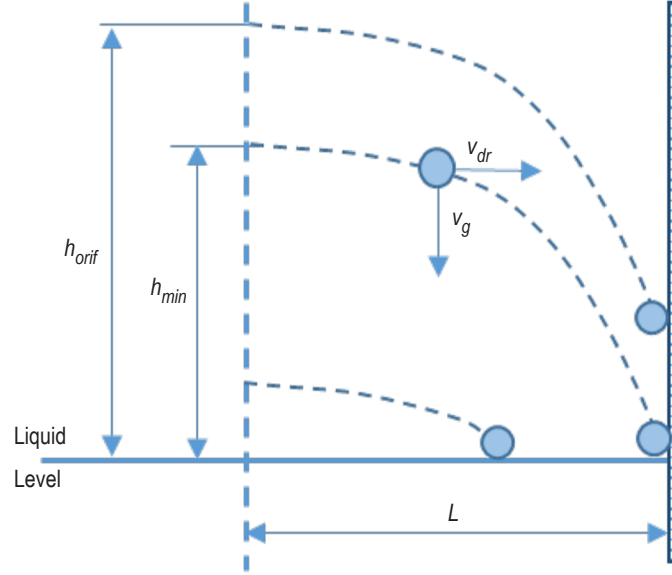


Figure 21. Droplet motion in the ullage.

The shortest time, at which droplets begin to reach the wall, is $t_{min} = L/v_{dr}$. The lowest height of the orifice corresponds to this time and can be found as:

$$h_{min} = \frac{g}{2} \left(\frac{L}{v_{dr}} \right)^2, \quad (92)$$

where L is a distance between injection tube and tank wall.

For calculating the droplets to ullage heat transfer, average velocities of droplets reaching and/or not reaching the wall need to be calculated as follows:

$$\bar{v}_{dr} = \left[v_{dr}^2 + \frac{g}{2} h_{orif} \right]^{1/2}, \quad \text{for droplets reaching the wall} \quad (93a)$$

and

$$\bar{v}_{dr} = \left[v_{dr}^2 + \left(\frac{g}{2} \frac{L}{v_{dr}} \right)^2 \right]^{1/2}, \quad \text{for droplets not reaching the wall.} \quad (93b)$$

6.3.2 Ullage Droplets Heat Transfer

The mass conservation equation for the ullage droplets according to figure 5 can be written as:

$$\frac{dM_{dr}}{dt} = \sum_i \dot{m}_i = \dot{m}_{mixu} + \dot{m}_{ucndr} - \dot{m}_{drboil} - \dot{m}_{drl} - \dot{m}_{drwl}. \quad (94)$$

Per figures 5 and 6, the energy conservation equation for ullage droplets is:

$$M_{dr} \frac{d(\bar{e}_{dr})}{dt} = q_{udr} + \dot{m}_{ucndr} h_{ul} + \dot{m}_{mixu} h_{mix} - \dot{m}_{drboil} h_{drl} - \dot{m}_{drl} h_{drl} - \dot{m}_{drwl} h_{drl} - \bar{e}_{dr} \sum_i \dot{m}_i - P_{dr} \frac{dV_{dr}}{dt}. \quad (95)$$

The heat transfer coefficient from ullage to a moving droplet can be calculated by Ranz and Marshall correlation³² for falling droplets:

$$h_{dr} = \frac{k_l}{D_{dr}} \left[2 + 0.6(Re_{dru})^{1/2} Pr_{dr}^{1/3} \right], \quad (96)$$

where

$$Re_{dru} = \frac{\rho_u D_{dr} \bar{v}_{dr}}{\mu_u} \quad \text{-- Reynolds number, calculated for droplet moving in ullage}$$

$$Pr_{dr} = \frac{\mu_l C_{pl}}{k_l} \quad \text{-- Prandtl number for droplet liquid.}$$

During the convective transfer stage, which occurs exactly after droplet creation and before droplet begins boiling, the heat flow rate can be calculated as:

$$q_{conv} = A_{dr} h_{dr} (T_u - T_{dr}). \quad (97)$$

On the boiling stage, the heat flow rate is:

$$q_{boil} = A_{dr} h_{dr} (T_u - T_{lsat}), \quad (98)$$

where T_{lsat} is the saturation temperature of the droplet liquid, calculated using ullage pressure.

6.3.3 Impinging Droplets—Wall Heat Transfer

For the heat transfer of droplets impinging on the wall, the Pasandideh-Fard et al.³³ model is used (see fig. 22). In this model, the diameter of impinging droplet and heat transfer coefficient can be found.

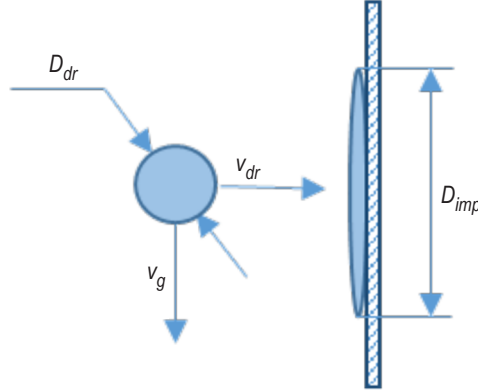


Figure 22. Droplet impingement model schematic.

The heat transfer coefficient of an impinging droplet is calculated by the following equation:

$$h_{imp} = \frac{k_l}{2D_{dr}} Re_{dr}^{1/2} Pr_{dr}^{0.4}, \quad (99)$$

where $Re_{dr} = \frac{\rho_l v_{dr} D_{dr}}{\mu_l}$ is the droplet Reynolds number with a velocity, normal to the wall.

The maximum diameter of an impinging droplet can be calculated as:

$$D_{imp} = D_{dr} \left[\frac{We_{dr} + 12}{3(1 - \cos\Theta) + 4(We_{dr}/Re_{dr}^{1/2})} \right]^{1/2}, \quad (100)$$

where Θ is the wetting angle, which is close to zero for cryogenic liquids. In that case, equation (100) will transform to:

$$D_{imp} = \frac{D_{dr}}{2} Re_{dr}^{1/4} \left(1 + \frac{12}{We_{dr}} \right)^{1/2}, \quad (101)$$

where $We_{dr} = \frac{\rho_l v_{dr}^2 D_{dr}}{\sigma_l}$ is a droplet Weber number with a velocity, normal to the wall.

Having a heat transfer coefficient and diameter of an impinging droplet, the heat flow rate for one droplet can be calculated as:

$$q_{imp} = \frac{\pi D_{imp}^2}{4} h_{imp} (T_{uw} - T_{dr}). \quad (102)$$

The total heat transfer from a hot surface to an impinging droplet during the time droplet spreading to its maximum diameter (D_{imp} in fig. 22) can be found by:

$$Q_{tot} = q_{imp} t_s, \quad (103)$$

where $t_s = 8D_{dr}/3v_{dr}$.

After impinging, there are two scenarios for the droplets' behavior—depositing on the surface or rebounding from it. According to Castanet³⁴, to distinguish between liquid rebounding from the solid surface and depositing on it, the so-called reference temperature, T^* , can be used:

$$T^* = \frac{T_w - T_{sat}}{T_{lf} - T_{sat}}, \quad (104)$$

where T_{lf} is a Leidenfrost temperature for impinging liquid.

If $0 < T^* < 1$ (which implies wall temperature is lower than Leidenfrost), liquid deposits on the wall. In this case, the contact temperature is used for heat transfer calculations:

$$T_{wf} = \frac{\varepsilon_w T_w + \varepsilon_l T_l}{\varepsilon_w + \varepsilon_l}, \quad (105)$$

where $\varepsilon_l = \sqrt{k_l \rho_l C_{pl}}$ and $\varepsilon_w = \sqrt{k_w \rho_w C_{pw}}$.

When the reference temperature is higher than unity, after interacting with the wall and warming up (or boiling), the liquid droplet reflects back to the ullage.

As it was found by Baumeister and Simon³⁵, the Leidenfrost temperature for cryogenic liquids, with good accuracy can be approximated as:

$$T_{lf} = 0.84375 T_{crit}, \quad (106)$$

where T_{crit} is a critical temperature of liquid.

6.3.4 Droplets Heat Transfer After Impinging in the Wall

As it was denoted earlier, after impacting into the wall, liquid remains on the wall and creates liquid film, or rebound to the ullage as depicted in figure 23.

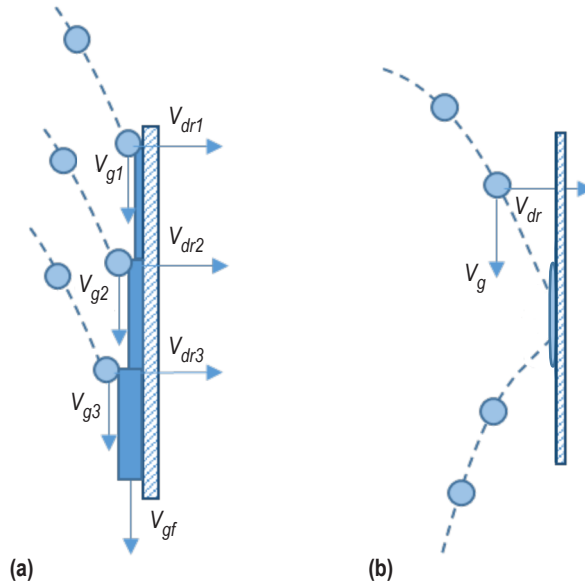


Figure 23. Droplet behavior after impingement: (a) Spreading and (b) rebounding.

6.3.4.1 Heat Transfer in the Liquid Film. After touching the wall and spreading on it, the sprayed droplets form a liquid film covering the wall, and during mixing, continually adds mass to it. For a description of the heat transfer in the liquid film, the model of Chun and Seban³⁵ was applied. By this model, heat transfer coefficients for the nonboiling liquid film are as follows:

$$h_{lam} = 0.821 \left(\frac{v_l^2}{gk_l^3} \right)^{-1/3} Re_f^{-0.22} \text{ for a laminar flow} \quad (107)$$

and

$$h_{turb} = 0.00381 \left(\frac{v_l^2}{gk_l^3} \right)^{-1/3} Re_f^{0.4} \left(\frac{v_l}{a_l} \right)^{0.65} \text{ for a turbulent flow,} \quad (108)$$

where v_l is a thermal diffusivity of the liquid in a film.

To specify a flow regime (laminar or turbulent), Chun and Seban suggested using film Weber number:

$$We^2 = \frac{\rho_l \delta u_l^2}{\sigma} = \frac{1}{16} \frac{\mu_l^2}{\rho_l \sigma \delta} Re_f^2. \quad (109)$$

If $We \leq 1$, there is a laminar film flow; otherwise, if $We > 1$, there is a turbulent flow. In equations (107) through (109),

$$Re_f = \frac{\rho_l \delta u_l}{\mu_l} = \frac{4\dot{M}}{\mu_l} \quad \text{– film Reynolds number}$$

$$\dot{M} = \frac{\rho^2 g \delta^3}{3\mu} \quad \text{– film mass flow rate per unit length of the wall, kg/m}\cdot\text{s}$$

$$\delta \quad \text{– film thickness, m.}$$

7. TANK AXIAL JET THERMODYNAMIC VENTING PRESSURE CONTROL SYSTEMS

7.1 Axial Jet Thermodynamic Venting System

Axial jet TVS is used for ullage pressure control and liquid destratification during long-term storage by mixing bulk liquid and condensation of vapor at the liquid-ullage interface. The axial jet system is compact, lightweight, and capable of being integrated with a compact heat exchanger. As shown in figure 24, it includes a recirculation pump, a TVS venting valve, a liquid cooling device, a J-T valve, a heat exchanger, a jet nozzle, and an external venting line with a back-pressure device (orifice or critical Venturi).

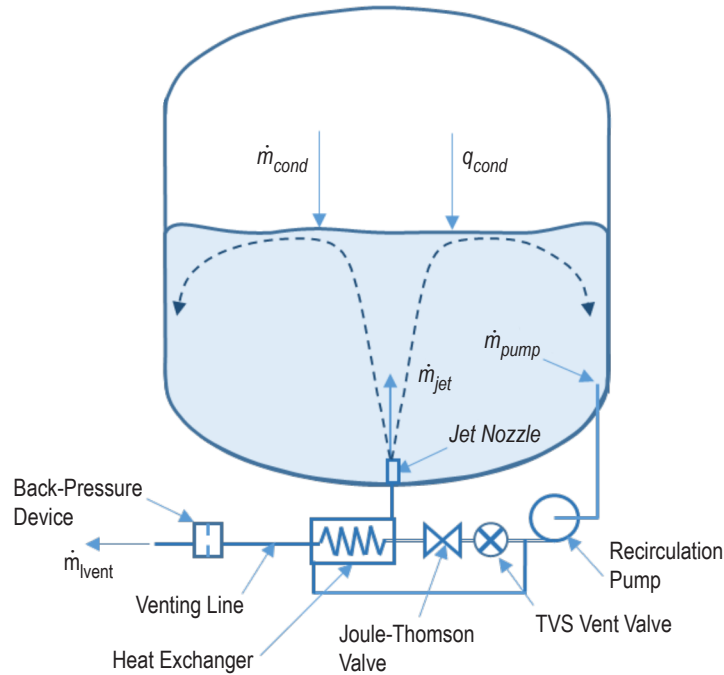


Figure 24. Axial jet TVS schematic.

7.2 Heat and Mass Transfer at the Ullage-Liquid Interface

There are two different cases of axial jet heat transfer models—high and low nozzle submergences, as depicted in figure 25. It can be shown analytically (see app. D.1) that these two cases can be divided as follows:

$$\frac{s}{D_{int}} \geq 2.458 \left(1 - \frac{d}{D_{int}} \right) \quad (\text{high nozzle submergence case}) \quad (110)$$

and

$$\frac{s}{D_{int}} < 2.458 \left(1 - \frac{d}{D_{int}} \right) \quad (\text{low nozzle submergence case}) \quad (111)$$

where d is a jet nozzle internal diameter.

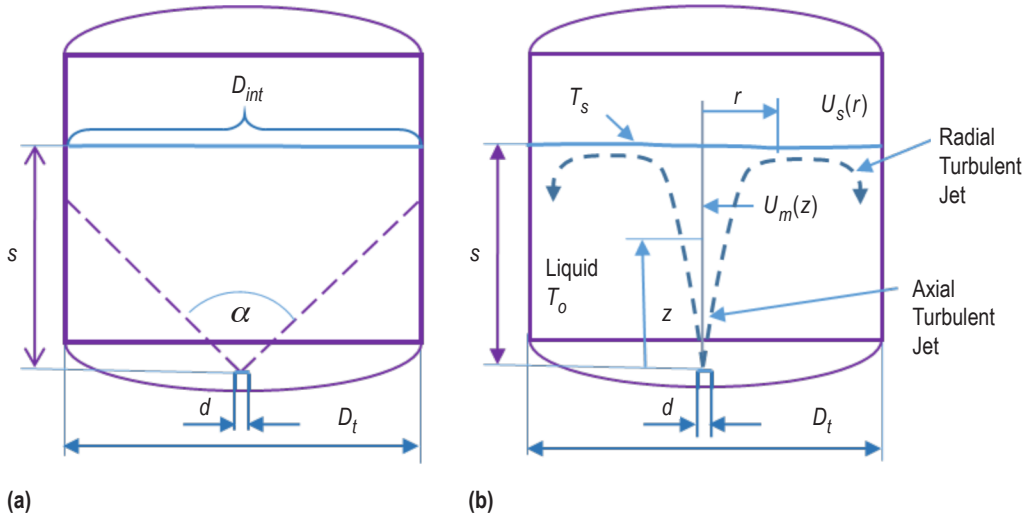


Figure 25. Axial jet TVS submergence cases schematic: (a) High submergence and (b) low submergence.

For high nozzle submergence, the jet fills the cylinder cross section before it reaches the interface region and the turbulence near the interface is uniform over the cross section (fig. 25(a)).

According to Carey²² and Sonin et al.³⁷, the average condensation mass flux from the ullage to the liquid at the interface can be calculated as:

$$\dot{m}_{avh} = \dot{M}_j \cdot 0.418 \exp \left(-1.2 \frac{s}{D_{int}} \right), \quad (112)$$

where \dot{m}_{avh} is the average mass flux at the interface at high nozzle submergence, $\text{kg/s} \cdot \text{m}^2$.

In the case of low nozzle submergence, the turbulent velocity field is quite different from the high submergence case, as illustrated in figure 25(b). Turbulent jet spreads from the nozzle, but remains confined to the axial region. The axial jet impinges on the free surface, and the bulk flow

associated with it turns radially outward and forms a radial jet just below the interface. The radial jet thickens and loses mean velocity (as well as turbulence intensity) as it moves outward, and is eventually deflected down into the bulk liquid at the wall, after which it mixes with the bulk liquid below. Mean flow in the bulk liquid outside the jet regions is low; however, some circulation and mixing does result from entrainment into the two jet regions and the return flow toward the outlet port. As shown by Thomas³⁸, the condensation mass flux for that case can be written as:

$$\dot{m}_{avl} = \dot{M}_j \times \left[0.26\beta_2 - (0.18\beta_2 - 0.077\beta_1) \frac{s}{D_{int}} \right], \quad (113)$$

where

\dot{m}_{avl} – average mass flux at the interface at low nozzle submergence, kg/s·m²
 β_1, β_2 – empirical coefficients which are $\beta_1 = 0.34$ and $\beta_2 = 0.24$ by the Brown³⁹ experiments and $\beta_1 = 0.33$ and $\beta_2 = 0.23$ by Lin and Hasan⁴⁰ numerical solution of the conservation equations for the k - ε turbulence model.

In equations (112) and (113),

$$\dot{M}_j = \frac{\rho_b c_{pb} \dot{m}_j \Delta T_0 (1 - Ja / 2)}{\rho_j h_{fg} d D_{int} Pr_b^{1/3}}, \quad (114)$$

where

\dot{m}_j – mass flow rate of the liquid flowing through the nozzle, kg/c
 ρ_j – density of the liquid flowing through the nozzle, kg/m³
 $Ja \equiv c_{pb} \Delta T / h_{fg}$ – a Jacob number, calculated by bulk liquid parameters
 $\Delta T = T_{sat} - T_{int}$ – ullage-liquid interface subcooling, K
 $\Delta T_0 = T_{sat} - T_0$ – a liquid subcooling at the nozzle outflow point, K.

Index “ b ” means that properties are calculated by bulk liquid temperature and pressure.

Average condensation heat transfer coefficient at the ullage-liquid interface can be calculated by:

$$h = \frac{\dot{m}_{av} h_{fg}}{\Delta T_0}. \quad (115)$$

From equations (112), (114), and (115) for high nozzle submergence, it can be written:

$$h_{avh} = H \times 0.418 \exp\left(-1.2 \frac{s}{D_{int}}\right). \quad (116)$$

For low nozzle submergence equations (113), (114), and (115),

$$h_{avl} = H \cdot \left[0.26\beta_2 - (0.18\beta_2 - 0.077\beta_1) \frac{s}{D_{int}} \right]. \quad (117)$$

In both equations (116) and (117), the coefficient H is:

$$H = \frac{\rho_b c_{pb} \dot{m}_j (1 - Ja / 2)}{\rho_j d D_{int} Pr_b^{1/3}}. \quad (118)$$

7.3 Helicoidally Coiled Tube-in-Shell Heat Exchanger Transfer

The model of heat and mass transfer in helicoidally coiled tube-in-shell heat exchanger based on two-phase forced convection and nucleate boiling inside the coiled tube, which in this case, is a venting line, and forced convection inside the annulus—created by internal spacer and external shell with the coiled tube inside it, as depicted in figure 26(b).

The total heat transfer coefficient from the shell side to the venting liquid inside the coiled tube calculates by a standard procedure⁴:

$$h_{mext} = \frac{1}{\frac{1}{h_{vpf}} + \frac{1}{h_{svp}} + \frac{\delta_{vp}}{k_{vp}}}, \quad (119)$$

where

- h_{vpf} – heat transfer coefficient from the venting pipe wall to the venting fluid, $W/m^2 \cdot K$
- h_{svp} – heat transfer coefficient from the shell side liquid to the venting pipe, $W/m^2 \cdot K$
- δ_{vp} – venting pipe wall thickness, m
- k_{vp} – thermal conductivity coefficient of the venting pipe metal wall, $W/m \cdot K$.

The heat transfer coefficient for inside the tube can be calculated by the Chen correlation²⁴ modified for a coiled tube:

$$h_{vpft} = \left(1 + 3.455 \frac{D_{hvp}}{D_c} \right) (h_{conv} + h_{boil}), \quad (120)$$

where

$$D_{hvp} = \frac{2Dd}{(D+d)[3-\sqrt{4-h}]} \quad \text{is an internal hydraulic diameter of coiled pipe, which usually}$$

has an elliptical shape with the major axis in the vertical direction (see app. D.3), and D_c is a coil diameter as shown in figure 26(a).

$$h = \left(\frac{D-d}{D+d} \right)^2, \text{ where } D \text{ and } d \text{ are the internal major and minor axes of the ellipse, respectively.}$$

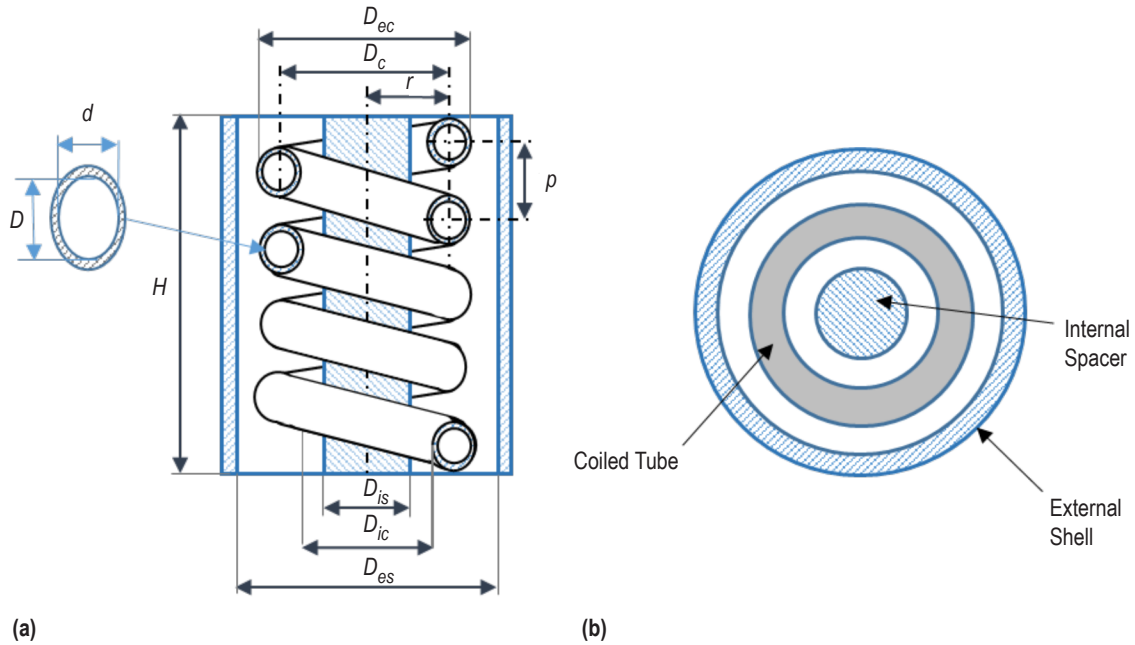


Figure 26. Helicoidally coiled tube-in-shell heat exchanger: (a) Exchanger measurements and (b) calculation schematic.

The convective heat transfer coefficient inside the coiled pipe is calculated by the Dittus-Boelter (see ref. 4) equation:

$$h_{conv} = 0.023 \frac{k}{D_{hvp}} Re^{0.8} Pr^{0.4}, \quad Re = \frac{4\dot{m}_{vent}}{\pi D_{hvp} \mu}, \quad Pr = \frac{\mu C_p}{k}. \quad (121)$$

For a single-phase flow, the Reynolds and Prandtl numbers are calculated using thermodynamic properties for a particular gas or liquid phase.

For the two-phase flow, the Reynolds number in equation (121) is replaced by:

$$Re_{tp} = Re_l [F(X_{lm})]^{1.25}, \quad Re_l = \frac{4\dot{m}_{vent}}{\pi D_{hvp} \mu_l} (1-X), \quad (122)$$

where X is vapor quality inside the coiled tube and $F(X_{lm})$ is the Reynolds number modification coefficient calculated by equation (81).

In this case, the Prandtl number is calculated using liquid thermodynamic properties. The boiling heat transfer coefficient is calculated by the Forster-Zuber equation (79) with the two-phase Reynolds number from equation (122) and the suppression factor from equation (80). The heat transfer coefficient from the liquid in the shell side to the venting pipe is calculated by the Dittus-Boelter correlation:

$$h_{svp} = 0.023 \frac{k_l}{D_{hs}} Re_l^{0.8} Pr_l^{0.4}, \quad Re_l = \frac{G_{shell} D_{hs}}{\mu_l}, \quad Pr_l = \frac{\mu_l C_{p_l}}{k_l}, \quad (123)$$

where

$$G_{shell} = \frac{4\dot{m}_{shell}}{\pi [D_{es}^2 - D_{is}^2 - 4D_c(d + 2\delta_{vp})]} \text{ is the mass flux in the shell side, kg/(m}^2\text{s)}$$

and

$$D_{hs} = 2 \frac{D_{is}^2 - D_{es}^2 - [Dd + 2\delta_{vp}(D + d)]\sqrt{1 + \gamma^{-2}}}{2(D_{is} + D_{es}) + (D + d + 4\delta_{vp})(3 - \sqrt{4 - h_s})\sqrt{1 + \gamma^{-2}}} \text{ is the hydraulic diameter of the shell side.}$$

Details of the G_{shell} and D_{hs} equations above are provided in appendix D.3.

7.4 Heat Transfer at Low Acceleration Conditions

At low accelerations, the heat transfer for the settled liquid can be modeled by the correlations described earlier with the special calculation of interface and dry wall areas. To do this, the Surface Evolver program⁴¹ can be used. In this program, the interface and dry wall areas as a function of Bond number, tank geometry, and liquid fill level are calculated. The liquid-ullage interface shapes calculated by Surface Evolver for hydrogen in the MHTB tank are presented in figure 27.

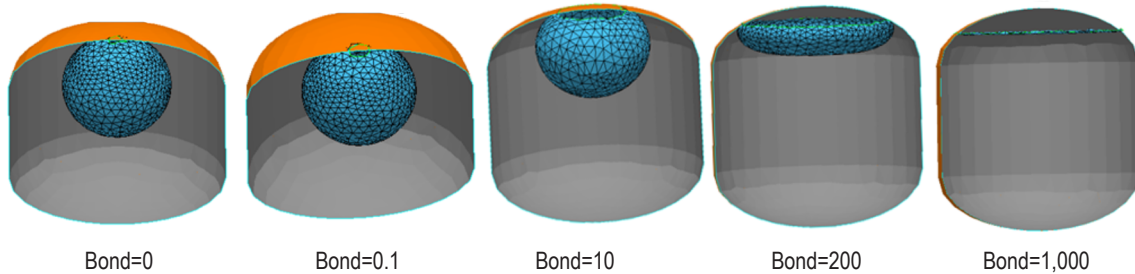


Figure 27. Liquid-ullage interface in MHTB tank with 90% fill level.

Interface and dry wall areas in dimensionless form (as a ratio of current value to the value at flat interface, or at high Bond numbers) are calculated with the Surface Evolver and can be approximated by the function:

$$A = a + b \frac{1 - \left(\frac{Bo}{Bo_3} \right)^m}{1 + k_a \left(\frac{Bo}{Bo_3} \right)^m}, \quad (124)$$

where coefficients a , b , and k_a are calculated from three points on the graph, and coefficient m can be found by the least squares method or graphically for best matching the Surface Evolver data (for details, see app. D.5). Figure 28 represents results of Surface Evolver calculations and their approximations.

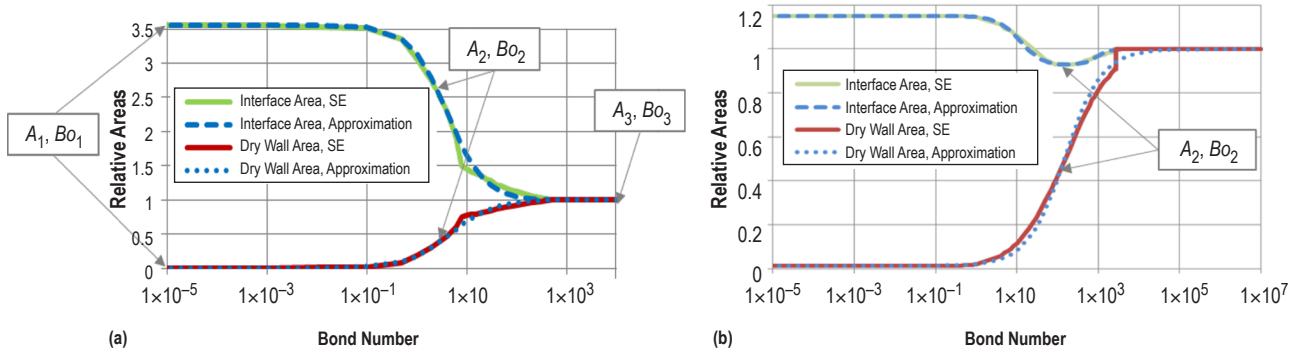


Figure 28. Interface and dry wall areas for hydrogen in MHTB tank: (a) 25% fill level and (b) 90% fill level.

It has to be noted that for different tank shapes and different fill levels, areas are different, so for each particular case it needs to find these functions using the Surface Evolver program.

7.4.1 Heat Transfer in Nonmixing Cases

For unsettled liquids during the nonmixing (self-pressurization) period for calculating heat transfer, the concentric spherical enclosure model is used. It includes an outer spherical tank shell and ullage sphere inside of it, divided by a liquid layer. The volume of the outer sphere is equal to the tank volume, the volume of the internal sphere is equal to the ullage volume, and the volume of the liquid layer is equal to the bulk liquid volume (fig. 3). Applying the Teertstra et al.⁴² method, the heat transfer to the ullage is calculated using $\sqrt{A_u}$ as a linear scale and conduction shape factor, S^* :

$$q_{mg} = k \sqrt{A_u} S^* (T_w - T_u). \quad (125)$$

In the case of ‘sphere in sphere,’ the shape factor is:

$$S^* = \left(\frac{4\pi}{3}\right)^{1/3} \frac{\sqrt{A_u}}{\left(V_{tot}^{1/3} - V_u^{1/3}\right)} + 2\sqrt{\pi} . \quad (126)$$

Heat flow rate from the tank wall to the ullage is:

$$q_{mg} = k_l \sqrt{A_u} (T_w - T_u) \left[\left(\frac{4\pi}{3}\right)^{1/3} \frac{\sqrt{A_u}}{\left(V_{tot}^{1/3} - V_u^{1/3}\right)} + 2\sqrt{\pi} \right] . \quad (127)$$

7.4.2 Heat Transfer During Mixing

To calculate heat transfer during mixing, a homogeneous fluid model was applied. In that model, all fluid inside the tank is assumed to be a homogeneous mixture of vapor, noncondensable gas (if any) and liquid. Thermodynamic and physical properties (density, viscosity, conduction coefficient, specific heat capacity, enthalpy, and other) are calculated as mass average values:

$$C_{mix} = \frac{C_{he}m_{he} + C_v m_v + C_l m_l}{m_{he} + m_v + m_l} . \quad (128)$$

8. COMPUTER MODEL DESCRIPTION

8.1 TankSIM Program Base

The code of the TankSIM program is based on FORTRAN 90 language and is released on the Intel Visual FORTRAN compiler for Windows, but it can be used at any platforms with minor adjustments just in external files operations.

The program is structured and consists of the main program and 75 subroutines. All subroutines can be divided into groups as follows:

- Service and error handling.
- Pressure and mission phases control.
- Initialization and input-output operations.
- Heat and mass transfer in the tank.
- Calculation by NIST procedures or tables interpolation to obtain fluids thermodynamic properties.
- Ullage venting and pressurization.
- Spray bar and axial jet TVS.
- Calculation of tank geometry.

8.2 Program Possibilities

The program TankSIM is created for predicting cryogenic tank temperatures and pressures under different external conditions. It is possible to use:

- Cylindrical tanks with different upper and lower domes geometries (flat, elliptical, and spherical) and different lengths of the cylindrical part.
- Different cryogenic fluids and incondensable pressurization gases.
- Different materials for a tank wall (properties of material are input parameters).
- Unbounded number of six mission phase combinations, which are:
 - Regular ('Slf')—self-pressurization with ullage venting, spray bar or axial jet pressure control systems.
 - Engine and feed system chilldown ('Chl').
 - Noncondensable gas ('Hep') prepressurization.
 - Autogenous ('Vap') prepressurization.
 - Engines firing ('Fir') with noncondensable gas or autogenous pressurization.
 - Vapor liquefaction ('Lqf').
- Different types of back-pressure devices—critical orifice or Venturi and pressure regulation.
- Three different types of pressure control logic.

8.3 Program Error Handling

Program error handling and control system includes two subroutines and more than 75 code segments. There are two types of code segments—custom error handling and these, which use the RefProp error procedures. When an error happens, the program pauses and an error message appears on the interactive screen. This message includes the name of a code block (main program or subroutine), serial number of error handling segment, time that the error happened (calculation time, not a system time), and error description. In addition, it includes four possibilities to continue calculations: just continue; continue without option message (error is printed on the screen, but program does not pause); continue without error message (does not print any messages); and stop (stop the program and error message is printed in the output file).

User needs to choose and input one option. Figure 29 is an example of an error message that appears on the screen.

```
Droplets_Transfer() 50, Time = 3.886600E+04 sec:
Time step (delt) > Droplet free moving time (tfall)

What Next?
   0 - Just Continue
   1 - Continue Without Printing Options Message
   2 - Continue Without Printing Error Message
   3 - Stop

Print option number below, then press "Enter"
_
```

Figure 29. Error message example.

It should be noted that the option chosen by the user (excluding ‘Stop’) will be applied only to a particular serial number. Each first appearance of the error handling segment will give the full set of options. See figure 30 for a typical custom error handling code segment.

```
!=====
  If (delt > tfall) Then                                     !
    subname = subname1                                     !
    reason = 'Time step (delt) > Droplet free moving time (tfall)!' !
    ier = 50                                              !
    Call Error_Action()                                   !
  End If                                                  !
!=====
```

Figure 30. Custom error handling code segment.

In this code segment, *subname* is the code block name (main program or subroutine), *reason* is a custom error description, *ier* is a unique serial number of the error handling code segment, and *Error_Action* is an error handling subroutine.

The typical error handling segment for the standard procedure is different from the custom sequence. In figure 31, *ierr* is a RefProp error number and *herr* is a RefProp error description.

```
!eeeeeeeeeeeeeeeeeeeeeeeeeeeeeeeeeeee
  If (ierr /= 0) Then !
    subname = subname1 !
    reason = Trim(herr)!
    ier = 42           !
    Call Error_Action()!
  End If              !
!eeeeeeeeeeeeeeeeeeeeeeeeeeeeeeeeeeee
```

Figure 31. Standard error handling code segment.

8.4 TankSIM Functionality

8.4.1 Program Flowcharts

Figures 32–34 represent working flowcharts for the regular mission phase, which include the self-pressurization and pressure control system for the cost time period, initialization subroutine, and heat exchanger transfer subroutine for the spray bar TVS system, respectively.

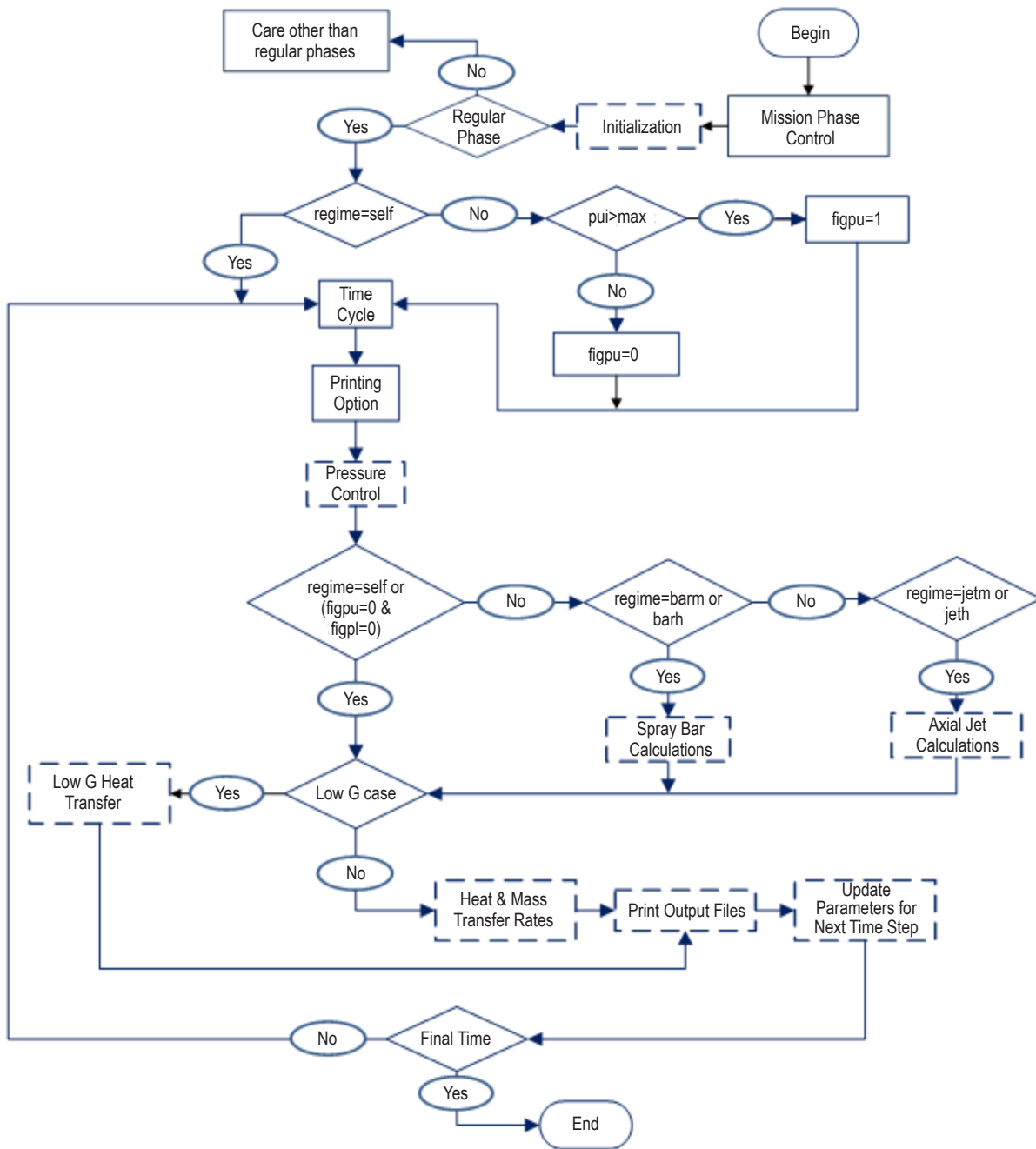


Figure 32. Program flowchart for regular mission phase.

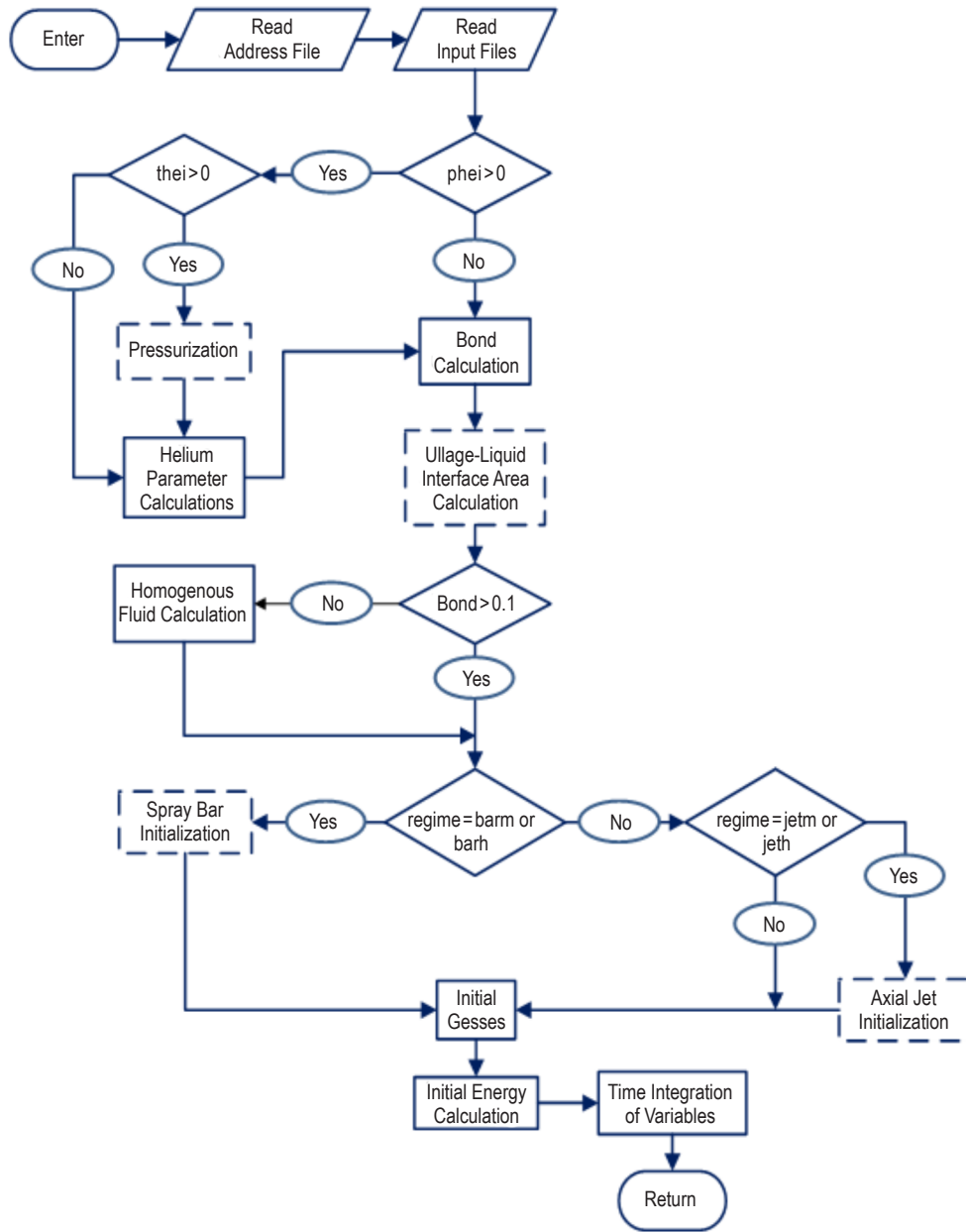


Figure 33. Initialization subroutine flowchart.

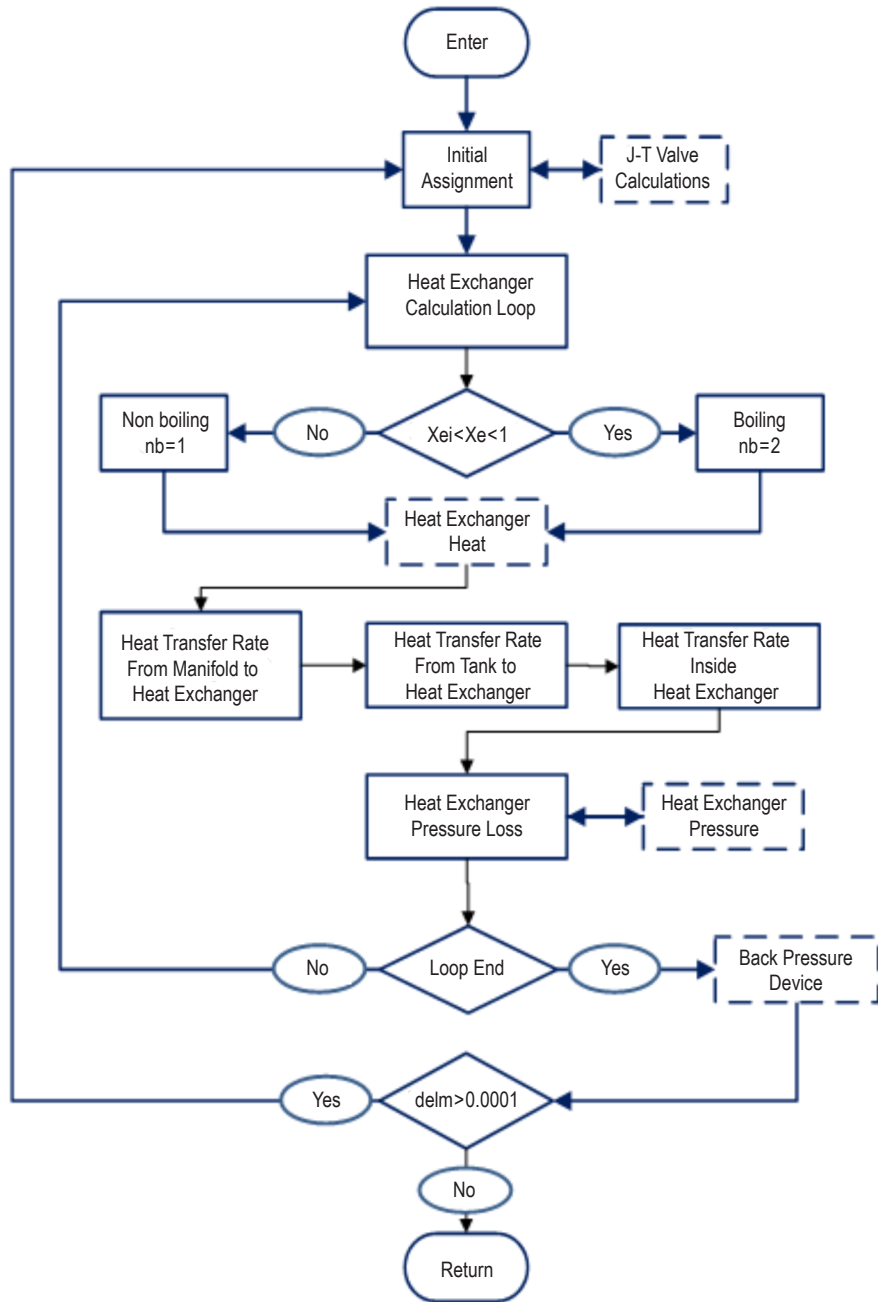


Figure 34. Heat exchanger transfer subroutine flowchart.

8.4.2 File System

The TankSIM file system includes program files, input files, service files, and several output files. The file structure and file names are hardcoded, excluding output files where names include date, time of creation, and short description of the case. The overall structure of the TankSIM file system is represented in figure 35. ‘TankSIM Main Folder’ can have any name and address, because all internal folders have relative addresses.

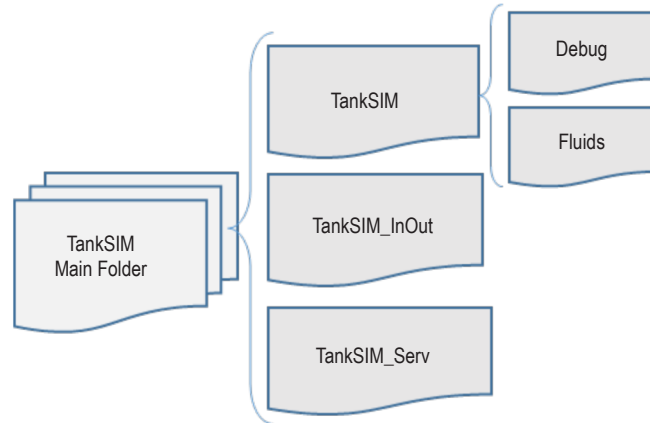


Figure 35. TankSIM file structure.

Folder ‘TankSIM’ contains the program source file, TankSIM FORTRAN project file, and several files for RefProp subroutines. In addition, the folder includes an address input file and two folders: ‘Debug,’ which is a compiler service folder (contains executable TankSIM file), and ‘Fluids,’ which contains the RefProp fluids description.

Folder ‘TankSIM_InOut’ contains working fluid and noncondensable gas property files, initial conditions input file, tank, spray bar, or axial jet measurements and properties, and mission profile input files. It also can include three optional files with external venting, filling, and pressurization line measurements, and properties for additional heat leak calculations. All input files are written in ‘text’ format.

Program output files are also included in the ‘TankSIM_InOut’ folder. The main output file, which includes input and calculated information in table form, is made in ‘comma separated values’ (CSV) format. That format allows an easy conversion to an Excel file to use all its possibilities for data analysis. If needed, the user can print several additional output files with more detailed information in ‘text’ format. Folder ‘TankSIM_Serv’ is used to write and read intermediate information during working with input files. All service files are automatically deleted after using and the folder remains empty, although it should still be there.

There is the possibility to use TankSIM executable file. In this case, the structure is the same as in figure 35, but the folder 'TankSIM' contains only a 'Fluids' subfolder and two files, executable and address.

A detailed description is provided in appendix E.

9. PROGRAM VALIDATION AND MULTIPHASE MISSION EXAMPLE

The main objective of this validation effort is to verify the TankSIM code using MHTB hydrogen tests and compare program prediction and test data and to demonstrate the program ability for modeling multiphase flight missions.

9.1 Multipurpose Hydrogen Test Bed Data Validation

In this section, TankSIM predictions are compared to MHTB test data. Validation was made for three different tank fill levels, 25%, 50%, and 90%. For calculations and analysis, two types of external heat leaks were used—heat leak estimated from boiloff tests and different heat leaks for self-pressurization and TVS operation, which were found for the best matching test data.

9.1.1 Hydrogen 25% Fill Level Test, File p263968kl, 1996

Results of calculations with constant values for heat leaks and test data for 25% fill level are presented in figures 36–40.

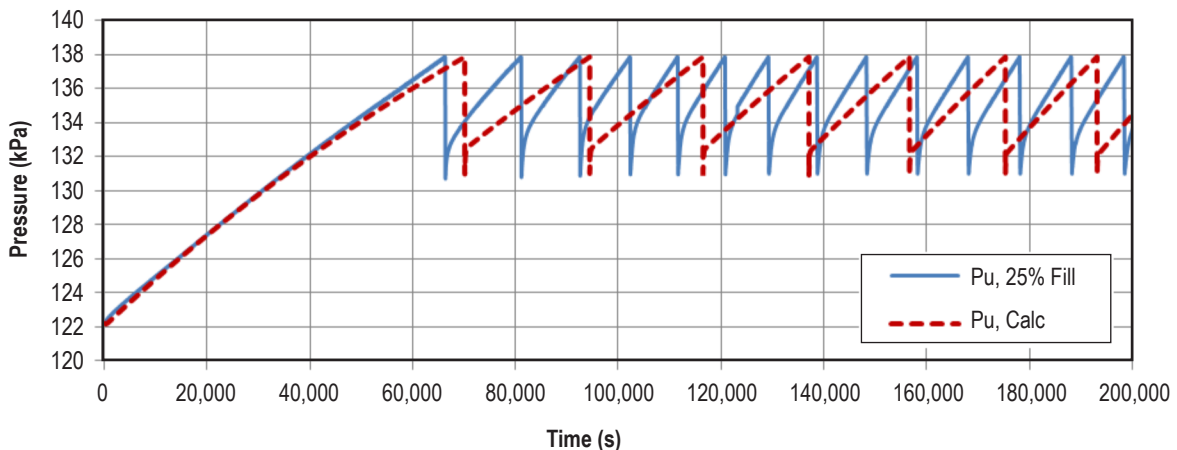


Figure 36. Ullage pressure, 25% fill level.

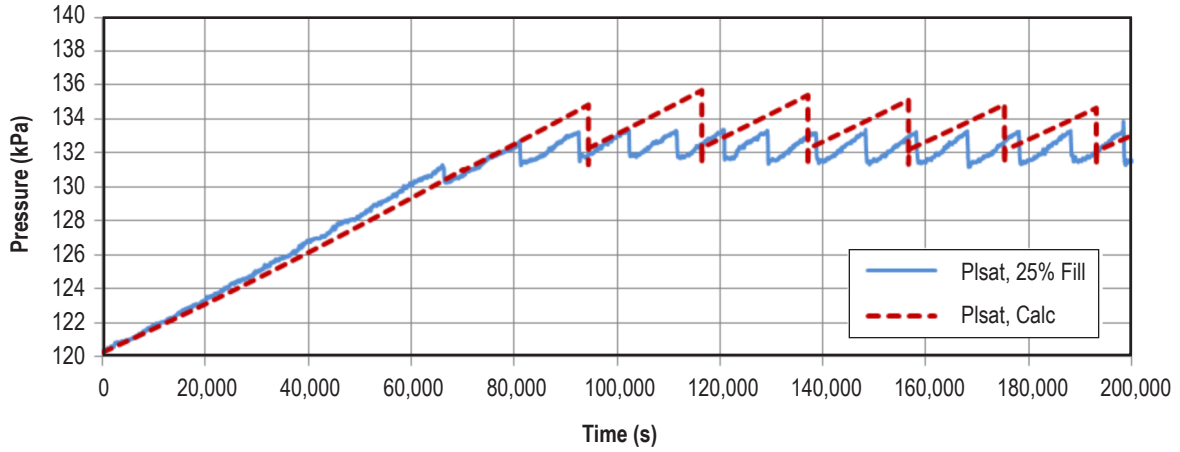


Figure 37. Liquid saturation pressure, 25% fill level.

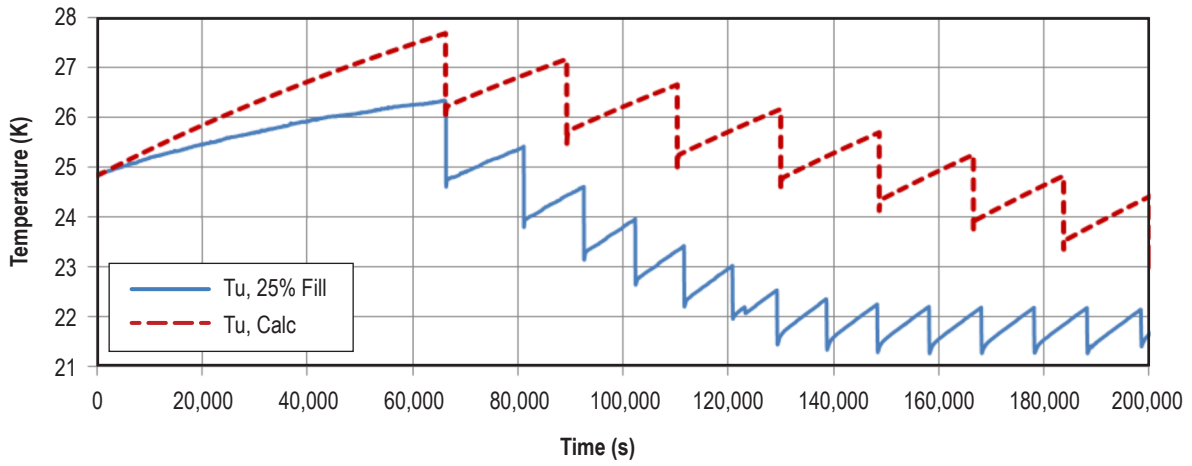


Figure 38. Ullage temperature, 25% fill level.

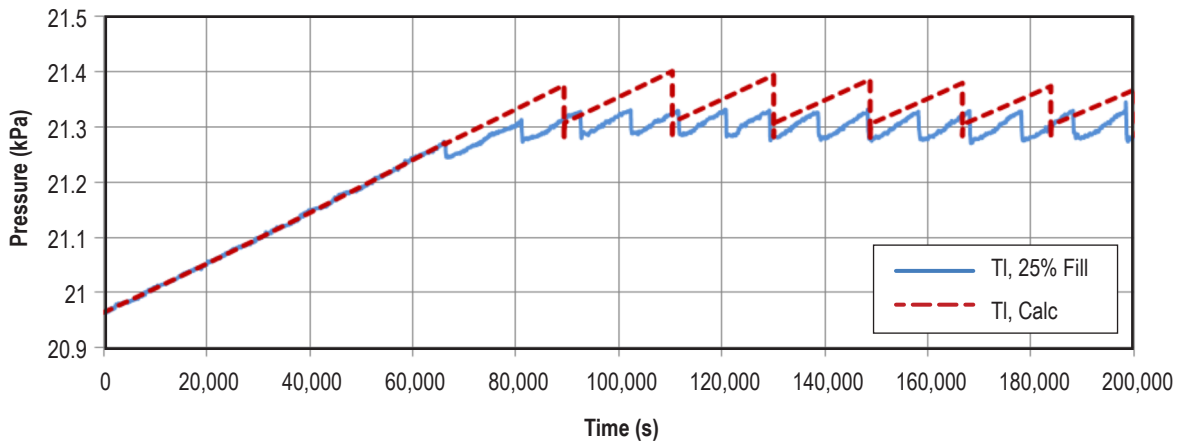


Figure 39. Liquid temperature, 25% fill level.

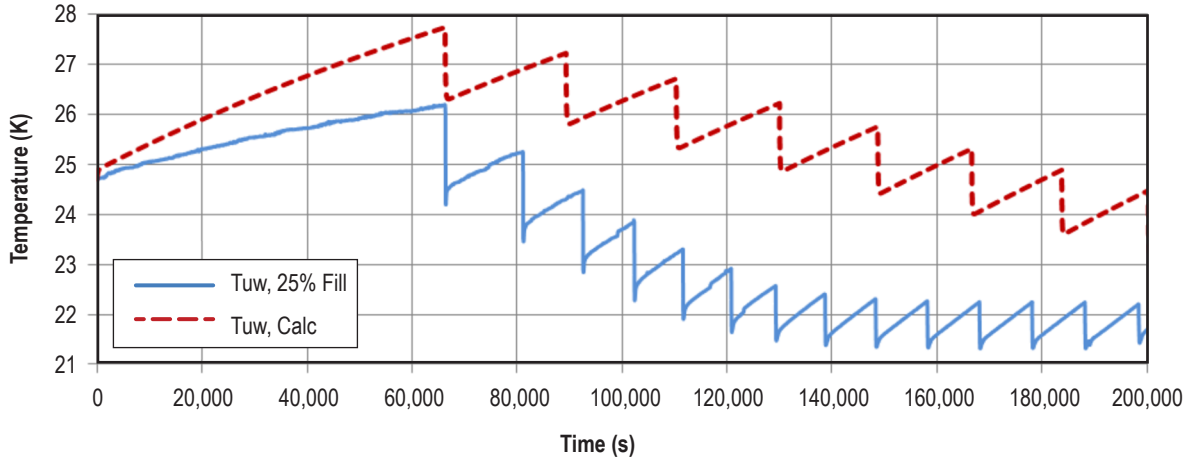


Figure 40. Ullage wall temperature, 25% fill level.

Comparison of predicted ullage pressure and liquid saturation pressure with test data are shown in figures 36 and 37. The ullage and liquid saturation pressure rising rates predicted by TankSIM during the tank lockup are in a good agreement with that of measured data. The ullage pressure and liquid saturation pressure drop rates during TVS operation also are in good agreement with those of the test data. However, ullage pressure predicted by TankSIM is slower than test data during the TVS operation. The number of cycles predicted by TankSIM and that of the test data are 11.5 and 18, respectively. The average cycling duration for prediction and test data are 23,050 and 14,821 s, respectively. The predicted liquid saturation pressure range and that of test data are 120.2 to 135.8 kPa and 120.2 to 134 kPa, respectively.

Figures 38 and 39 show a comparison of present predicted ullage and liquid temperatures with that of measured data. The predicted ullage temperature is within the 23.3 to 27.7 K range, while measured values are within the 21.3 to 26.2 K range. Predicted liquid temperature is in good agreement with that of the test data during the self-pressurization regime but the agreement is slightly different during the TVS operation. Predicted liquid temperature changes are within the 21 to 21.4 K range, while the measured values are within the 21 to 21.35 K range. From figure 40, it can be seen that the ullage predicted wall and test data temperatures are in very close agreement.

Figures 41 to 45 show calculating results with the best matching heat leaks, which are 10 W (ullage) and 10.1 W (liquid) for initial self-pressurization and 14.5 W (ullage) and 15 W (liquid) during the TVS operation period. By comparing predicted values with the test data one can conclude good agreement with the test data during the TVS operation.

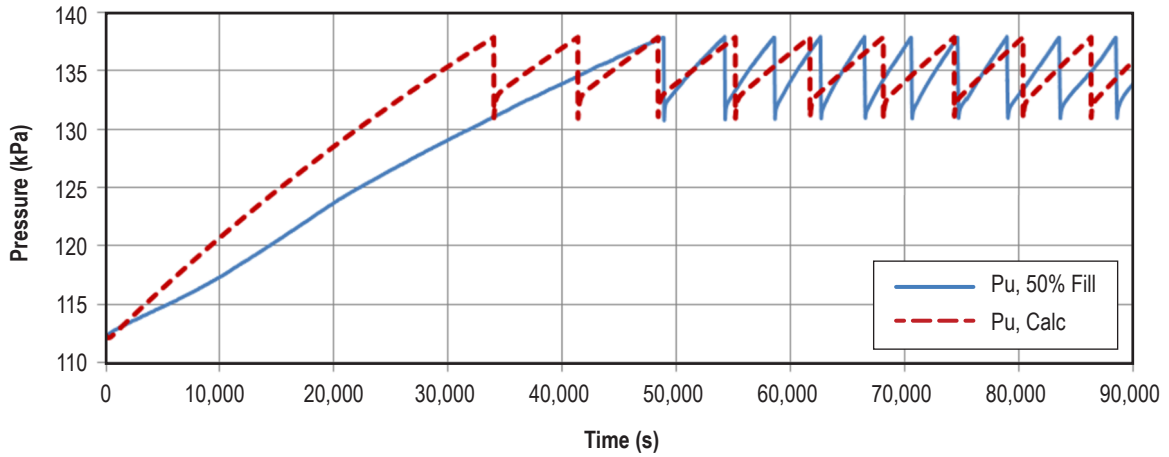


Figure 41. Ullage pressure, 50% fill level.

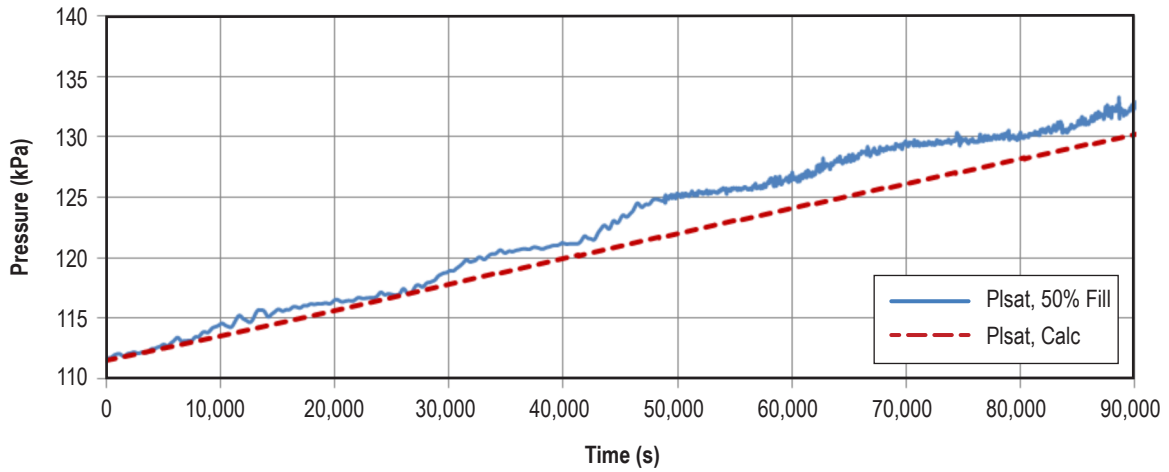


Figure 42. Liquid saturation pressure, 50% fill level.

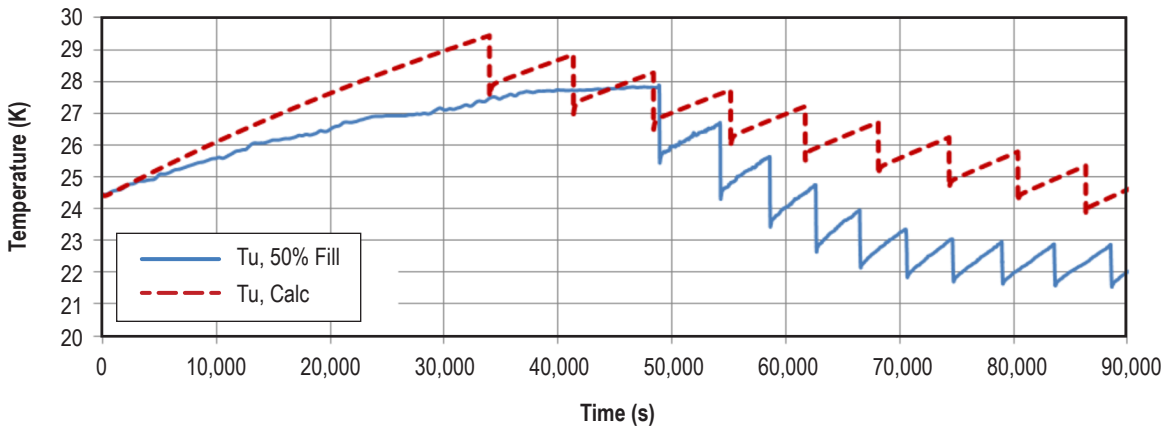


Figure 43. Ullage temperature, 50% fill level.

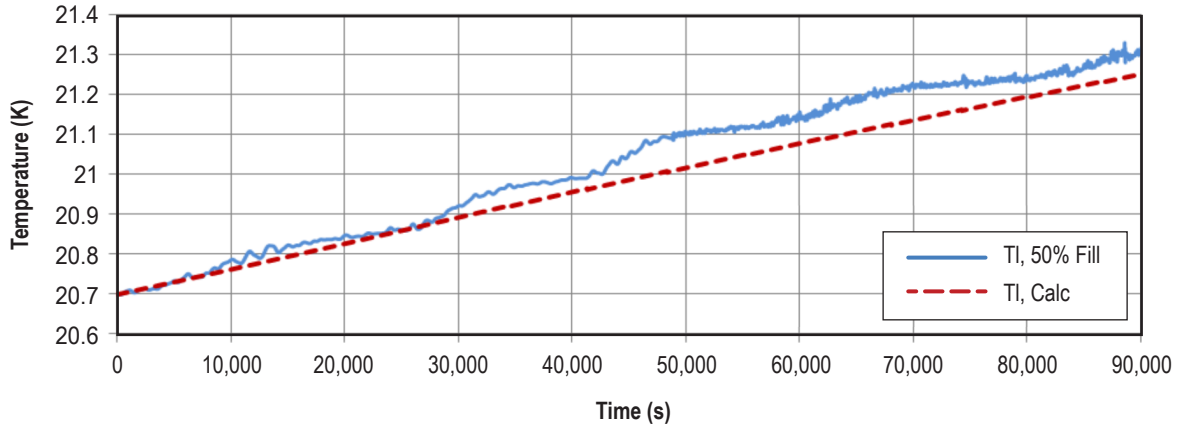


Figure 44. Liquid temperature, 50% fill level.

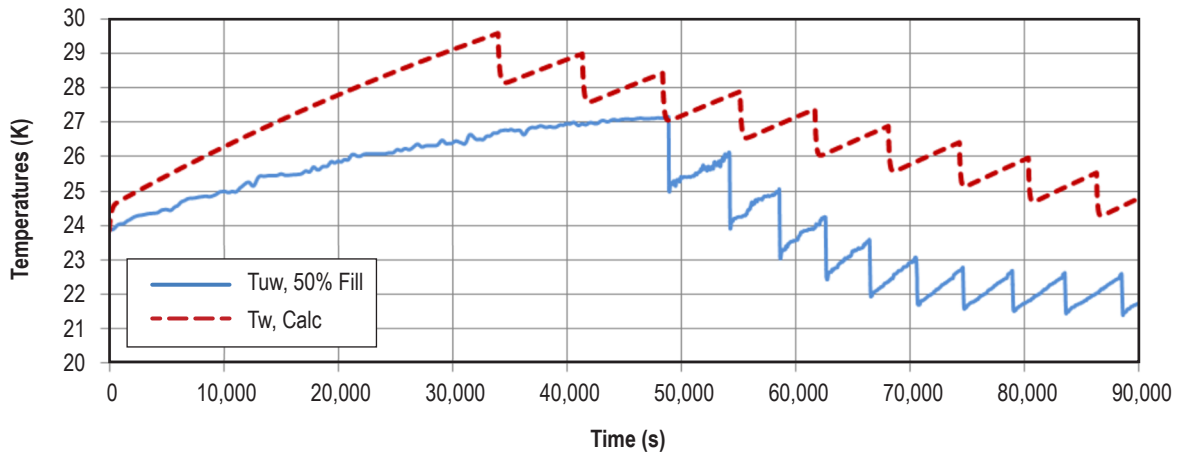


Figure 45. Ullage wall temperature, 50% fill level.

9.1.2 Hydrogen 50% Fill Level Test, File p263981t, 1998

Figure 41 presents a comparison of ullage pressure predicted by TankSIM and that of test data. Pressure rise predicted by TankSIM during the tank lockup increases faster than that of measured data. However, ullage pressure predicted by TankSIM is somewhat slower than test data during TVS operation. The ullage pressure drop rate predicted by TankSIM is in a reasonable agreement with that of test data. The number of cycles predicted by TankSIM and that of test data are 9 and 10, respectively, which are in close agreement. The average cycling duration for prediction and test data are 6,770 and 6,053 s, respectively.

TankSIM predicted liquid saturation pressure is in a good agreement with that of test data as shown in figure 42. The predicted liquid saturation pressure range and that of test data are 112 to 130.6 kPa and 112 to 133.1 kPa, respectively.

Comparison between TankSIM predicted ullage temperature with that of test data is shown in figure 43. The TankSIM predicted ullage temperature range is 29.5 to 23.8 K, while measured ullage temperature is 27.9 to 22.2 K.

Figure 44 compares predicted liquid temperature with that of measured data. The predicted liquid temperature is 20.7 to 21.26 K, while the measure liquid temperature range is 20.7 to 21.35 K.

A comparison between the predicted ullage wall temperature and that of test data is provided in figure 45. The predicted TankSIM ullage wall temperature range is 24.3 to 29.5 K, while the measured ullage wall temperature range is 21.6 to 27.1 K.

9.1.3 Hydrogen 90% Fill Level Test, File p263981d, 1998

Figure 46 presents a comparison of ullage pressure predicted by TankSIM and that of test data. Pressure rise predicted by the tank during the tank lockup is faster than that of measured data. However, ullage pressure rate predicted by TankSIM is somewhat slower than test data during TVS operation. The ullage pressure drop rate predicted by TankSIM is in a reasonable agreement with that of test data. The number of cycles predicted by TankSIM and that of test data are 8 and 14, respectively. The average cycling durations for prediction and test data are 3,800 and 2,150 s, respectively. TankSIM predicted liquid saturation pressure is in good agreement with that of test data as shown in figure 47. The predicted liquid saturation pressure range and that of test data are 110.4 to 117.4 kPa and 110.4 to 121.1 kPa, respectively.

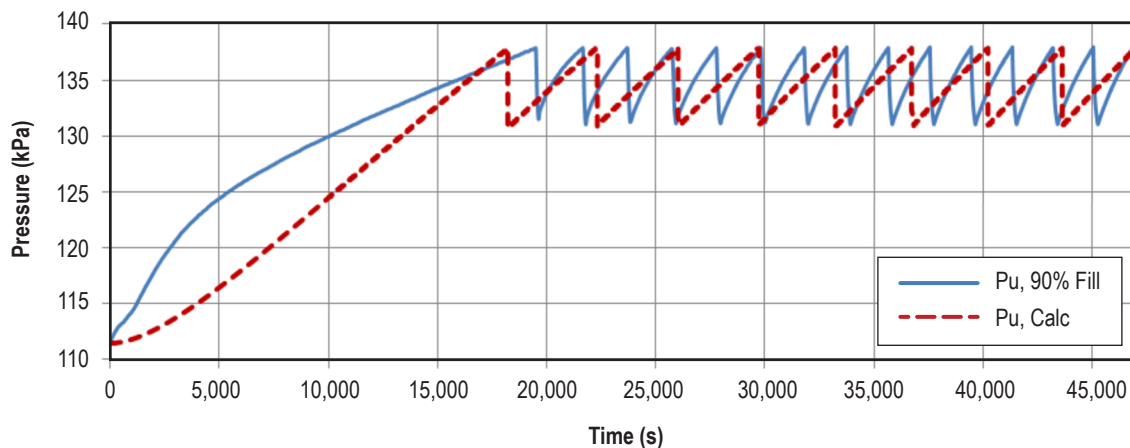


Figure 46. Ullage pressure, 90% fill level.

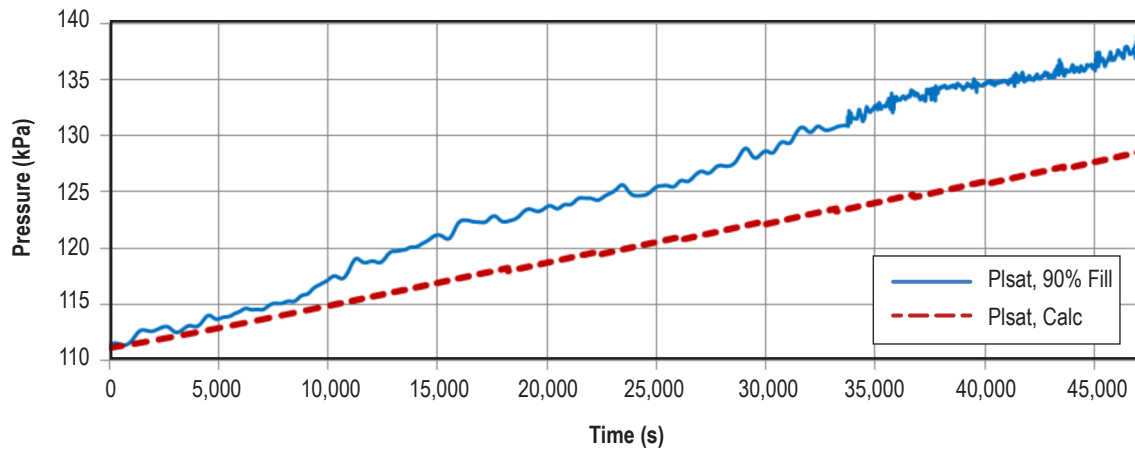


Figure 47. Liquid saturation pressure, 90% fill level.

Comparison between TankSIM predicted ullage temperature with that of test data is shown in figure 48. The TankSIM predicted ullage temperature range is 20.9 to 25 K, while the measured ullage temperature is 20.9 to 24.2 K.

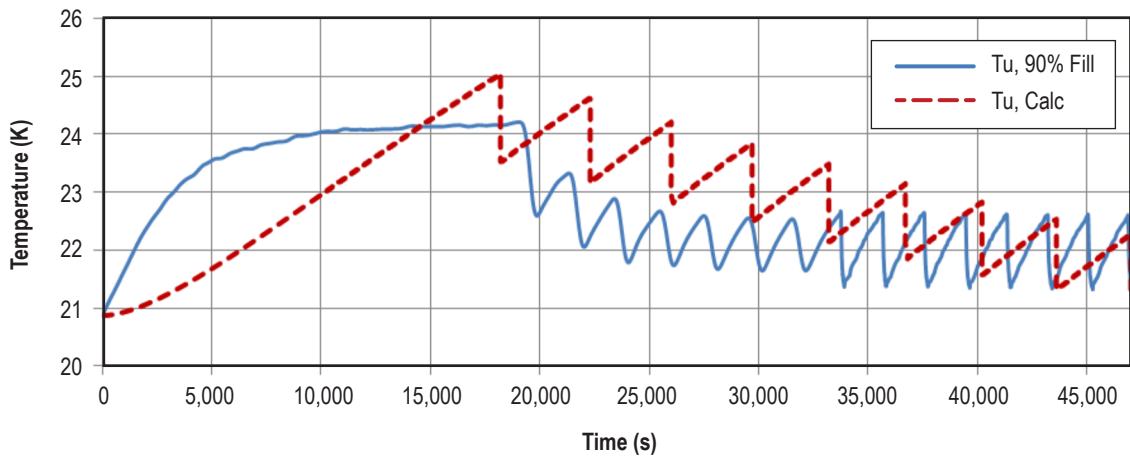


Figure 48. Ullage temperature, 90% fill level.

Figure 49 presents predicted liquid temperature with that of measured data. The predicted liquid temperature is 20.7 to 21 K while the measured liquid temperature range is 20.7 to 20.9 K.

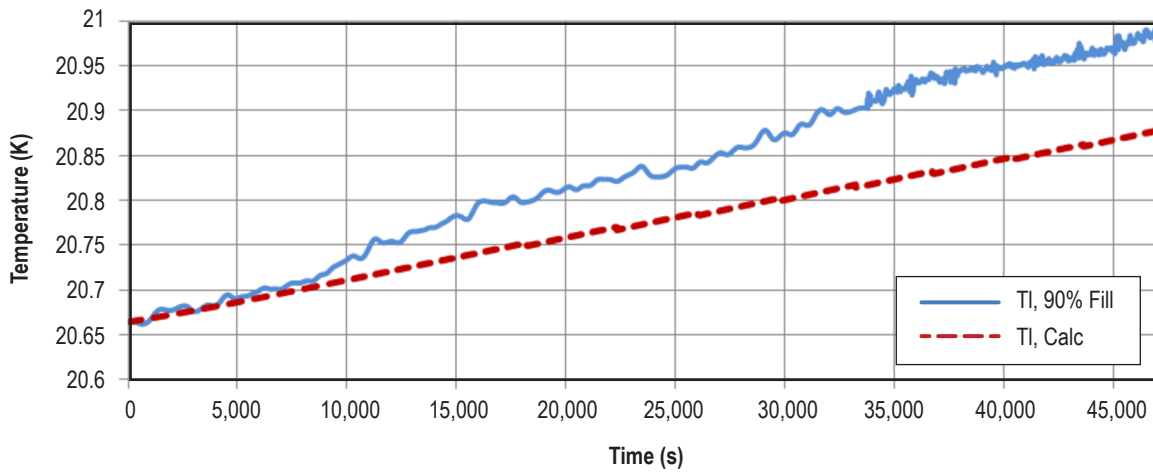


Figure 49. Liquid temperature, 90% fill level.

9.1.4 Hydrogen 25% Fill Level Test, File p263968kl, 1996, Adjusted Heat Loads

The example of adjusted heat loads is provided in this section. Three sets of heat loads are shown in table 2. The first set is estimated from the boiloff test, which is usually made before tank lockup. The second set is the best matched heat leaks during self-pressurization. As shown in table 2, these values are close to the estimated values. The third set is values for the best matched during the TVS operation.

Table 2. Heat leaks in 25% fill level test, adjusted heat loads.

Fill Level 25%	Estimated From Boiloff	Best Matching Lock-up Values	Best Matching TVS Values
Ullage	9.64	10.0	14.5
Liquid	9.06	10.1	15.0
Total	18.70	20.1	29.5

Results of modeling compared to test data are presented in figures 50–54. By comparing figures 36–40 with figures 50–54, one can conclude that the calculated parameters for the adjusted heat leaks lead to much closer agreements with the test data.

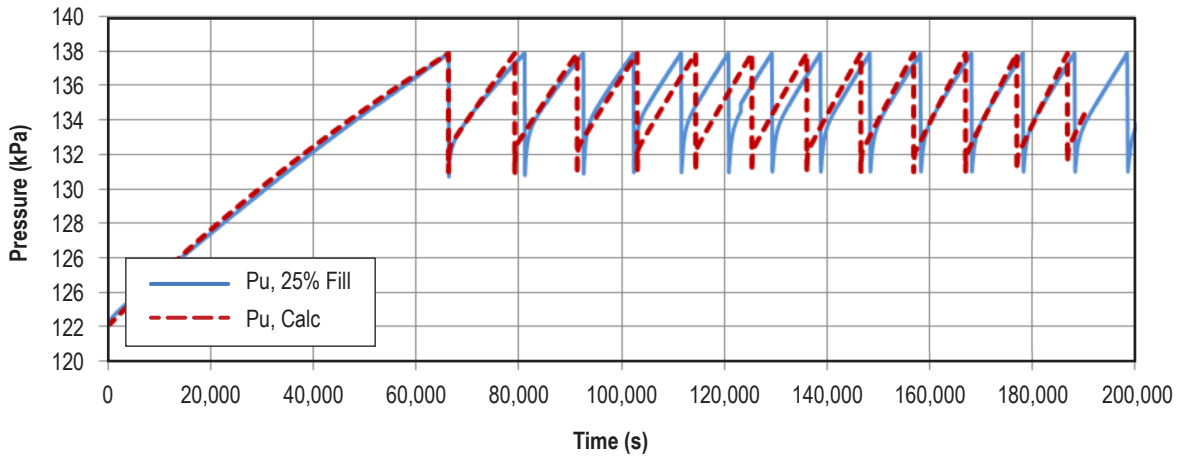


Figure 50. Ullage pressure, adjusted heat loads, 25% fill level.

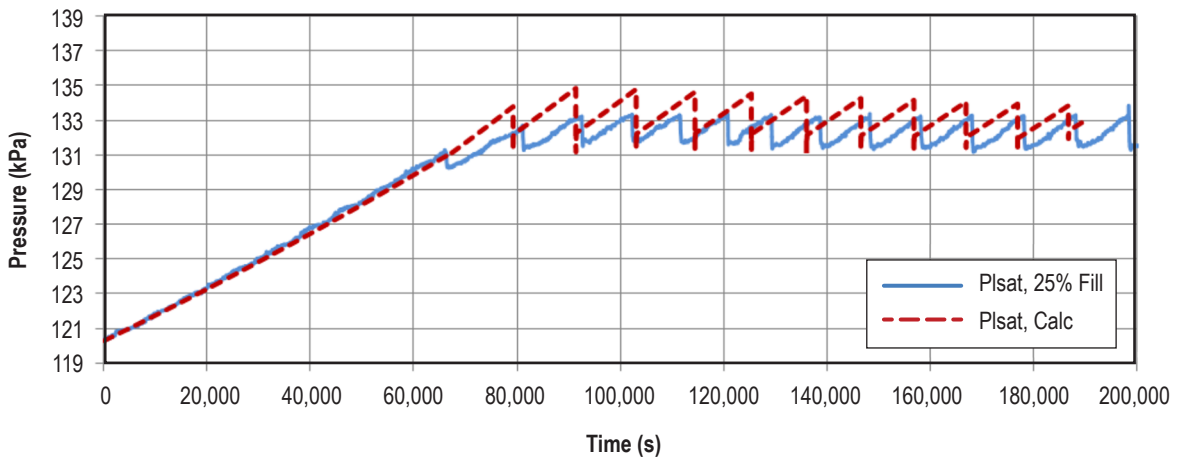


Figure 51. Liquid saturation pressure, adjusted heat loads, 25% fill level.

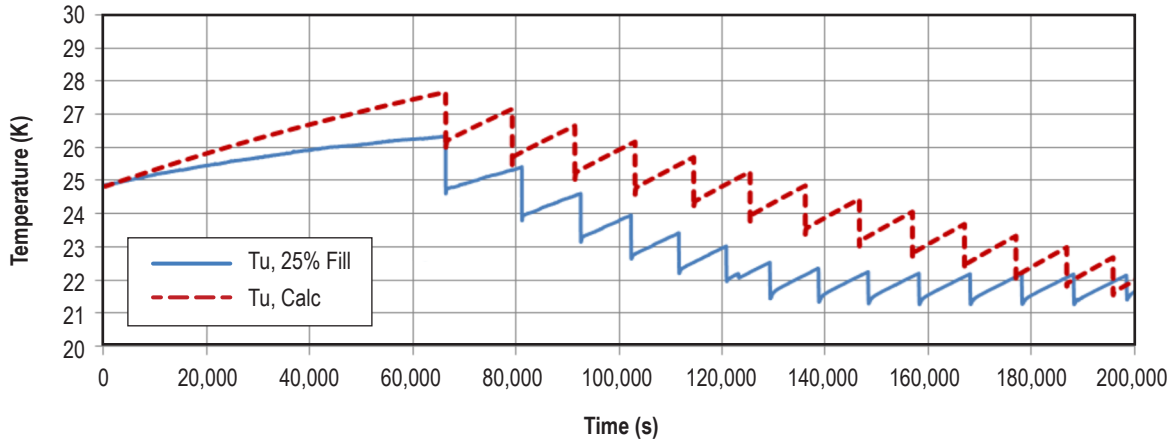


Figure 52. Ullage temperature, adjusted heat loads, 25% fill level.

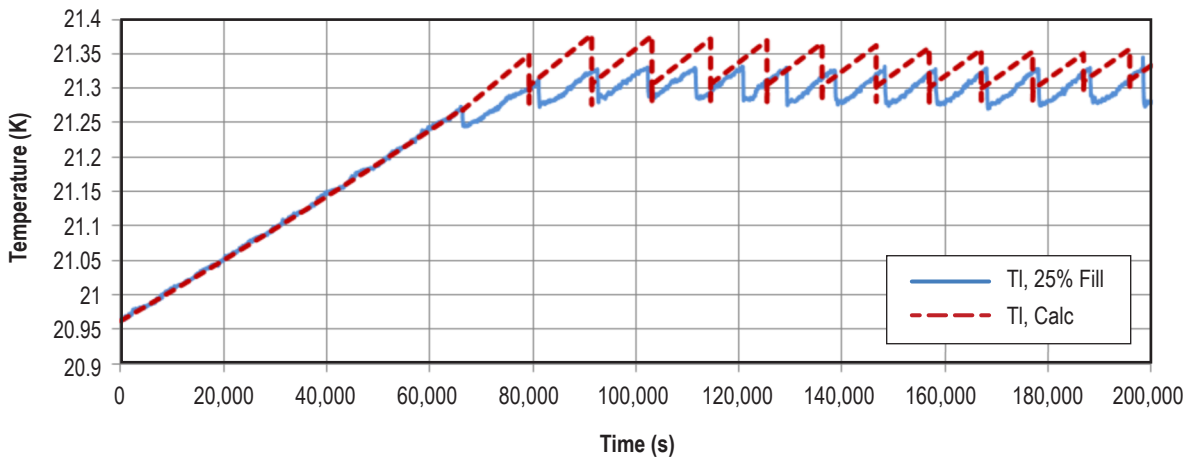


Figure 53. Liquid temperature, adjusted heat loads, 25% fill level.

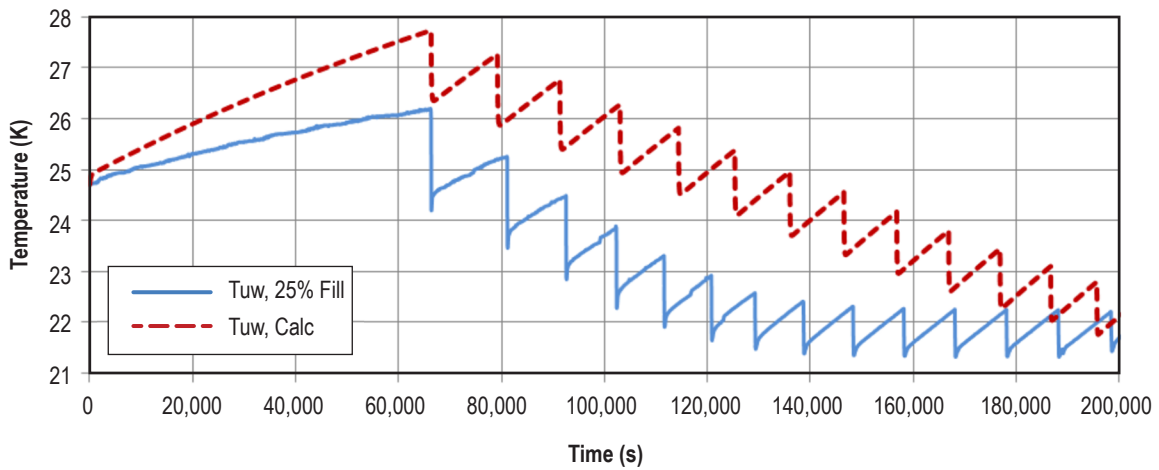


Figure 54. Ullage wall temperature, adjusted heat loads, 25% fill level.

9.2 Multiphase Mission Example With Ullage Venting

TankSIM allows combining the number of mission phases, such as:

- Self-pressurization (or tank lockup) with different pressure control systems.
- Autogenous or noncondensable gas prepressurization.
- Feed lines chilldown.
- Engine firing with tank pressurization.
- Propellant liquefaction.

Each of these phases could have its own duration, heat leaks, acceleration, mass flow rates, and other parameters. Usually, each mission is a combination of the first four phases. Figures 55–57 present the model predictions for results for ullage and liquid saturation pressures as well as ullage and liquid temperatures. The model simulates a mission, which consist of the following nine phases:

- (1) First self-pressurization with cycling ullage venting.
- (2) Second self-pressurization with different heat leaks and acceleration.
- (3) First prepressurization with noncondensable gas.
- (4) First feed lines chilldown.
- (5) First engine firing.
- (6) Third self-pressurization with cycling ullage venting.
- (7) Second prepressurization with noncondensable gas.
- (8) Second feed lines chilldown.
- (9) Second engine firing.

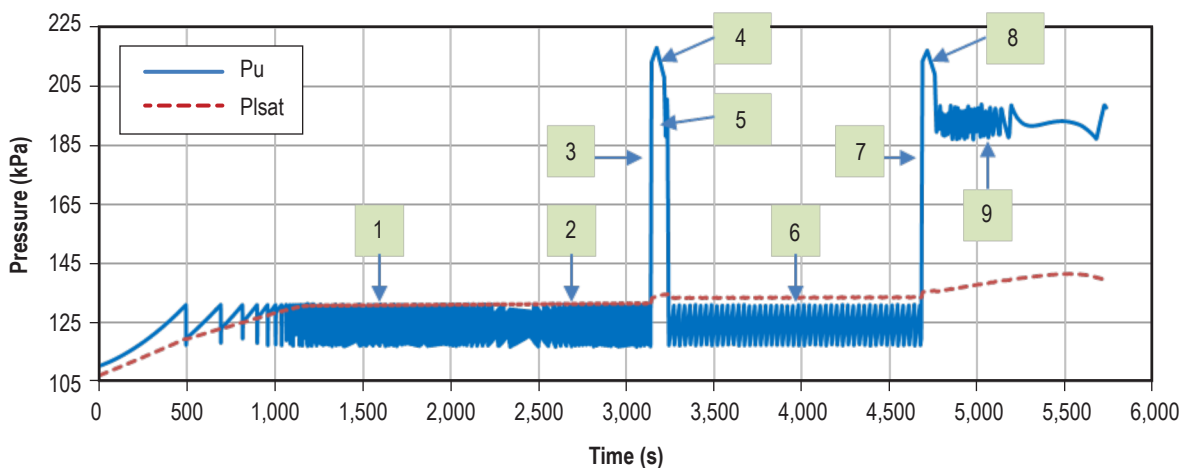


Figure 55. Ullage and liquid saturation pressures (cycling ullage venting).

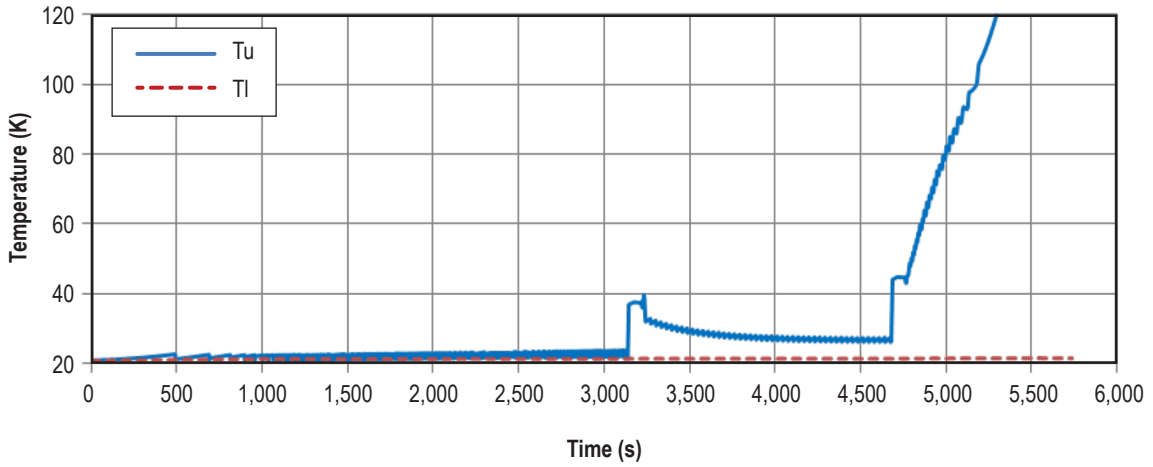


Figure 56. Ullage and liquid temperatures (cycling ullage venting).

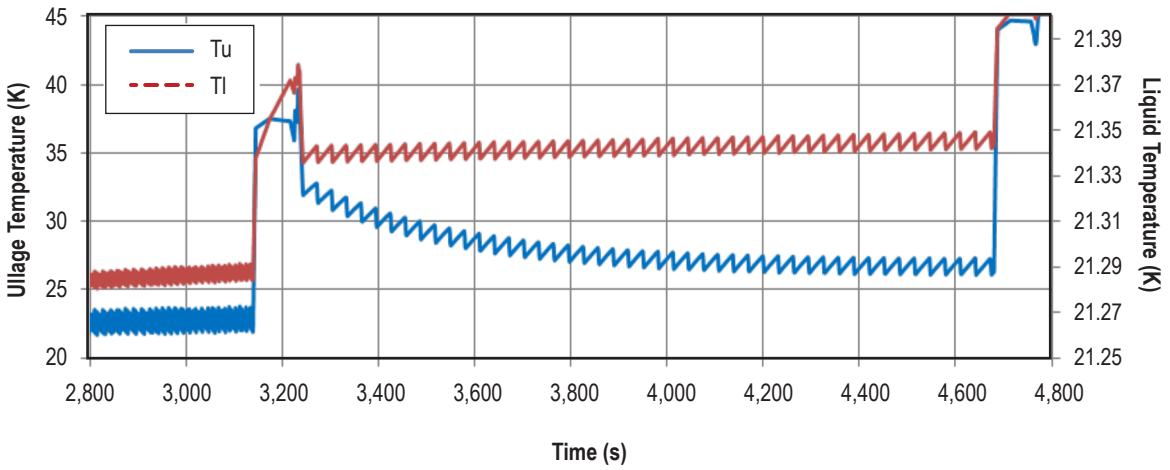


Figure 57. Ullage and liquid temperatures (cycling ullage venting, large scale).

10. SUMMARY AND FUTURE PROGRAM IMPROVEMENT

10.1 Summary

A full and detailed description of the TankSIM program is presented in this TM. At this time, TankSIM is one of the most robust non-computational fluid dynamics (CFD) programs for predicting heat and mass transfer inside cryogenic propellant tanks with different external and internal conditions. Program features include the following:

- Use of different tank shapes, working fluids, and noncondensable gases.
- Use of different types of pressure control systems—ullage venting in permanent and cycling regimes, spray bar and axial jet TVS, and their combinations in different mission phases.
- Simulation of full mission profiles by combining different mission phases in needed sequences with the ability to add new phases as required.
- Computations with relatively high precision and acceptable run time.

10.2 Future TankSIM Improvements

For future improvement of TankSIM, the following tasks are recommended:

- Develop new correlation equations for tank wall-to-ullage, tank wall-to-liquid, and liquid-to-ullage interface heat transfer under normal and low gravity, dependent on tank geometry, endcaps ratio, barrel section height, and fill level. This can be done using CFD software and regression analysis.
- Improve calculation of the ullage-to-liquid and tank wall-to-ullage interface areas, dependent on Bond number, fill level, and shape of the tank. This can be done using ‘Surface Evolver’ software and regression analysis.
- Develop calculation of the concentration-dependent coefficient for condensation mass flow rate when noncondensable gas is present in the tank.
- Replace nonsettled liquid heat transfer calculations during mixing from homogeneous fluid model to gas ullage and set of liquid spheres; diameters can be found from the mixer jet spray Weber number.
- Create a graphical user interface with Visual Studio tools.
- Continue to validate the program paying special attention to preparation of test data and develop an algorithm for estimating experimental heat leaks. Find the sources of discrepancies between predictions and test data at TVS operation and improve the program to reduce differences.

APPENDIX A—CONSERVATION EQUATIONS FOR MULTINODE ANALYSIS OF CRYOGENIC STORAGE TANKS

A.1 Leibnitz's Theorem

The following theorem is useful in expressing the mass and energy conservation equations in integral form. From Panton⁴³, the Leibnitz's Theorem for the time derivative of a volume integral of a scalar, f , where the control volume, V , changes with time, t , may be written as:

$$\frac{d}{dt} \left\{ \int_{V(t)} f dV \right\} = \int_{V(t)} \frac{\partial f}{\partial t} dV + \int_{S(t)} f (\vec{V}_S \cdot \hat{n}_S) dS. \quad (129)$$

In equation (129), the scalar function, f , may be a function of time and space, $f = f(t, \vec{r})$; S is the surface bounding the volume, V ; \vec{V}_S is the surface velocity, and \hat{n}_S is the outward unit normal to surface S . The above equation may also be rearranged to express the volume integral of $\partial f / \partial t$ as

$$\int_{V(t)} \frac{\partial f}{\partial t} dV = \frac{d}{dt} \left\{ \int_{V(t)} f dV \right\} - \int_{S(t)} f (\vec{V}_S \cdot \hat{n}_S) dS. \quad (130)$$

By applying equation (129) to the scalar function $f=1$, a useful relationship between the rate of volume change and surface velocity is found:

$$\frac{dV}{dt} = \frac{d}{dt} \left\{ \int_{V(t)} f dV \right\} - \int_{S(t)} (\vec{V}_S \cdot \hat{n}_S) dS. \quad (131)$$

If the control volume, V , is constant (i.e., V is not changing with time), then

$$\frac{d}{dt} \left\{ \int_V f dV \right\} = \int_V \frac{\partial f}{\partial t} dV, \quad \frac{dV}{dt} = 0. \quad (132)$$

A.2. Conservation of Mass

The conservation of mass for no creation or destruction sources within the volume, V , follow Panton⁴⁰ and may be written in integral form as

$$\frac{d}{dt} \left\{ \int_{V(t)} \rho dV \right\} + \int_{S(t)} \rho (\vec{V} - \vec{V}_S) \cdot \hat{n}_S dS = 0. \quad (133)$$

This also follows directly from integrating the differential form of conservation of mass:

$$\frac{\partial \rho}{\partial t} + \nabla \cdot (\rho \vec{V}) = 0. \quad (134)$$

Over the control volume, V , while applying the Gauss's theorem to the $\nabla \cdot (\rho \vec{V})$ term,

$$\int_V \nabla \cdot (\rho \vec{V}) dV = \int_S \rho \vec{V}_S \cdot \hat{n}_S dS, \quad (135)$$

and applying equation (130) to the term $\int_{V(t)} \frac{\partial \rho}{\partial t} dV$ where the scalar function, f , in equation (130) corresponds to the fluid density, ρ .

Using the following definitions for the terms of equation (132),

$$m = \int_{V(t)} \rho dV; \quad \dot{m}_k = \int_{S(t)} \rho (\vec{V} - \vec{V}_S) \cdot \hat{n}_S dS; \quad S(t) = \sum_k S_k(t), \quad (136)$$

where

- m – fluid mass within the volume
- V – volume
- \dot{m}_k – mass flow rate out of the volume through the surface element
- S – total surface
- S_k – surface element.

Using the above definitions, the integral form for the conservation of mass previously given by equation (132) as

$$\frac{d}{dt} \{m\} + \sum_k \dot{m}_k = 0. \quad (137)$$

A volume-average density also can be defined as $m = \bar{\rho}V$, where $\bar{\rho} = \frac{1}{V} \int_{V(t)} \rho dV$, and the conservation of mass written as

$$\frac{d}{dt} \{\bar{\rho}V\} + \sum_k \dot{m}_k = 0. \quad (138)$$

A.3 Conservation of Thermal Energy

The conservation of thermal energy in differential form written in terms of specific internal energy, e , is

$$\frac{\partial(\rho e)}{\partial t} + \nabla \cdot (\rho e \vec{V}) = -(\nabla \cdot \vec{q}) - P(\nabla \cdot \vec{V}) + \phi, \quad (139)$$

or written in terms of specific enthalpy, h , is

$$\frac{\partial(\rho h)}{\partial t} + \nabla \cdot (\rho h \vec{V}) = -(\nabla \cdot \vec{q}) + \frac{\partial P}{\partial t} + (\vec{V} \cdot \nabla P) + \phi, \quad (140)$$

where ϕ is the viscous dissipation function (which is always positive). Integrating over a control volume, $V(t)$, and applying Leibnitz's rule given by equation (130) to the volumes integrals, $\partial(\rho e)/\partial t$ and $\partial(\rho h)/\partial t$, the above two thermal energy equations become

$$\frac{d}{dt} \left\{ \int_{V(t)} \rho e dV \right\} + \int_{S(t)} \rho e (\vec{V} - \vec{V}_S) \cdot \hat{n}_S dS = - \int_{S(t)} \vec{q} \cdot \hat{n}_S dS - \int_{V(t)} P(\nabla \cdot \vec{V}) dV + \int_{V(t)} \phi dV \quad (141)$$

and

$$\frac{d}{dt} \left\{ \int_{V(t)} \rho h dV \right\} + \int_{S(t)} \rho h (\vec{V} - \vec{V}_S) \cdot \hat{n}_S dS = - \int_{S(t)} \vec{q} \cdot \hat{n}_S dS - \int_{V(t)} \left[\frac{\partial P}{\partial t} + (\vec{V} \cdot \nabla P) \right] dV + \int_{V(t)} \phi dV. \quad (142)$$

For a constant control volume, V (i.e., V is not changing with time), the control volume surface velocity is $\vec{V}_S = 0$.

Volumes integrals in equations (140) and (141) can be simplified by ignoring the spatial variation of pressure within the control volume, $P(\vec{r}, t) \approx P(t)$, which is a reasonable approximation for low speed flows.

For the thermal energy equation in terms of specific internal energy, the above described approximation for P is used to simplify the following integral involving pressure:

$$\begin{aligned} \int_{V(t)} P(\nabla \cdot \vec{V}) dV &\approx P \int_{V(t)} (\nabla \cdot \vec{V}) dV = P \int_{S(t)} \vec{V} \cdot \hat{n}_S dS \\ &= P \int_{S(t)} (\vec{V} - \vec{V}_S) \cdot \hat{n}_S dS + P \int_{S(t)} \vec{V}_S \cdot \hat{n}_S dS = P \int_{S(t)} (\vec{V} - \vec{V}_S) \cdot \hat{n}_S dS + P \frac{dV}{dt}, \end{aligned} \quad (143)$$

where equation (131) was used to relate the surface integral of $(\vec{V}_S \cdot \hat{n}_S)$ to the rate of volume change dV/dt . For the thermal energy equation in terms of specific enthalpy, h , $P(\vec{r}, t) \approx P(t)$ is used to simplify the following integral involving pressure:

$$\int_{V(t)} \left[\frac{\partial P}{\partial t} + (\vec{V} \cdot \nabla P) \right] dV = \int_{V(t)} \frac{dP}{dt} dV = \frac{dP}{dt} \int_{V(t)} dV = \frac{dP}{dt} V. \quad (144)$$

Using the simplifications given above which are valid when $P(\vec{r}, t) \approx P(t)$, the integral form of the thermal energy equations in terms of specific internal energy, e , is

$$\frac{d}{dt} \left\{ \int_{V(t)} \rho e dV \right\} + \int_{S(t)} \rho h (\vec{V} - \vec{V}_S) \cdot \hat{n}_S dS = - \int_{S(t)} \vec{q} \cdot \hat{n}_S dS - P \frac{dV}{dt} + \int_{V(t)} \phi dV, \quad (145)$$

and the integral form of the thermal energy equations in terms of specific enthalpy, h , is

$$\frac{d}{dt} \left\{ \int_{V(t)} \rho h dV \right\} + \int_{S(t)} \rho h (\vec{V} - \vec{V}_S) \cdot \hat{n}_S dS = - \int_{S(t)} \vec{q} \cdot \hat{n}_S dS + V \frac{dP}{dt} + \int_{V(t)} \phi dV. \quad (146)$$

In equation (143), for the internal energy, the relation $\rho e + P = \rho h$ was employed. For the case in which the control volume is constant in size and shape, ($dV/dt = 0$ and $\vec{V}_S = 0$), the above thermal energy equations simplify to

$$\frac{d}{dt} \left\{ \int_V \rho e dV \right\} + \int_S \rho h \vec{V} \cdot \hat{n}_S dS = - \int_S \vec{q} \cdot \hat{n}_S dS + \int_V \phi dV \quad (147)$$

and

$$\frac{d}{dt} \left\{ \int_V \rho h dV \right\} + \int_S \rho h \vec{V} \cdot \hat{n}_S dS = - \int_S \vec{q} \cdot \hat{n}_S dS + V \frac{dP}{dt} + \int_V \phi dV. \quad (148)$$

Defining mass-averaged internal energy, \bar{e} , enthalpy, \bar{h} , and a total fluid mass, m , within the control volume as

$$\bar{e} = \frac{1}{m} \int_{V(t)} \rho e dV, \quad \bar{h} = \frac{1}{m} \int_{V(t)} \rho h dV, \quad m = \int_{V(t)} \rho dV, \quad (149)$$

The equation can be written as

$$\frac{d}{dt} \left\{ \int_{V(t)} \rho e dV \right\} = \frac{d}{dt} \{ m \bar{e} \}; \quad \frac{d}{dt} \left\{ \int_{V(t)} \rho h dV \right\} = \frac{d}{dt} \{ m \bar{h} \}. \quad (150)$$

Using mass conservation equation (137), the time derivative of mass, the equation can be written as

$$\frac{d}{dt} \{ m \bar{e} \} = \bar{e} \frac{dm}{dt} + m \frac{d\bar{e}}{dt} = m \frac{d\bar{e}}{dt} - \bar{e} \sum_k \dot{m}_k \quad (151)$$

and

$$\frac{d}{dt} \{ m \bar{h} \} = \bar{h} \frac{dm}{dt} + m \frac{d\bar{h}}{dt} = m \frac{d\bar{h}}{dt} - \bar{h} \sum_k \dot{m}_k. \quad (152)$$

After replacing integrals in equations (147) and (148) by the definition from equation (150), the thermal energy equations in integral form become

$$m \frac{d\bar{e}}{dt} - \sum_k \dot{m}_k \bar{e} + \int_{S(t)} \rho h (\vec{V} - \vec{V}_S) \cdot \hat{n}_S dS = - \int_{S(t)} \bar{q} \cdot \hat{n}_S dS - P \frac{dV}{dt} + \int_{V(t)} \phi dV \quad (153)$$

and

$$m \frac{d\bar{h}}{dt} - \sum_k \dot{m}_k \bar{h} + \int_{S(t)} \rho h (\vec{V} - \vec{V}_S) \cdot \hat{n}_S dS = - \int_{S(t)} \bar{q} \cdot \hat{n}_S dS + V \frac{dP}{dt} + \int_{V(t)} \phi dV. \quad (154)$$

The only assumption in deriving the above equations was that pressure was spatially uniform.

The viscous dissipation contribution is expected to be small, although when the fluid mixer device is operating, the kinetic energy introduced into the fluid will eventually dissipate and lead to an increase in thermal energy. For now, the following term will be carried:

$$\dot{S}_{visc} = \int_{V(t)} \phi dV. \quad (155)$$

One further simplification is to treat the enthalpy along the various surface elements, S_k , as spatially constant ($h_k(\vec{r}, t) \approx h_k(t)$) for the integration over the control surface, S , so that

$$\int_{S(t)} ph(\vec{V} - \vec{V}_S) \cdot \hat{n}_S dS = \sum_k \int_{S_k} ph(\vec{V} - \vec{V}_S) \cdot \hat{n}_S dS \approx \sum_k h_k \int_{S_k} h(\vec{V} - \vec{V}_S) \cdot \hat{n}_S dS = \sum_k \dot{m}_k h_k. \quad (156)$$

For consistency, the heat flux surface integral will be split into the same surface elements, S_k , and be written as

$$- \int_{S(t)} \vec{q} \cdot \hat{n}_S dS = - \sum_k \int_{S_k} \vec{q} \cdot \hat{n}_S dS = \sum_k q_k, \quad (157)$$

where Q_k is the heat rate into the fluid through surface element, S_k .

Using the above relations consistent with the approximation $h_k(\vec{r}, t) \approx h_k(t)$, the thermal energy equations in integral form become

$$\frac{d}{dt} \{m\bar{e}\} + \sum_k \dot{m}_k h_k = \sum_k q_k - P \frac{dV}{dt} + \dot{S} \quad (158)$$

and

$$\frac{d}{dt} \{m\bar{h}\} + \sum_k \dot{m}_k h_k = \sum_k q_k + V \frac{dP}{dt} + \dot{S}_k, \quad (159)$$

or

$$m \frac{d\bar{e}}{dt} + \sum_k \dot{m}_k (h_k - \bar{e}) = \sum_k q_k - P \frac{dV}{dt} + \dot{S}_k \quad (160)$$

and

$$m \frac{d\bar{h}}{dt} + \sum_k \dot{m}_k (h_k - \bar{h}) = \sum_k q_k + V \frac{dP}{dt} + \dot{S}_k. \quad (161)$$

APPENDIX B—HEAT AND MASS TRANSFER INSIDE THE TANK

B.1 Ullage-Bulk Liquid Interface Temperature

Temperature of the interface is calculated by Alabovskii's equation, suggested in reference 1:

$$\frac{\Theta_u}{\Theta_l} = \frac{k_l}{k_u} \left(\frac{\mu_u \rho_l}{\mu_l \rho_u} \right)^{0.5} \left(\frac{\mu_l}{\rho_l a_l} \right)^{0.5} (1+m), \quad (162)$$

where

$$\Theta_u = T_u - T_{int} = \text{ullage temperature difference, K}$$

$$\Theta_l = T_l - T_{int} = \text{liquid temperature difference, K}$$

$$\mu_u, \mu_l = \text{viscosity of ullage and liquid respectively, kg/m}\cdot\text{s}$$

$$a_l = \frac{C_{pl} \rho_l}{k_l} = \text{liquid thermal diffusivity, m}^2/\text{s}$$

$$m = \frac{q_{evap}}{q_{intl}} = \text{evaporation to total heat flows through interface ratio.}$$

Because interface temperature, in most cases, is higher than liquid temperature and lower than ullage temperature, and the right side of equation (162) is positive, the temperature difference for the liquid needs to be reassigned to the positive value as:

$$\Theta_l = T_{int} - T_l. \quad (163)$$

After rearranging, equation (162) can be written as:

$$\frac{T_u - T_{int}}{T_{int} - T_l} = \frac{k_l}{k_u} \left(\frac{\mu_u \rho_l}{\mu_l \rho_u} Pr_l \right)^{0.5} (1+m). \quad (164)$$

Suppose

$$K = \frac{k_l}{k_u} \left(\frac{\mu_u \rho_l}{\mu_l \rho_u} Pr_l \right)^{0.5} (1+m), \quad (165)$$

and equation (164) is resolved for the interface temperature, T_{int} ,

$$T_{int} = \frac{KT_l + T_u}{K+1} = \frac{T_l + T_u / K}{1+1/K}. \quad (166)$$

Table 3 presents coefficient K for some cryogenic fluids; hydrogen, oxygen, methane, and nitrogen are calculated with assuming $(1+m)$ is close to unity, which implies evaporation from the interface is relatively low. As can be seen from equations (165) and (166), if evaporation is not negligible, the interface temperature will be even closer to liquid temperature.

Table 3. Coefficient K from equation (165).

Fluid	Saturation Temperature (K)	Coefficient K	Fluid	Saturation Temperature (K)	Coefficient K
Hydrogen			Oxygen		
	18	20.16		85	116.42
	19	17.24		88	95.21
	20	14.88		90	83.79
	21	12.94		95	62.01
Methane			Nitrogen		
	105	99.60		75	87.80
	110	76.31		78	70.45
	115	59.51		80	61.24
	120	47.10		82	53.51

As can be seen from table 3 and equation (166), the interface temperature is always closer to the liquid temperature than to the ullage temperature.

B.2 Requirements for Using Flat Plate Correlations to the Cylindrical Segment of the Tank

Conditions when the flat plate model can be used follow. For thermal conductivity (the heat flow rate through the cylindrical wall) (see fig. 58), the tank is:

$$q_{cyl} = \frac{2\pi h_{cyl} k (T_2 - T_1)}{\ln(r_2 / r_1)}, \quad (167)$$

where h_{cyl} is the height of the wall and $T_2 > T_1$.

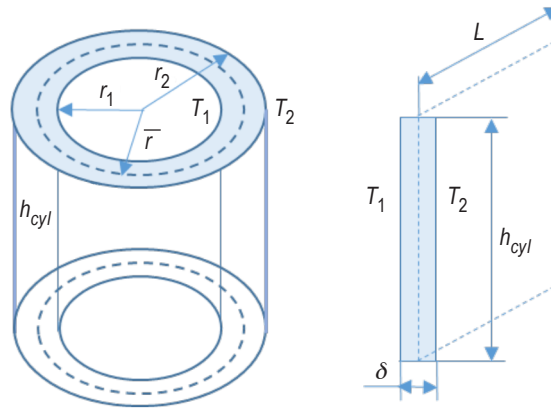


Figure 58. Cylindrical to flat tank wall transformation.

For a flat wall, the heat flow rate can be written as:

$$q_{flat} = \frac{Ak(T_2 - T_1)}{\delta}, \quad (168)$$

where A is a wall surface area, δ is a thickness of the wall, and $\delta = r_2 - r_1$. It can be found using the length of the cylindrical wall calculated with the average of the radius of the cylinder, $r = (r_1 + r_2)/2$, and height, h_{cyl} , $A = 2\pi r h_{cyl}$, or

$$q_{flat} = \frac{\pi(r_1 + r_2)h_{cyl}k(T_2 + T_1)}{\delta}. \quad (169)$$

Suppose temperatures, wall lengths and thicknesses, and wall heights are the same for both cylindrical and flat walls. In this case, the relative difference between heat flow rates as a function of the ratio of wall thickness to radius can be written as:

$$\Delta = \frac{q_{flat} - q_{cyl}}{q_{flat}}, \text{ or } \Delta = 1 - (0.5 + 1/x)\ln(1+x), \quad (170)$$

where $x = \delta/r_1$.

Figure 59 presents this function in the ratio range, which takes place in propellant tank applications.

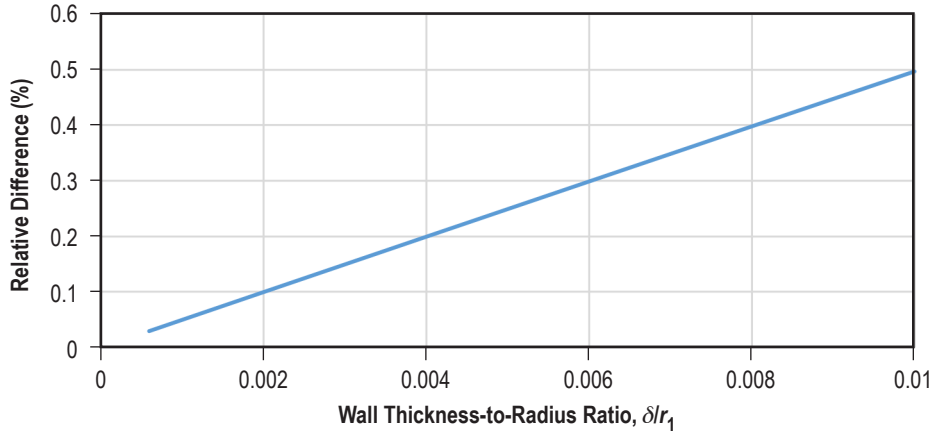


Figure 59. Relative difference between heat flow rates through circular and flat tank walls.

B.3 Free Convection Heat Transfer From the Tank Wall Inside the Tank

Following Elenbaas⁴⁴, the Nusselt number can be accepted for the internal convection in a circular cylinder as:

$$Nu_r = \frac{\alpha r}{k_l(T_w)} = \frac{1}{16} \frac{r}{h} Ra_r \left\{ 1 - \exp \left[- \left(\frac{h}{r} \frac{20}{Ra_r} \right)^{C_2} \right] \right\}^{C_3}. \quad (171)$$

Equation (171) was developed, assuming a radius of cylinder $r \rightarrow \infty$. Equation (171) should match the Schmidt-Pohlhausen-Beckmann⁴⁵ solution with the experimental adjustment for the flat vertical plate:

$$Nu_h = \frac{\alpha h}{k_u(T_w)} = 0.6 Ra_h^{1/4}. \quad (172)$$

Using these equations,

$$C_2 \cdot C_3 = 3/4, \quad Ra_h = \frac{g\beta C_p \rho_u \Delta T h^3}{\nu k_u}, \quad \text{and} \quad Ra_r = \frac{g\beta C_p \rho_u \Delta T r^3}{\nu k_u}. \quad (173)$$

and from equations (172), it can be found that:

$$Ra_r = Ra_h r^3 / h^3, \quad Nu_r = Nu_h r / h. \quad (174)$$

Using equations (170)–(172), the cylindrical Nusselt to flat plate Nusselt ratio can be created:

$$\frac{Nu_r}{Nu_h} = \frac{1}{c_1} \frac{r}{h} Ra_r \left\{ 1 - \exp \left[- \left(\frac{h}{r} \frac{20}{Ra_r} \right)^{C_2} \right] \right\}^{C_3} / Ra_h^{1/4}, \quad (175)$$

where $c_1 = 16 \times 0.6 = 9.6$.

Simplifying equation (175),

$$\frac{Nu_r}{Nu_h} = \frac{1}{c_1} \left(\frac{r}{h} \right)^{7/4} Ra_r^{3/4} \left\{ 1 - \exp \left[- \left(\frac{h}{r} \frac{20}{Ra_r} \right)^{C_2} \right] \right\}^{C_3}. \quad (176)$$

For cylindrical vertical channels, Elenbaas⁴⁴ suggested $C_2 = 3/4$, $C_3 = 1$. With this assumption, equation (176) becomes:

$$\frac{Nu_r}{Nu_h} = \frac{1}{c_1} \left(\frac{r}{h} \right)^{7/4} Ra_r^{3/4} \left\{ 1 - \exp \left[- \left(\frac{h}{r} \frac{20}{Ra_r} \right)^{3/4} \right] \right\}. \quad (177)$$

For a small argument, the exponent in equation (177) can be expanded into the Taylor series. Keeping linear and quadratic terms only, gives:

$$\exp \left[- \left(\frac{h}{r} \frac{20}{Ra_r} \right)^{3/4} \right] \approx 1 - \left(\frac{h}{r} \frac{20}{Ra_r} \right)^{3/4} + \frac{1}{2} \left(\frac{h}{r} \frac{20}{Ra_r} \right)^{3/2}. \quad (178)$$

This series converges when $\left(\frac{h}{r} \frac{20}{Ra_r} \right)^{3/4} < 1$. Using equation (174), it can be found that

$$\frac{r}{h} > \left(\frac{20}{Ra_h} \right)^{1/4}. \quad (179)$$

The lowest ratio value, $\frac{r}{h} = \left(\frac{20}{Ra_h} \right)^{1/4}$, is depicted in figure 60.

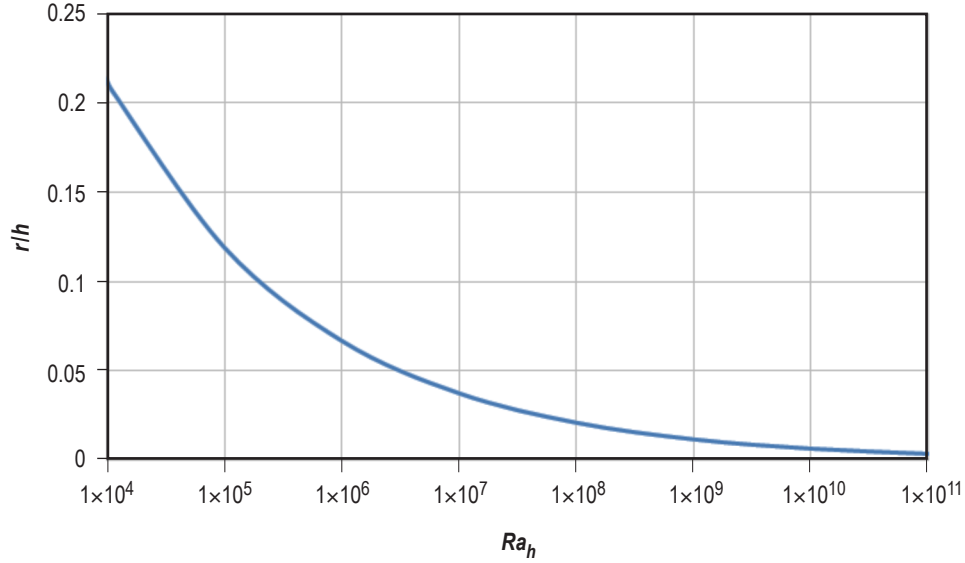


Figure 60. Minimal radius-to-height ratio value allows using the flat wall convective heat flow model for cylindrical walls.

By substituting equation (178) into equation (177),

$$\frac{Nu_r}{Nu_h} = \frac{1}{c_1} \left(\frac{r}{h}\right)^{7/4} Ra_r^{3/4} \left(\frac{h}{r} \frac{20}{Ra_r}\right)^{3/4} \left[1 - \frac{1}{2} \left(\frac{h}{r} \frac{20}{Ra_r}\right)^{3/4}\right] = \frac{20^{3/4}}{c_1} \frac{r}{h} \left[1 - \frac{1}{2} \left(\frac{h}{r} \frac{20}{Ra_r}\right)^{3/4}\right]. \quad (180)$$

Using equation (174),

$$Nu_r = Nu_{r \rightarrow h} \frac{r}{h}, \text{ or } \frac{Nu_r}{Nu_h} = \frac{Nu_{r \rightarrow h}}{Nu_h} \frac{r}{h}. \quad (181)$$

Now, equation (180) can be rewritten as:

$$\frac{Nu_{r \rightarrow h}}{Nu_h} \frac{r}{h} = \frac{20^{3/4}}{c_1} \frac{r}{h} \left[1 - \frac{1}{2} \left(\frac{h}{r} \frac{20}{Ra_r}\right)^{3/4}\right], \text{ or } \frac{Nu_{r \rightarrow h}}{Nu_h} = \frac{20^{3/4}}{c_1} \left[1 - \frac{1}{2} \left(\frac{h}{r} \frac{20}{Ra_r}\right)^{3/4}\right]. \quad (182)$$

Because this ratio should be equal to unity for large radius-to-height ratios, $\frac{20^{3/4}}{c_1} = 1$.

Calculating Nu relative difference and using equation (182),

$$\delta Nu = 1 - \frac{Nu_{r \rightarrow h}}{Nu_h} = \frac{20^{3/4}}{2} \left(\frac{h}{r}\right)^3 Ra_h^{-3/4} \approx 4.7287 \left(\frac{h}{r}\right)^3 Ra_h^{-3/4}. \quad (183)$$

The relative difference, δNu , calculated by equation (182) for $10^4 \leq Ra_r \leq 10^{11}$ is presented in figure 61.

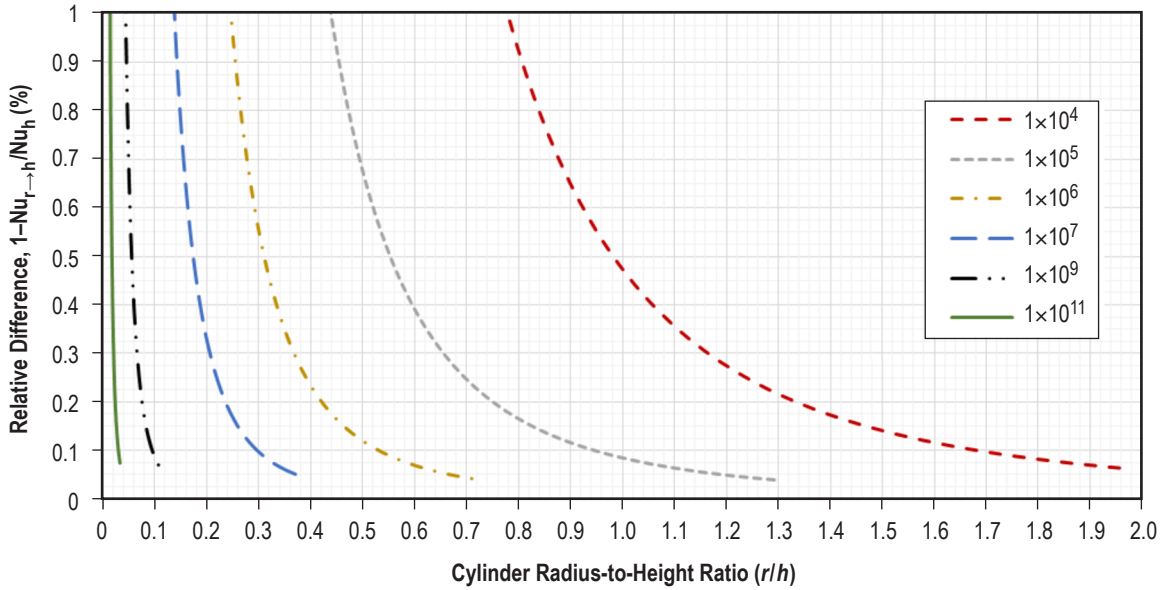


Figure 61. Relative Nusselt numbers difference versus radius-to-height ratio for different Rayleigh numbers.

B.4 Ullage Wall Condensation Model

B.4.1 Vertical Cylindrical Wall

Condensation on the internal side of the cylindrical wall segment is shown in figure 62.

For this system with the boundary layer approximation, the momentum equation can be expressed as reported by Incropera and DeWitt⁴⁶:

$$\frac{\partial^2 u}{\partial y^2} = -\frac{g}{\mu_l} (\rho_l - \rho_v). \quad (184)$$

Integrating twice with boundary conditions $\frac{\partial u}{\partial y} \Big|_{\delta=0} = 0$; $u(0) = 0$, results in:

$$u(y) = \frac{g(\rho_l - \rho_v)}{\mu_l} \left[y\delta - \frac{y^2}{2} \right]. \quad (185)$$

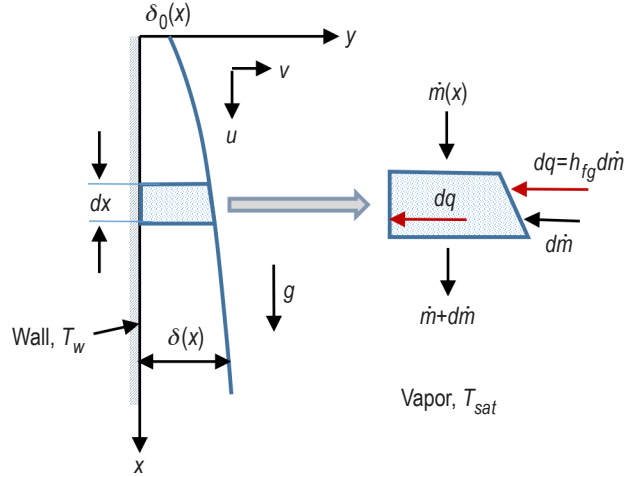


Figure 62. Condensation on the internal side of cylindrical wall segment.

Integrating this velocity across the film, results in the following relation for the mass flow rate per unit width of surface:

$$\dot{m}' = \rho_l \int_{\delta_0}^{\delta} u dy = \frac{\rho_l (\rho_l - \rho_v) g}{\mu_l} \left(\frac{y^2 \delta}{2} - \frac{y^3}{6} \right)_{\delta_0}^{\delta} = \frac{\rho_l (\rho_l - \rho_v) g}{3 \mu_l} \left[\delta^3 - \frac{\delta_0^2}{2} (3\delta - \delta_0) \right]. \quad (186)$$

Differentiating equation (185) with respect to δ yields:

$$\frac{d\dot{m}'}{d\delta} = \frac{\rho_l (\rho_l - \rho_v) g}{\mu_l} \left[\delta^2 - \frac{\delta_0^2}{2} \right]. \quad (187)$$

Assuming that heat flux across the film is mainly due to conduction, and using conservation of energy from the condensation, one can get:

$$\frac{k_l \Delta T}{\delta} dx = h'_{fg} d\dot{m}', \quad (188)$$

where referring to Rohsenow⁴⁷, $h'_{fg} = h_{fg} (1 + 0.68 Ja)$ and $Ja = \frac{C_{pl} (T_{sat} - T_w)}{h_{fg}}$.

Combining equations (187) and (188), the following differential equation is obtained for δ :

$$dx = \frac{\rho_l (\rho_l - \rho_v) g h'_{fg}}{\mu_l k_l \Delta T} d\delta \left[\delta^3 - \frac{\delta_0^2 \delta}{2} \right]. \quad (189)$$

Integrating equation (189) and solving for δ , the following can be obtained:

$$\delta(x) = \left[\frac{\delta_0^2 + (\delta_0^4 + 4kx)^{1/2}}{2} \right]^{1/2}, \quad (190)$$

where $k = \frac{4\mu_l k_l \Delta T}{\rho_l (\rho_l - \rho_v) g h'_{fg}}$.

Because heat transfer across the film is by conduction alone, the heat transfer coefficient is given by

$$h_l(x) = k_l / \delta(x) = k_l \left(\frac{2}{\delta_0^2 + \sqrt{\delta_0^4 + 4kx}} \right)^{1/2}. \quad (191)$$

The mean heat transfer coefficient is:

$$\bar{h}_l = \frac{1}{L} \int_0^L h_l(x) dx = \frac{k_l}{L} \int_0^L \left(\frac{2}{\delta_0^2 + \sqrt{\delta_0^4 + 4kx}} \right)^{1/2} dx = \frac{k_l}{k^{1/4} L} \int_0^L \frac{1}{(\sqrt{a} + \sqrt{a+x})^{1/2}} dx, \quad (192)$$

where $a = \delta_0^4 / 4k$.

Integrating equation (192), one gets:

$$\bar{h}_l = \frac{4}{3\sqrt{2}} \left[\frac{g\rho_l(\rho_l - \rho_v)k_l^3 h'_{fg}}{\mu_l \Delta T L} \right]^{1/4} \left[(\sqrt{b+1} - 2\sqrt{b})(\sqrt{b} + \sqrt{b+1})^{1/2} + \sqrt{2}b^{3/4} \right], \quad (193)$$

where $b = \delta_0^4 / 4kL$.

Supposing $\delta_0 = 0$ results in the Nusselt equation for the mean laminar heat transfer coefficient on the vertical wall,

$$\bar{h}_l = 0.9428 \left[\frac{g\rho_l(\rho_l - \rho_v)k_l^3 h'_{fg}}{\mu_l \Delta T L} \right]^{1/4}. \quad (194)$$

The average Nusselt number can be expressed in the form:

$$\bar{Nu}_l = \frac{\bar{h}_l L}{k_l} = 0.9428 \left[\frac{g \rho_l (\rho_l - \rho_v) h'_{fg} L^3}{k_l \mu_l (T_{sat} - T_w)} \right]^{1/4} \left[(\sqrt{b+1} - 2\sqrt{b})(\sqrt{b} + \sqrt{b+1})^{1/2} + \sqrt{2b}^{3/4} \right]. \quad (195)$$

The thickness of the film will be:

$$\delta = (kL)^{1/4} \left(\sqrt{b} + \sqrt{b + \frac{x}{L}} \right)^{1/2} = \left(\frac{4\mu_l k_l (T_{sat} - T_w) L}{\rho_l (\rho_l - \rho_v) g h'_{fg}} \right)^{1/4} \left(\sqrt{b} + \sqrt{b + \frac{x}{L}} \right)^{1/2}. \quad (196)$$

The dimensionless parameter b that depends on the initial liquid film thickness is:

$$b = \frac{\delta_0^4}{4kL} = \frac{\delta_0^4}{16} \frac{\rho_l (\rho_l - \rho_v) g h'_{fg}}{\mu_l k_l (T_{sat} - T_w) L}. \quad (197)$$

B.4.2 Upper Dome

The condensation appears in the underside of inclined surfaces for this case. Following Gerstmann and Griffith⁷, the following assumptions were made:

- Flow is laminar.
- Angle of inclination is small.
- Pressure in the film is hydrostatic.
- Vapor exerts negligible shear on the interface.
- Wall temperature and the vapor temperature are uniform.
- Group $k_l \Delta T / \mu_l h'_{fg}$ is much less than unity.
- Group $Ja = c_{pl} \Delta T / h'_{fg}$ is much less than unity.
- Capillary length scale is accepted in the form:

$$\psi = \left[\frac{\sigma}{g(\rho_l - \rho_v) \cos(\alpha)} \right]^{1/2}. \quad (198)$$

Using previous assumptions and figure 63, the governing equations may be written as:

$$\frac{\partial p}{\partial x} = \mu_l \frac{\partial^2 v_x}{\partial x^2}, \quad (199)$$

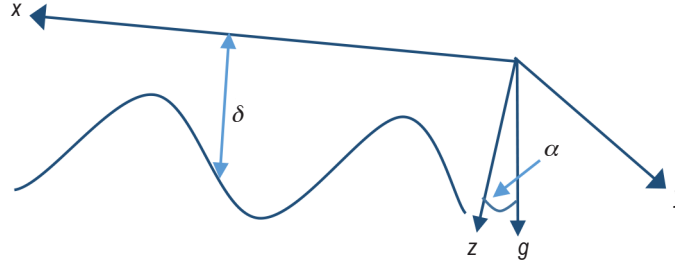


Figure 63. Condensation on the upper dome.

$$p = p_{sat} - (\rho_l - \rho_v) g \cos(\alpha) (\delta - z) - \sigma \frac{d^2 \delta}{dx^2}, \quad (200)$$

$$\frac{\partial v_x}{\partial x} + \frac{\partial v_z}{\partial z} = 0, \quad (201)$$

and

$$\frac{Q}{A} = \frac{k_l (T_{sat} - T_w)}{\delta}. \quad (202)$$

By differentiating equation (200) and substituting in equation (199), the following equation can be obtained:

$$\mu_l \frac{\partial^2 v_x}{\partial x^2} = -(\rho_l - \rho_v) g \cos(\alpha) \frac{d\delta}{dx} - \sigma \frac{d^3 \delta}{dx^3}. \quad (203)$$

Integrating equation (203) with boundary conditions of zero velocity at the wall and zero shear stress at the interface gives:

$$v_x = \frac{1}{\mu_l} \left[(\rho_l - \rho_v) g \cos(\alpha) \frac{d\delta}{dx} + \sigma \frac{d^3 \delta}{dx^3} \right] \left(z\delta - \frac{z^2}{2} \right). \quad (204)$$

Integrating equation (200) over the film thickness, using equations (201) and (203), equation (205) can be obtained:

$$\delta \frac{d}{dx} \left\{ \frac{1}{3\mu_l} \left[(\rho_l - \rho_v) g \cos(\alpha) \frac{d\delta}{dx} + \sigma \frac{d^3\delta}{dx^3} \right] \left[\delta^3 - \frac{\delta_0^2}{2} (3\delta - \delta_0) \right] \right\} = \frac{k_l \Delta T}{\rho_l h_{fg}}. \quad (205)$$

Equation (204) can be made dimensionless by defining the following new variables: $\hat{\delta} = \frac{\delta}{\psi}$ and $\hat{x} = \frac{x}{\psi}$.

Using primes to signify differentiation with respect to x , equation (204) may be restated as

$$\hat{\delta} \left[\hat{\delta}^3 - \frac{\hat{\delta}_0^2}{2} (3\hat{\delta} - \hat{\delta}_0) \right] (\hat{\delta}'' + \hat{\delta}''''') + 3\hat{\delta} \left(\hat{\delta}^2 - \frac{\hat{\delta}_0^2}{2} \right) \left[\hat{\delta}''' \hat{\delta}' + (\hat{\delta}')^2 \right] = \Theta, \quad (206)$$

where

$$\Theta = \frac{3k_l \Delta T \mu_l}{\psi \rho_l h_{fg} \sigma}.$$

Assuming that $\hat{\delta}_0^2 \ll \hat{\delta}^2$ in equation (206) results in the same equation as obtained by Gerstmann⁷:

$$\hat{\delta}^4 (\hat{\delta}'' + \hat{\delta}''''') + 3\hat{\delta}^3 \left[\hat{\delta}''' \hat{\delta}' + (\hat{\delta}')^2 \right] = \Theta. \quad (207)$$

The solution of this equation is given in reference 6 for $Ra > 10^6$:

$$\bar{Nu} = \frac{0.9}{Ra^{1/6} (1 + 1.1 Ra^{-1/6})}, \quad (208)$$

where Ra is a modified Rayleigh number:

$$Ra = \frac{\rho_l \sigma h_{fg}}{k_l \mu_l (T_{sat} - T_w)} \left[\frac{\sigma}{g (\rho_l - \rho_v) \cos(\alpha)} \right]^{1/2}. \quad (209)$$

It was recommended by Gerstmann and Griffith⁷ that equations (208) and (209) could be used for small inclinations, $\alpha < 20^\circ$.

For angles $20^\circ < \alpha < 90^\circ$, the modified Nusselt model was recommended. At this model, the free-fall acceleration g in equations (195)–(197) should be replaced by $g \sin(\alpha)$. In this case, equations (195)–(197) result in:

$$\bar{N}u_l = \frac{\bar{h}_l L}{k_l} = 0.9428 \left[\frac{g \sin(b) \rho_l (\rho_l - \rho_v) h'_{fg} L^3}{k_l \mu_l (T_{sat} - T_w)} \right]^{1/4} \left[(\sqrt{b+1} - 2\sqrt{b})(\sqrt{b} + \sqrt{b+1})^{1/2} + \sqrt{2}b^{3/4} \right], \quad (210)$$

$$\delta = \left(\frac{4\mu_l k_l (T_{sat} - T_w) L}{\rho_l (\rho_l - \rho_v) g \sin(\alpha) h'_{fg}} \right)^{1/4} \left(\sqrt{b} + \sqrt{b + \frac{x}{L}} \right)^{1/2}, \quad (211)$$

and

$$b = \frac{\delta_0^4 \rho_l (\rho_l - \rho_v) g \sin(\alpha) h'_{fg}}{16 \mu_l k_l (T_{sat} - T_w) L}. \quad (212)$$

The tangent line equation for the ellipse is:

$$\frac{xx_0}{h_b^2} + \frac{yy_0}{r^2} = 1. \quad (213)$$

From equation (213), points $(0, y^*)$ and $(x^*, 0)$ can be found:

$$(0, y^*): y^* = \frac{h_b^2}{y_0}; \quad (x^*, 0): x^* = \frac{r^2}{x_0}. \quad (214)$$

From figure 64, coordinates x_0 and y_0 can be found:

$$y_0 = h_b - h_1; \quad x_0 = r \sqrt{\frac{h_1}{h_d} \left(2 - \frac{h_1}{h_d} \right)}. \quad (215)$$

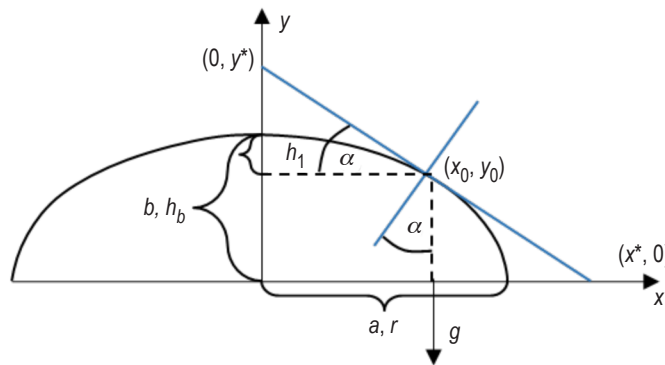


Figure 64. Angle α calculation schematic.

From figure 64, equations (214) and (215), it can be found that:

$$\tan(\alpha) = \frac{y^*}{x^*} = \frac{h_d}{r} \sqrt{\frac{\bar{h}_1(2-\bar{h}_1)}{(1-\bar{h}_1)^2}}, \quad (216)$$

where $\bar{h}_1 = \frac{h_1}{h_d}$,

and

$$\sin(\alpha) = \frac{\tan(\alpha)}{\sqrt{1+\tan^2(\alpha)}}, \quad \cos(\alpha) = \frac{1}{\sqrt{1+\tan^2(\alpha)}}. \quad (217)$$

B.4.3 Lower Dome

As shown by Oosthuizen⁸, the condensation on the upper side of the inclined plate can be described by the Nusselt equations, where the free-falling acceleration is replaced by the product $g \sin(\beta)$. In this case, β is an angle between the tangent line and free-fall acceleration. For the condensation on the lower dome, equations (210)–(212) convert to:

$$\bar{N}u_l = \frac{\bar{h}_l L}{k_l} = 0.9428 \left[\frac{g \sin(\beta) \rho_l (\rho_l - \rho_v) h'_{fg} L^3}{k_l \mu_l (T_{sat} - T_w)} \right]^{1/4} \left[(\sqrt{b+1} - 2\sqrt{b})(\sqrt{b} + \sqrt{b+1})^{1/2} + \sqrt{2}b^{3/4} \right] \quad (218)$$

and

$$\delta = (kL)^{1/4} \left(\sqrt{b} + \sqrt{b + \frac{x}{L}} \right)^{1/2} = \left(\frac{4\mu_l k_l (T_{sat} - T_w) L}{\rho_l (\rho_l - \rho_v) g \sin(\beta) h'_{fg}} \right)^{1/4} \left(\sqrt{b} + \sqrt{b + \frac{x}{L}} \right)^{1/2}, \quad (219)$$

where

$$b = \frac{\delta_0^4}{4kL} = \frac{\delta_0^4}{16} \frac{\rho_l (\rho_l - \rho_v) g \sin(\beta) h'_{fg}}{\mu_l k_l (T_{sat} - T_w) L},$$

$$k = \frac{4\mu_l k_l \Delta T}{\rho_l (\rho_l - \rho_v) g \sin(\beta) h'_{fg}},$$

$$h'_{fg} = h_{fg} (1 + 0.68Ja),$$

$$Ja = \frac{c_{pl} (T_{sat} - T_w)}{h_{fg}}.$$

Figure 65 shows the condensation on the lower dome.

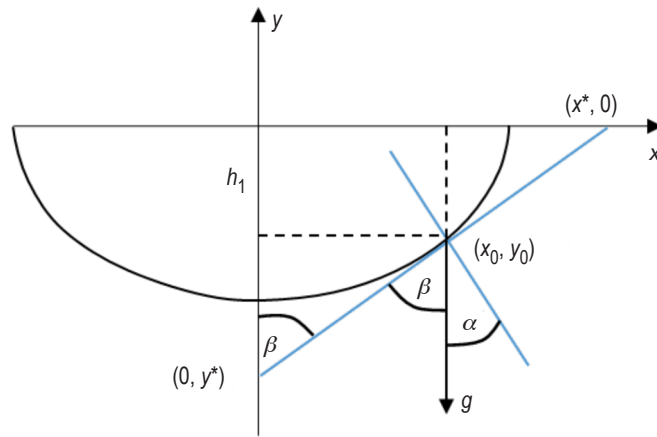


Figure 65. Condensation on the lower dome.

B.4.4 Angle β Calculation.

Because $\alpha + \beta = 90^\circ$, $\tan(\beta) = \cot(\alpha) = \frac{1}{\tan(\alpha)}$, or $\tan(\beta) = \frac{r}{h_b} \sqrt{\frac{(1 - \bar{h}_l)^2}{\bar{h}_l(2 - \bar{h}_l)}}$,

and $\sin(\beta) = \frac{\tan(\beta)}{\sqrt{1 + \tan^2(\beta)}}$.

APPENDIX C—TANK THERMODYNAMIC VENTING PRESSURE CONTROL SYSTEMS

C.1 Liquid Film Heat Transfer

To make calculations, the wall is divided into layers and the number of these layers are equal to the number of sprays receiving the wall. For each layer, the mass flow rate, velocity of the liquid, and thickness of the liquid film can be found. Assume that droplets in the ullage and liquid in the film on the wall have no friction losses. In this case, the distance between two sequential droplets reaching the wall can be found using the initial distance between the orifices and orthogonal component of the droplet velocity (fig. 66).

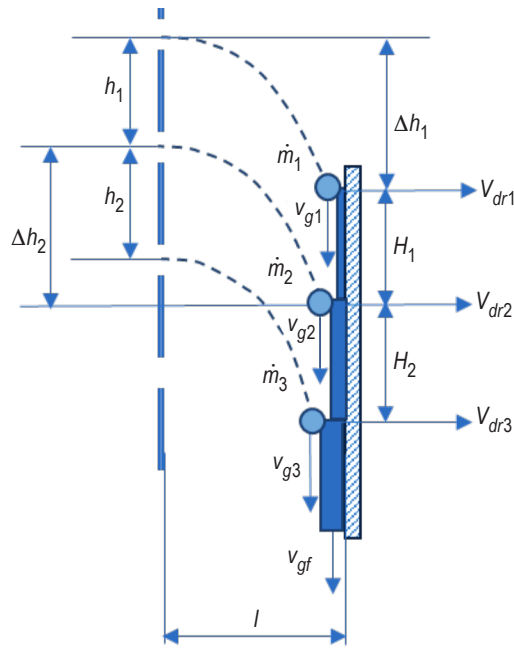


Figure 66. Heat and mass transfer in the liquid film.

$$H_1 = h_1 + \Delta h_2 - \Delta h_1; \quad \Delta h_1 = \frac{g}{2} \left(\frac{l}{V_{dr1}} \right)^2; \quad \Delta h_2 = \frac{g}{2} \left(\frac{l}{V_{dr2}} \right)^2. \quad (220)$$

From equation (220), one can get:

$$H_1 = h_1 + \frac{gl^2}{2} \left(\frac{1}{V_{dr2}^2} - \frac{1}{V_{dr1}^2} \right), \quad H_2 = h_2 + \frac{gl^2}{2} \left(\frac{1}{V_{dr3}^2} - \frac{1}{V_{dr2}^2} \right). \quad (221)$$

In general, for each orifice H_i can be written as:

$$H_i = h_i + \frac{gl^2}{2} \left(\frac{1}{V_{dr(i+1)}^2} - \frac{1}{V_{dri}^2} \right). \quad (222)$$

In the beginning and in the end of each layer, the mass flow rates and velocities of the liquid can be found. In the beginning of the layer,

$$\dot{m}_{b(i+1)} = \dot{m}_{fi} + \dot{m}_{i+1} - \Delta\dot{m}_{imp(i+1)} \quad (223)$$

and

$$v_{b(i+1)} = \frac{\dot{m}_{fi} v_{fi} + [\dot{m}_{i+1} - \Delta\dot{m}_{imp(i+1)}] v_{i+1}}{\dot{m}_{fi} + [\dot{m}_{i+1} - \Delta\dot{m}_{imp(i+1)}]}. \quad (224)$$

In the end of the layer,

$$\dot{m}_{f(i+1)} = \dot{m}_{b(i+1)} - \Delta\dot{m}_{evap(i+1)} \quad (225)$$

and

$$v_{f(i+1)} = v_{b(i+1)} + \sqrt{2gH_{i+1}}. \quad (226)$$

APPENDIX D—TANK AXIAL JET THERMODYNAMIC VENTING PRESSURE CONTROL SYSTEMS

D.1 Heat and Mass Transfer on the Ullage-Liquid Interface During Axial Jet Mixing

To calculate heat and mass transfer on the interface, the following assumptions were made:

- Buoyancy effects are insignificant, $Ri \equiv \frac{\beta_b g \Delta T L_b}{v_b^2} < 1$.
- Bulk liquid Prandtl number is lower than 6, $1 < Pr_b \equiv \frac{\mu_b c_{pb}}{k_b} < 6$.
- Bulk liquid Jacob number is small, $Ja \equiv \frac{c_{pb} \Delta T}{h_{fg}} < 0.2$.
- Ullage-liquid interface is turbulent, $350 < Re \equiv \frac{\rho_b v_b L_b}{\mu_b} < 11,000$.
- Jet is fully turbulent, $Re_j \equiv \frac{\rho_j v_j d}{\mu_j} > 2,300$.
- Jet nozzle diameter is small compared to the nozzle submergence, $d \ll s$.
- L_b is a turbulent linear scale.

From figure 67, the jet diameter at any height, x , can be calculated as $D(x) = d + 2 \tan(\alpha/2)x$. When a jet reaches the interface, its diameter is $D_j = d + 2 \tan(\alpha/2)s$. If a diameter of the jet is larger than the interface diameter, the result is high nozzle submergence; if smaller, low nozzle submergence. The boundary between these two cases can be found when diameters are equal: $D_j = D_{int}$, or $D_{int} = d + 2 \tan(\alpha/2)s$.

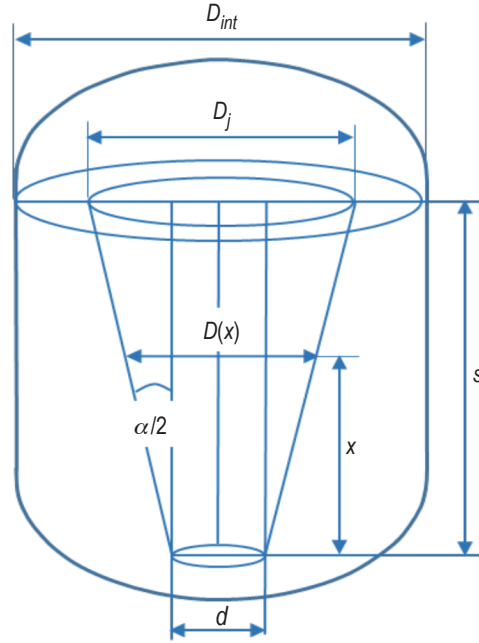


Figure 67. Geometrical parameters of axial jet.

The boundary submergence, s/D_{int} , follows:

$$\frac{s}{D_{int}} = \frac{1}{2 \tan(\alpha/2)} \left(1 - \frac{d}{D_{int}} \right) . \quad (227)$$

From equation (227), it follows that $\frac{s}{D_{int}} < \frac{1}{2 \tan(\alpha/2)} \left(1 - \frac{d}{D_{int}} \right)$ is a low nozzle submergence

and $\frac{s}{D_{int}} \geq \frac{1}{2 \tan(\alpha/2)} \left(1 - \frac{d}{D_{int}} \right)$ is a high nozzle submergence.

As shown by Tollmien⁴⁸, angle α of the jet expansion in the same liquid is about $11^\circ \div 12^\circ$. Dominick⁴⁹ suggested correlation for the expansion angle, which for SI units is as follows:

$$\tan\left(\frac{\alpha}{2}\right) = 0.8252(\nu)^{0.135}, \quad (228)$$

where ν is a kinematic viscosity of liquid, m^2/s .

D.2 Helicoidally Coiled Tube-in-Shell Heat Exchanger Transfer

Hydraulic diameter for the flow inside a coiled pipe can be found by the standard equation $D_{hvp} = 4A/P$.

From figure 68, the area of ellipse is $A = \pi Dd/4$. The first Ramanujan's formula for the perimeter of the ellipse follows:

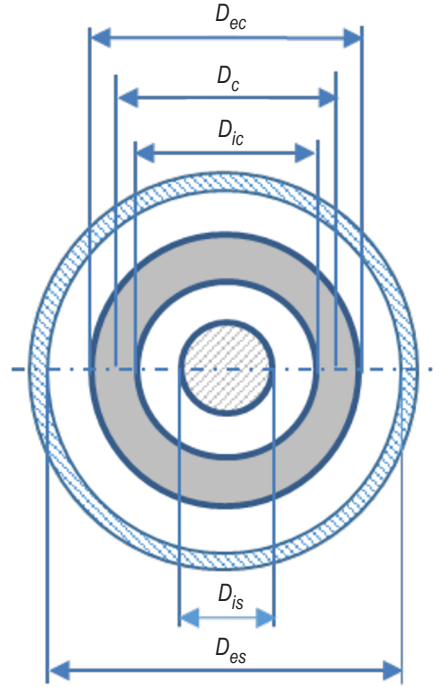


Figure 68. Geometrical parameters of helicoidally coiled tube-in-shell heat exchanger.

$$P = \frac{\pi}{2} \left[3(D+d) - \sqrt{(3a+b)(a+3b)} \right] \quad (229)$$

can be modified to

$$P = \frac{\pi}{2} (D+d) \left(3 - \sqrt{4 - h_{in}} \right), \quad (230)$$

where $h_{in} = \left[\frac{(D-d)}{(D+d)} \right]^2$ (from fig. 26(a)).

From equation (230), the hydraulic diameter for the elliptical tube can be found:

$$D_{hvp} = \frac{4A}{P} = \frac{2Dd}{(D+d)(3-\sqrt{4-h_{in}})} \quad (231)$$

As can be seen in figure 68, the open area on the shell can be calculated as:

$$A_s = \frac{\pi}{4} \left[D_{es}^2 - D_{is}^2 - (D_{ec}^2 - D_{ic}^2) \right] \quad (232)$$

From figure 26(a), $D_{ec} = D_c + d + 2\delta$ and $D_{ic} = D_c - d - 2\delta$. In this case, the open area is:

$$A_s = \frac{\pi}{4} \left[D_{es}^2 - D_{is}^2 - 4D_c(d + 2\delta_{vp}) \right] \quad (233)$$

The mass flux in the shell side can be found by:

$$G_{shell} = - \frac{4\dot{m}_{shell}}{\pi \left[D_{es}^2 - D_{is}^2 - 4D_c(d + 2\delta_{vp}) \right]} \quad (234)$$

Hydraulic diameter for the shell side can be found by $D_{hs} = 4V/S$, as suggested by Patil⁵⁰, which is equivalent to the standard formula $D_h = 4A/P$ for the cylindrical geometry. The free volume for the shell side can be calculated as follows (assume the heat exchanger takes n coils with total length, L):

$$L = n\sqrt{\pi^2 D_c^2 + p^2} = np\sqrt{1 + \left(\frac{\pi D_c}{p}\right)^2} = np\sqrt{1 + \gamma^{-2}}, \quad (235)$$

where

p is pitch of a helicoidally coiled pipe, m
 $\gamma = p/\pi D_c$ is a dimensionless pitch.

With this assumption, the open (free) volume of the shell side is:

$$\begin{aligned} V_s &= np\frac{\pi}{4} (D_{es}^2 - D_{is}^2) - np\frac{\pi}{4} \left[(D + 2\delta_{vp})(d + 2\delta)\sqrt{1 + \gamma^{-2}} \right] \\ &= np\frac{\pi}{4} \left\{ (D_{es}^2 - D_{is}^2) - \left[(Dd + 2\delta_{vp})(D + d) \right] \sqrt{1 + \gamma^{-2}} \right\}. \end{aligned} \quad (236)$$

Total area of the shell side can be calculated as:

$$A_s = np\pi(D_{es} + D_{is}) + npP_s\sqrt{1+\gamma^{-2}} = np\left[\pi(D_{es} + D_{is}) + P_s\sqrt{1+\gamma^{-2}}\right]. \quad (237)$$

Replacing the external perimeter of the coiled pipe by Ramanujan's formula gives:

$$A_s = np\left[\pi(D_{es} + D_{is}) + \frac{\pi}{2}np(D + d + 4\delta_{vp})(3 - \sqrt{4 - h_s})\sqrt{1+\gamma^{-2}}\right]. \quad (238)$$

In this case, the shell side hydraulic diameter is:

$$D_{hs} = 2 \frac{D_{is}^2 - D_{es}^2 - [Dd + 2\delta_{vp}(D + d)]\sqrt{1+\gamma^{-2}}}{2(D_{is} + D_{es}) + (D + d + 4\delta_{vp})(3 - \sqrt{4 - h_s})\sqrt{1+\gamma^{-2}}}, \quad (239)$$

where $h_{is} = \left[\frac{(D - d)}{(D + d + 4\delta_{vp})}\right]^2$.

D.3 Heat Transfer at Low Acceleration Conditions

Assuming that the plot of the approximation function would go through three points of the graph calculated by Surface Evolver, from figure 28 the following can be found:

$$A_1 = a + b \frac{1 - \left(\frac{Bo_1}{Bo_3}\right)^m}{1 + k_a \left(\frac{Bo_1}{Bo_3}\right)^m}, \quad A_2 = a + b \frac{1 - \left(\frac{Bo_2}{Bo_3}\right)^m}{1 + k_a \left(\frac{Bo_2}{Bo_3}\right)^m}, \quad \text{and} \quad A_3 = a + b \frac{1 - \left(\frac{Bo_3}{Bo_3}\right)^m}{1 + k_a \left(\frac{Bo_3}{Bo_3}\right)^m}. \quad (240)$$

Solving the system of equations (240), it can be found that

$$a = A_3, \quad (241)$$

$$k_a = \frac{(A_1 - A_3)(1 - Bo_{23}) - (A_2 - A_3)(1 - Bo_{13})}{(A_2 - A_3)(1 - Bo_{13})Bo_{23} - (A_1 - A_3)(1 - Bo_{23})Bo_{13}}, \quad (242)$$

and

$$b = (A_1 - A_3) \left(\frac{1 + k_a Bo_{23}}{1 - Bo_{23}} \right), \quad (243)$$

where

$$Bo_{13} = \left(\frac{Bo_1}{Bo_3} \right)^m \quad \text{and} \quad Bo_{23} = \left(\frac{Bo_2}{Bo_3} \right)^m ,$$

A_1, A_2, A_3 – interface areas or dry wall areas corresponding to three chosen points on the graph

Bo_1, Bo_2, Bo_3 – Bond numbers corresponding to the same three chosen points on the graph
 m – a coefficient that can be found with the least squares method or graphically for the best match with the Surface Evolver data.

Point 1 on figure 28 corresponds to very low Bond numbers (actually, $Bo = 0$), when all gas volume is inside the liquid phase and the dry wall area disappears. Point 3 corresponds to high Bond numbers, where gas-liquid interface is flat and both relative areas are equal to the unit. Point 3 can be taken as inflection points of the graph (fig. 28(a)) or as a minimum point on the interface area graph and an inflection point on the dry wall area (fig. 28(b)). On both interface and dry area lines, point 2 can be different.

APPENDIX E—COMPUTER MODEL DESCRIPTION

E.1 Input Files Description

The following eight items describe the input files:

(1) Address file (fig. 69)

– ‘*TankSIM_Addr_Input.txt*’

– Includes Input-Output folder address and file number assignments for TankSIM input and output open file procedures.

– Should be in the same folder as the TankSIM (‘*TankSIM.f90*’) source file.

All files in figure 69 should be in the In-Out folder.

```
TanSIM.F90 Address Input File
-----
Path, 40 positions
-----
'..\TankSIM_InOut'
-----
PathServ, 40 positions
-----
'..\TankSIM_Serv'
-----
Fn1  Fn2  Fn3  Fn4  Fn5  Fn6  Fn7  Fn8  Fn9  Fn10  Fn11  Fn12  Fn13  Fn14  Fn15  Fn16  Fn17
-----
1    2    3    4    5    6    7    8    9    10   11   12   13   14   15   16   17
-----
```

Figure 69. TankSIM address input file.

(2) TankSIM input file (fig. 70)

– ‘*TankSIM_Input.txt*’

– Includes fluid, initial conditions—pressures, temperatures, flow rates, external heat flows, calculation time, and time steps for regular and mixing regimes.

```

TankSIM.f90 Input File
-----
fluid,8pos.
-----
'Hydrogen'
-----
pheini,kPa  pvini,kPa  tuini,K  tlini,K  tuwini,K  tlwini,K  tkwlini,m  full,%
-----
0.0          110.117    20.8021  20.6632  20.9443   20.675    0.0         90.0
-----
phest,kPa   thesti,K    dhest,mm tkhest,mm vhest,m^3  Helium
-----
0.0         294.0      4.0       1.0       2.7835
-----
Tank
-----
brktime,s   iplotreg,-  iplotmix,-  itesti,-  flgpri,-
-----
8360.5      1           1           5         3
-----
tent,K      penv,kPa    casenum,25pos.
-----
210.0      103.0      1234567890123456789012345--
'H2_90%d3_9-50_2W_81d'
-----

```

Figure 70. TankSIM input file.

(3) Mission profile input file (fig. 71)

– ‘*TankSIM_Mission_Profile.txt*’

– Includes mission profile information—number of mission phases, regimes information, mission time, time steps, heat loads, pressure regulation ranges, flow rates, pump parameters, and other information.

```

TankSIM Mission Profile Input File
-----
nmtl
-----
6
-----
===== Lift - Off =====1
flgmis,3pos dtmis,s  tmstep,s  prtmis,-
-----8
'Slf'      1.0d5    0.1      1
-----
qext,W  qheatu,W  qheatl,W  gr,-  teta,degr  pumin,kPa  pumax,kPa  plmin,kPa  plmax,kPa  flgpcl  regime,4pos
-----10
100.0   0.0       0.0       1.0    0.0        131.0      138.0      131.0      133.0    1      'barh'
-----
flgback,7pos.  kfri,-  kdevi,-  mdvent,kg/s  Lohm,1/ft^2  pbacki,kPa  dback,mm  cdor,-  deltmix,s  iptmix,
-----
'orifice'      0.0     880.0    1.0e-3    1000.0     20.7       4.4       0.6       0.1       1
-----
vdgpm,gpm  JT & Pump
----- data  20
30.0
-----
p0,kPa  p1,-  p2,-  p3,-  p4,-  p5,-  Pump
----- Dp
4.85910d+00  -3.72393d-02  8.40148d-03  -4.45719d-04  5.24202d-6  0.0  curve
-----
e0,W  e1,-  e2,-  e3,-  e4,-  e5,-  Pump
----- energy
25.8  0.0  0.0  0.0  0.0  0.0  curve
-----
===== Coast 1 =====30
flgmis,3pos dtmis,s  tmstep,s  prtmis,-
-----
'Slf'      2645.146  0.1      200
-----

```

Figure 71. TankSIM mission profile input file.

```

qext,W qheatu,W qheatl,W gr,- teta,degr pumin,kPa pumax,kPa plmin,kPa plmax,kPa flgpcc regime,4pos
-----
300.0 0.0 0.0 0.003 0.0 131.0 138.0 131.0 132.0 1 'ullg'
-----
flgback,7pos. kfri,- kdevi,- mdvent,kg/s Lohm,1/ft^2 pbacki,kPa dback,mm cdor,- deltmix,s iprtmix,-
-----
'orifice' 0.0 880.0 1.0 1.0 1.0 4.4 0.6 0.1 20
-----
vdgpm,gpm Pump
----- flow data
1.0
-----
p0,kPa p1,- p2,- p3,- p4,- p5,- Pump
----- Dp
5.38106d+00 1.90193d-03 -2.13456d-04 0.0 0.0 0.0 curve
----- 50
e0,W e1,- e2,- e3,- e4,- e5,- Pump
----- energy
30.0 0.0 0.0 0.0 0.0 0.0 curve
-----
===== Chillover =====3
flgmis,3pos dtmis,s tmstep,s prtmis
-----
'Chl' 10.0 0.1 1
-----
mdch,kg/s
----- 60
0.9
===== Pre-Press =====4
flgmis,3pos dtmis,s tmstep,s prtmis
-----
'Hep' 20.0 0.1 1
-----
puhp,kPa dpuhp,-
-----
193.0 0.05
===== Firing =====70=====5
flgmis,3pos dtmis,s tmstep,s prtmis
-----
'Fir' 44.88 0.1 1
-----
mdlf,kg/s pufir,kPa dpufir,kPa flgprs pvp,kPa tvp,K hvp,kJ/kg gr,- teta,degr
-----
2.0125 186.2 0.03 0 4585.0 175.0 2217.2 0.193 0.0
-----
===== Cost 2 =====6
flgmis,3pos dtmis,s tmstep,s prtmis,-
----- 80
'Slf' 250000.0 0.1 10000
-----
qext,W qheatu,W qheatl,W gr,- teta,degr pumin,kPa pumax,kPa plmin,kPa plmax,kPa flgpcc regime,4pos
-----
54.0 0.0 0.0 0.003 0.0 131.0 138.0 131.0 132.0 1 'barh'
-----
flgback,7pos. kfri,- kdevi,- mdvent,kg/s Lohm,1/ft^2 pbacki,kPa dback,mm cdor,- deltmix,s iprtmix,-
-----
'orifice' 0.0 880.0 1.0e-3 1000.0 20.7 4.4 0.7 0.1 1
-----
vdgpm,gpm Pump
----- flow data
30.0
-----
p0,kPa p1,- p2,- p3,- p4,- p5,- Pump
----- Dp
5.001696E+00 6.405861E-02 -5.161413E-03 3.415321E-05 0.0 0.0 curve
-----
e0,W e1,- e2,- e3,- e4,- e5,- Pump
----- energy 100
4.28571E-01 -8.77778E-02 5.14286E-03 2.84444E-03 0.0 0.0 curve
-----

```

Figure 71. TankSIM mission profile input file (Continued).

(4) Tank input file (fig. 72)

– ‘TankSIM_Tank.txt’

– Includes tank information—material, shape, tank measurements, and tank material specific heat and heat conduction table as a function of temperature.

```
TankSIM Tank input file, MHTB
-----
tmater,8pos.   tshape,10pos.   flgadd,-
-----
'Alum5083'     'Elliptical '   0
-----
dtank,m       hcyl,m         hbulk,m        tkw,m          vaddt,m^3      ptmax,kPa      rhow,kg/m^3    ksi,-
-----
3.048         1.524          0.762          0.0127        0.0            344.0         2700.0         0.0
-----
nmet
-----
16
```

----- Tank Material properties -----		
tm _{met} ,K	cp _{met} ,J/(kg*K)	k _{met} ,W/(m*K)
10	1.573040847	8.426670258
15	3.853604493	12.84981814
20	8.854270289	17.21229475
30	33.44547565	25.42986843
40	81.95717957	32.88862558
50	148.8382155	39.66304975
60	223.6378248	45.85432776
70	298.2954404	51.54876507
80	368.6691736	56.8145777
90	433.333574	61.70539924
100	492.1981761	66.26405365
110	545.6466744	70.52547741
120	594.1292376	74.51880941
130	638.0174392	78.26885478
140	677.5840155	81.79711056
150	713.0313602	85.12249119

Figure 72. TankSIM tank input file.

- (5) Spray bar, heat exchanger, and pump input file (fig. 73)
 – ‘*TankSIM_SprayBar.txt*’
 – Includes spray manifold, injection pipes, and heat exchanger measurements and properties.

```

Spray Bar, Heat Exchanger and Pump Input File, MHTB
-----
dmno,m    thmn,m    lmn,m    kmn,W/(m*K)  ltop,m  nbar,-  Spray
-----
0.03175   8.89d-4   2.7877   10.2         0.054   1       manifold
-----
kmni,-    kmnf,-
-----
314.5     1242.8
-----
dito,m    thit,m    lit,m    dzsi,m    norsi,-  norit   ninj,-  Injection
-----
0.0127    7.1d-4    2.645    0.061     42      1       4       tube
-----
ditom,m   thitm,m   litm,m   dzsim,m   nortop,-  norimn  lspr,m  flgtop,-  Injection
-----
0.051     0.0413    0.14     0.089     1       4       1.5     1       tube
manifold
-----
ks,-      cds,-     nlim
-----
1.56      0.8       200
-----
nsec
-----
1
-----
node(nsec)  dorf(nsec),mm
-----
43         1.7
-----
dexo,m     thex,m     lex,m     xei,-     nex,-     alhex,deg  Heat
-----
0.0381     8.89d-4    2.67      0.0       21       0.0       exchanger
-----
kvent,-    Pump
-----
1          flow
-----
1          data
  
```

Figure 73. TankSIM spray bar input file.

- (6) Axial jet input file (fig. 74)
 - ‘*TankSIM_AxialJet.txt*’
 - Includes axial jet nozzle and helicoidally coiled heat exchanger measurements and pressure drop coefficients.

```

TankSIM Axial Jet Input File
-----
bet1,-    bet2,-    hj,m      dj,m      nzj,-
-----
0.34      0.24      1.3       0.08382  1
-----
dexo1,m   dexo5,m   thex,m    dmno,m    dmni,m    alhex,deg
-----
3.4925d-2 3.4925d-2 1.651d-3  0.3175    0.05715   90.0
-----
dcoil,m   pitch,m   nex,-     kex,W/(m*K) xei
-----
0.187325  3.9688d-2 51        17.22     0.12
-----
kmni,-    kmnf,-
-----
2.44      3.13
-----
kvent,-   Qexji,W
-----
1         15720
-----

```

Figure 74. TankSIM axial jet input file.

- (7) Optional external lines input (fig. 75)
 - ‘*TankSIM_Tank_Add_Feed.txt*’
 - ‘*TankSIM_Tank_Add_Pres.txt*’
 - ‘*TankSIM_Tank_Add_Vent.txt*’ (example of this file presented in fig. 75)
 - These files have the same structure and include internal volume, connected to the ullage, environmental and approximate pipe temperatures, line segment measurements, and constant thermophysical properties.


```

TankSIM Tank Vent Line input file
-----
vaddv,m^3      tcv,K      thv,K      tenv,K      tcgv,K      thgv,K
-----
2.2733E-02    140.0     179.0     250.0     113.0     114.0
-----
nsegv,-
-----
5
*****
lv,           dv,           tkwv,         epsv,         rhowv,        cpav,         kav,          rthv
m            m            m            -            kg/m^3        J/(kg*K)     W/(m*K)      m
-----
0.26416     0.0603     1.5875E-03   0.0015     7920.        300.0        10.2         1.5E-05
7.7724     0.0603     1.5875E-03   0.015      7920.        300.0        10.2         1.5E-05
0.762      0.0221     1.651E-03    0.015      7920.        300.0        10.2         1.5E-05
1.524      0.01021    1.2446E-03   0.015      7920.        300.0        10.2         1.5E-05
5.791      0.00472    8.128E-04    0.015      7920.        300.0        10.2         1.5E-05
*****

```

Figure 75. TankSIM external venting line input file.

(8) Main output file (fig. 76)

– ‘*TankSIM_20160830_110721_1_Out-H2_90%d3_9-50_2W_81d.csv*’

– Includes all initial and calculated information. The length of the record (line) may consist of 55 columns of data depending on TVS type.

TankSIM - Tank System Integrated Model - .CSV output																			
File:	TankSIM_20160830_110721_1_Out-H2_90%d3_9-50_2W_81d.csv																		
Fluid:	Hydrogen																		
Tank Measurements																			
Tmater	Tshape	Flgadd	Dtank	Hcyl	Hbulk	Tkw	Vaddt	Ptmax	Rhow										
Alum5083	Elliptical	0	3.05E+00	1.52E+00	7.62E-01	1.27E-02	0.00E+00	3.44E+05	2.70E+03										
Mission Profile																			
Phase	Duration	Fin time	Delt reg	Prt reg															
Sif	4.80E+04	4.80E+04	1.00E-01	100	Qext	Qheatu	Qheatl	Gr	Teta	Pumin	Pumax	Plmin	Plmax	Flgpcl	Regime	Flgback			
					0.00E+00	5.90E+00	4.82E+01	1.00E+00	0.00E+00	1.31E+02	1.38E+02	1.31E+02	1.32E+02	2	barh	orifice			
					Vdgp	P0	P1	P2	P3	P4	P5	E0	E1	E2	E3	E4			
					3.00E+01	4.86E+00	-3.72E-02	8.40E-03	-4.46E-04	5.24E-06	0.00E+00	2.58E+01	0.00E+00	0.00E+00	0.00E+00	0.00E+00			
Regime	Time	Time h	Pu	Plsat	Tu	TI	Tuw	Tlw	Tint	Pv	Phe	Bond	MI	MI Lost	Fill	Del Fill			
-	sec	hour	kPa	kPa	K	K	K	K	K	kPa	kPa	-	kg	kg	%	%			
Sif	0	0	110.1172	110.4056	20.80212	20.6632	20.94451	20.67536	20.67272	110.1172	0	8.32E+05	1.15E+03	2.98E-06	90				
Sif	10	0.003	110.1489	110.4056	20.80548	20.6632	20.9652	20.69187	20.67295	110.1489	0	8.32E+05	1.15E+03	7.30E-04	89.9983				
Sif	20	0.006	110.2186	110.4056	20.8107	20.6632	20.98571	20.69398	20.67331	110.2186	0	8.32E+05	1.15E+03	1.77E-03	89.9981				
Sif	30	0.008	110.291	110.4056	20.81613	20.6632	21.00605	20.69423	20.67369	110.291	0	8.32E+05	1.15E+03	2.84E-03	89.9979				
Sif	40	0.011	110.3637	110.4057	20.82158	20.6632	21.02622	20.69426	20.67407	110.3637	0	8.32E+05	1.15E+03	3.93E-03	89.9977				
Sif	50	0.014	110.4073	110.4066	20.82482	20.66323	21.04623	20.69428	20.67432	110.4073	0	8.32E+05	1.15E+03	4.57E-03	89.9976				
Sif	60	0.017	110.4096	110.4089	20.82495	20.66331	21.06607	20.69435	20.6744	110.4096	0	8.32E+05	1.15E+03	4.58E-03	89.9977				
Sif	70	0.019	110.412	110.4113	20.82509	20.66338	21.08574	20.69443	20.67448	110.412	0	8.32E+05	1.15E+03	4.59E-03	89.9978				
Sif	80	0.022	110.4144	110.4136	20.82523	20.66345	21.10525	20.69451	20.67456	110.4144	0	8.32E+05	1.15E+03	4.60E-03	89.9979				
Sif	90	0.025	110.4161	110.416	20.82533	20.66353	21.12459	20.69459	20.67463	110.4161	0	8.32E+05	1.15E+03	4.60E-03	89.998				
Sif	100	0.028	110.4185	110.4183	20.82549	20.6636	21.14377	20.69467	20.67471	110.4185	0	8.32E+05	1.15E+03	4.61E-03	89.9981				
Sif	110	0.031	110.421	110.4207	20.82565	20.66367	21.16279	20.69475	20.67479	110.421	0	8.32E+05	1.15E+03	4.63E-03	89.9982				
Sif	120	0.033	110.4236	110.423	20.82582	20.66375	21.18166	20.69483	20.67487	110.4236	0	8.32E+05	1.15E+03	4.64E-03	89.9983				
Sif	130	0.036	110.4254	110.4254	20.82594	20.66382	21.20037	20.69491	20.67495	110.4254	0	8.32E+05	1.15E+03	4.64E-03	89.9984				

Figure 76. TankSIM main output file.

E.2 Variables Description for Input and Output Files

Table 4 lists the description of the variables for the input and output files.

Table 4. Variables description for input and output files.

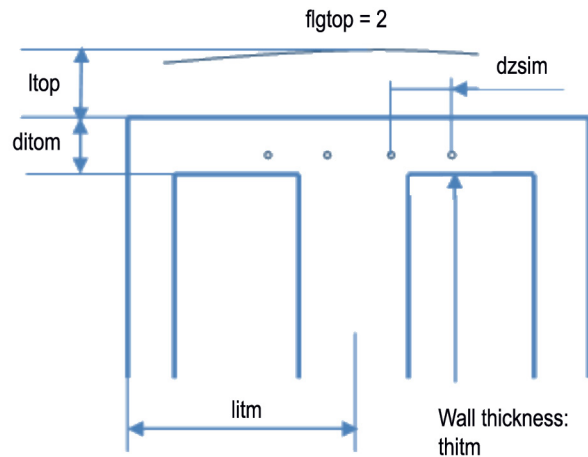
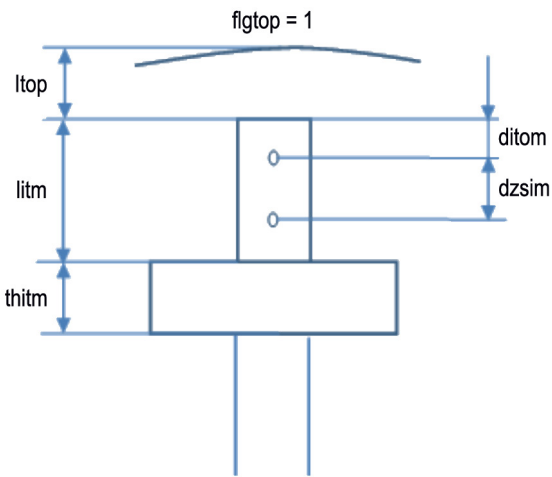
Description of TankSIM Input and Output Files Variables		
Address File (TankSIM_Addr_Input.txt)		
Path	Path to the InOut folder	40 pos.
PathServ	Path to the folder for service files	40 pos.
FN1-FN17	Working file numbers	-
Mission Profile File (TankSIM_Mission_Profile.txt)		
Common		
flgmis	Mission phase flag: 'Sif' - self pressurization; 'Chl' - feed line chilldown; 'Hep' - non-condensable gas pressurization; 'Fir' - engine firing; 'Lqf' - wall liquefaction	3 pos.
dtmiss	Mission duration	sec
tmstep	Time step for calculation	sec
prtmis	Number of records, skipping during printing	-
'Sif'		
qext	Uniformly distributed heat loads	W
qheatu	Constant flow rate to the ullage (usually from supporting elements, manholes, etc.)	W
qheatl	Constant flow rate to the liquid (usually from supporting elements, manholes, etc.)	W
gr	Vehicle acceleration-to-g ratio	-
teta	Angle between thrust vector and tank longitudinal axis	degree
pumin	Minimum required ullage pressure	kPa
pumax	Maximum required ullage pressure	kPa
plmin	Minimum required liquid saturation pressure	kPa
plmax	Maximum required ullage liquid saturation pressure	kPa
flgpcl	Ullage pressure control logic flag: 1 - control by ullage and liquid saturation pressures independently 2 - control by ullage pressure only 3 - control by liquid saturation pressure only	-
regime	Pressure control regime: 'barm' - spray bar mixing, no venting; 'barh' - spray bar TVS; 'jetm' - axial jet mixing, no venting; 'jeth' - axial jet TVS; 'ullg' - ullage venting; 'sbul' - ullage venting and spray bar mixing; 'preg' - ullage pressure regulation; 'prbm' ---"--- with spray bar mixing; 'prbh' ---"--- spray bar TVS; 'prjm' ---"--- axial jet mixing; 'prjh' ---"--- axial jet TVS; 'prul' ---"--- ullage venting; 'boff' - boil-off	4 pos.
flgback	Back pressure device: 'orifice' - critical orifice; 'venturi' - critical Venturi; 'prconst' - constant backpressure	7 pos.

Description of TankSIM Input and Output Files Variables (Continued)		
kfri	Friction pressure lost coefficient from the pump to the heat exchanger (vent line)	
kdevi	Device pressure lost coefficient from the pump to the vent line (valves, flowmeters)	
mdvent	Initial vent flow rate	kg/sec
Lohm	Joule-Thomson device resistance (for Lee equation)	1/ft ²
pbacki	Initial backpressure	kPa
dback	Diameter of backpressure device	mm
cdor	Back pressure orifice discharge coefficient	-
deltmix	Time step for calculation during TVS functioning	sec
iprtmix	Number of records, skipping during printing (TVS functioning)	
vdgpm	Pump volumetric flow rate	gpm
p0	Constant pump Delta P (all other coefficients = 0) or free term in Delta P vs. Flow Rate curve	kPa
p1...p5	Coefficients for Delta P (kPa) vs. Flow Rate (gpm) curve (5-th order maximum)	-
e0	Constant pump Power (all other coefficients = 0) free term in Power vs. Flow Rate curve	W
e1...e5	Coefficients for Power (W) vs. Flow Rate (gpm) curve (5-th order maximum)	-
'Chl'		
mdch	Feed line chilling down mass flow rate	kg/sec
'Hep'		
puhp	Nominal start box pressure	kPa
dpuhp	Start box pressure margin (ratio)	-
'Fir'		
mdlf	Propellant mass flow rate during firing	kg/sec
pufir	Nominal run box pressure	kPa
dpufir	Run box pressure margin (ratio)	-
figprs	Pressurization flag: 0 - autogenous; 1 - non-condensable	-
pvp	Pressure of pressurization vapor or gas entering tank	kPa
typ	Temperature of pressurization vapor or gas entering tank	K
hvp	Enthalpy of pressurization vapor or gas entering tank	kJ/kg
gr	Vehicle acceleration-to-g ratio	-
teta	Angle between thrust vector and tank longitudinal axis	degree
'Lqf'		
qext	Uniformly distributed heat loads	W
qcrc	Uniformly distributed heat eliminating by cryocooler	W
qheatu	Constant flow rate to the ullage (usually from supporting elements, manholes, etc.)	W
qheatl	Constant flow rate to the liquid (usually from supporting elements, manholes, etc.)	W
gr	Vehicle acceleration-to-g ratio	-
teta	Angle between thrust vector and tank longitudinal axis	degree
mdlqf	Propellant vapor mass flow rate liquefaction	kg/sec
pulqf	Nominal run box pressure	kPa
dpulqf	Run box pressure margin (ratio)	-
pvp	Pressure of vapor entering tank	kPa
typ	Temperature of vapor entering tank	K
hvp	Enthalpy of vapor entering tank	kJ/kg
Input File (TankSIM_Input.txt)		
fluid	Working fluid: "Methane_', 'Hydrogen', 'Oxygen_', 'Nitrogen', 'Parahydr'	8 pos.

Description of TankSIM Input and Output Files Variables (Continued)		
pheini	Initial pressurization gas pressure	kPa
pvini	Initial vapor pressure	kPa
tuini	Initial ullage temperature	K
tlini	Initial liquid temperature	K
twini	Initial ullage wall temperature	K
tlwini	Initial liquid wall temperature	K
tkwlini	Initial thickness of ullage wall liquid film	m
full	Liquid fill level in volume percent	%
phest	Bottle helium pressure in the beginning of the mission	kPa
thesti	Bottle helium temperature in the beginning of the mission	K
dhest	Helium regulator orifice diameter	mm
tkhest	Thickness of regulator orifice diameter	mm
vhest	Helium bottles total volume	m ³
brktime	Program breaking time, used for debugging	sec
iplotreg	Number of time steps between output plotting, pump is off	NOT USED NOW
iplotmix	Number of time steps between output plotting, pump is on	NOT USED NOW
itesti	Initial printing flag (usually use 5)	-
flgprt	Print flag:	-
	0 - only inputs and summary outputs, no details;	
	1 - basic printing with details;	
	2 - Ullage venting printing;	
	3 - Spray bar TVS printing;	
	4 - Axial jet TVS printing;	
	5 - Combination of ullage venting & spray bar TVS;	
	6 - Combination of ullage venting & axial jet TVS;	
	7 - Liquefaction;	
tent	Environmental temperature	K
penv	Environmental pressure	kPa
casnum	Any text, used for file name and naming a case	20 pos
Tank File (TankSIM_Tank.txt)		
tmater	Tank wall material: 'SS 304', 'Aluminum', 'Titanium', etc.	8 pos.
tshape	Tank bulkhead shape: 'Spherical', 'Elliptical', 'Flat'	10 pos.
flgadd	'1' indicates additional external lines attached to the tank wall: feed, vent, pressure.	-
dtank	Tank outside diameter	m
hcyl	Tank cylinder part (barrel) height	m
hbulk	Tank bulkhead height	m
tkw	Tank wall thickness	m
vaddt	Additional volume added to the Ullage from additional lines	m ³
ptmax	Tank design maximum pressure	kPa
rhow	Tank material average density	kg/m ³
ksi	Surface average heat absorption coeff. (used in Stephan-Boltzmann equation)	-
nmet	Number of points in tank material properties table	-
tmet	Temperature in tank material properties table	K
cpmet	Tank material specific heat table	J/(kg•K)
kmet	Tank material thermal conductivity table	W/(m•K)

Description of TankSIM Input and Output Files Variables (Continued)

Spray Bar File (TankSIM_Spray_Bar.txt)



dmno	spray manifold external diameter	m
thmn	spray manifold wall thickness	m
lmn	spray manifold length	m
kmn	spray manifold material average thermal conductivity	W/(m•K)
ltop	distance from top of the tank to top part of spray manifold (flagtop = 1) or distance from top of the tank to the top of the injection line manifold (flagtop = 2)	m
nbar	number of spray bars in tank	-
kmni	total pressure lost coefficient from the pump to the spray manifold	-
kmnf	total pressure lost coefficient from the spray manifold to injection lines	-
dito	injection line external diameter	m
thit	injection line wall thickness	m
lit	injection line length	m
dzsi	distance between orifices on the injection lines	m
norsi	number of orifice levels on the injection line	-
norit	number of orifices on the each orifice level	-
ninj	number of injection lines per spray bar	-
ditom	distance from the top to the first top orifice (flagtop = 1), or injection line manifold external diameter (flagtop = 2)	m

Description of TankSIM Input and Output Files Variables (Continued)		
thitm	Manifold height (flgtop = 1), or injection line manifold wall thickness (flgtop = 2)	m
litm	Spray manifold top part length (flgtop = 1), or injection line manifold length (flgtop = 2)	m
dzsim	Distance between orifices on the top part (flgtop = 1), or injection lines manifold (flgtop = 2)	m
nortop	Number of orifice levels on the top part of the spray bar manifold (flgtop = 1), or on the injection line manifold (flgtop = 2)	-
norimn	Number of orifices on the each orifice level on the top part of spray bar manifold (flgtop = 1), or on the injection lines manifold (flgtop = 2)	-
lspr	Distance from the injection line spray orifice to the tank wall (used for calculating amounts of liquid spraying to the wall and falling to the bulk liquid)	m
flgtop	Type of the spray bar top part: 1 - MHTB with perforated spray manifold top part; 2 - SLS type with perforated injection line manifold (large tanks)	-
ks	Spray orifice loss coefficient	-
cds	Spray orifice discharge coefficient	-
nlim	Maximum number of iterations	-
nsec	Number of sections with the same orifice sizes	-
node	Node number (number of different orifices in injection line table (if all same orifices - node = 1)	-
dorf	Orifice nodes diameter table	m
dexo	Heat exchanger external diameter	m
thex	Heat exchanger wall thickness	m
lex	Heat exchanger length	m
xei	Heat exchanger initial gas quality	-
nex	Number of points heat exchanger divided	-
alhex	Angle between heat exchanger and tank longitudinal axis	degree
kvent	Kvent = 1, vent line begins after pump (flow rate subtracts from pump flow rate)	-
Axial Jet File (TankSIM_AxialJet.txt)		
bet1	Coefficient in axial jet equation (0.34)	-
bet2	Coefficient in axial jet equation (0.24)	-
hj	Axial jet nozzle exit height	m
dj	Axial jet internal nozzle diameter	m
nzj	Axial jet number of nozzles	-
dexol	Heat exchanger pipe minor axis	m
TankSIM Output File		
File	Name of the current file	-
Fluid	Working fluid	-
	Thank Measurement	
	Same as in tank input file	
	Mission Profile	
	Same as in mission profile input file	
	Regular printing for 'Slf' and common part for all other regimes	
Regime	Working regime during phase: 'Slf' - self pressurization (no mixing and TVS working); 'Chl' - lines chill-down);	3 pos.

Description of TankSIM Input and Output Files Variables (Continued)		
	'Chp' - chill-down with autogenous pressurization;	
	'Hep' - non-condensable gas pressurization;	
	'Hec' - pressurization phase with zero non-condensable flow rate (no pressurization during pressurization phase, ullage pressure higher than required max);	
	'Fir' - engine firing without pressurization;	
	'Fip' firing with autogenous pressurization;	
	'Bar' - spray bar TVS is switched on (cycling);	
	'MiB' spray bar only mixing (cycling);	
	'PhB' - spray bar TVS working permanently;	
	'PmB' spray bar only mixing permanently;	
	'Jet' - axial jet TVS is switched on (cycling);	
	'MiJ' - axial jet only mixing (cycling);	
	'PhJ' - axial jet TVS working permanently;	
	'PmJ' - axial jet only mixing permanently;	
	'Ull' - ullage venting (open valve).	
	'Lqf' - liquefaction	
Time	Time from the beginning of the mission	sec
Time h	Time from the beginning of the mission	hour
Pu	Ullage pressure	kPa
Plsat	Liquid saturation pressure corresponds to liquid temperature	kPa
Tu	Ullage temperature	K
Tl	Liquid temperature	K
Tlw	Temperature of the wall interfacing with liquid	K
Tw	Temperature of the wall interfacing with ullage	K
Tint	Liquid - ullage interface temperature	K
Pv	Vapor pressure in ullage	kPa
Phe	Non-condensable gas pressure in ullage	kPa
Bond	Bond number by tank diameter	-
Ml	Bulk liquid mass	kg
Ml lost	Total mass lost by chill-down, liquid venting and through ullage-liquid interface	kg
Fill	Volumetric tank fill level	%
Del Fill Sw	Difference between initial liquid volumetric fill level and liquid level swell	%
Liq Lev	Bulk liquid level	m
Del Lev Sw	Difference between initial liquid level and liquid level swell	m
Mv	Mass of vapor in ullage	kg
Mhe Ul	Mass of non-condensable in ullage	kg
Mhe Lost	Non-condensable gas lost mass	kg
Md Evap	Evaporation-condensation mass flow rate through ullage liquid interface	kg/sec
Md Boff	Bulk liquid boil-off mass flow rate	kg/sec
Md Cond	Ullage condensation mass flow rate	kg/sec
Mlost int	Liquid total mass lost through ullage-liquid interface (evaporation and boil-off)	kg
M Drop U	Mass of liquid droplets in ullage (from ullage condensation and mixing)	kg
Err_Etot	Total energy balance error compare to the external heat loads	%
Err_Mtot	Total fluid mass balance error compare to the total fluid mass	%
Err_Mds	Spayed mass flow rate error compare to the flow rate in manifold	%

Description of TankSIM Input and Output Files Variables (Continued)		
Addition to Common print for all regimes excluding 'SIF'		
Mix.Cycl	Number of cycles during mixing (no TVS) or ullage venting	–
Hex.Cycl	Number of cycles during TVS working or ullage venting by liquid saturation pressure	–
Dutypu	Duty cycle for ullage pressure controlling	%
Dutypl	Duty cycle for liquid saturation pressure controlling addition to all regimes for Ullage Venting	%
Md Uvent	Ullage venting mass flow rate	kg/sec
M Uv tot	Mass venting from the ullage	kg
Time Uven	Total ullage venting time	sec
Addition to all regimes for Spray bar or Axial jet		
Md Pump	Pump mass flow rate	kg/sec
Qd Pump	Pump volumetric flow rate	GPM
Dp Pump	Pressure increase at the pump	kPa
Md Lvent	Liquid venting mass flow rate	kg/sec
Qman tot	Power eliminating from the manifold	W
Tman End	Temperature at the manifold end	K
Pman End	Pressure at the manifold end	kPa
Qex tot	Power eliminating by heat exchanger	W
Lefex/Xsef	Relative length where liquid fully evaporated in the heat exchanger, or vapor quality if it does not fully evaporated	–
Tex End	Temperature at the heat exchanger end	K
Pex End	Pressure at the heat exchanger end	kPa
Dt J-T	Temperature drop at the Joule-Thomson device	K
Dp J-T	Pressure drop at the Joule-Thomson device	kPa
X J-T	Vapor quality after the Joule-Thomson device	–
Pback	Back pressure at venting device	kPa
Addition to all regimes for Liquefaction		
Md Ull	Ullage condensation flow rate	kg/sec
Md Uwall	Ullage wall condensation flow rate	kg/sec
Md Vapor	External vapor added to the tank flow rate	kg/sec
Qwu	Heat eliminated from the ullage	W
Tsat-Twu	Ullage wall subcooling compare to the vapor saturation temperature	K

REFERENCES

1. Alabovskii, N.: "Thermal Interaction at the Gas-Liquid Interface in an Apparatus with an Immersed Burner," Kiev Polytechnical Institute. Translated from *Inzhenerno-Fizicheskii Zhurnal*, Vol. 22, No. 1, pp. 117–122, January 1972.
2. Delhaye, J.M.: "Jump conditions and entropy sources in two-phase systems. Local instant formulation," *Int. J. Multiphase Flow*, Vol. 1, Issue 3, pp. 395–409, 1974.
3. Meserole, J.S.; Jones, O.S.; Brennan, S.M.; and Fortini, A.: "Mixing-Induced Ullage Condensation and Fluid Destratification," AIAA-87-2018, 23rd Joint Propulsion Conference, San Diego, CA, doi.org/10.2514/6.1987-2018, 1987.
4. Rohsenow, W.M.; Hartnett, J.P.; and Cho, Y.I.: "Handbook of Heat Transfer," 3rd ed., McGraw-Hill, NY, 1998.
5. Churchill, S.W.; and Usagi, R.: "A General Expression for the Correlation of Rate of Transfer and Other Phenomena," *AIChE Journal*, Vol. 18, pp. 1121–1128, 1972.
6. Gerstmann, J.; and Griffith, P.: "The Effects of Surface Instabilities on Laminar Film Condensation," Technical Report No. 5050-36, MIT, 1965.
7. Gerstmann, J.; and Griffith, P.: "Laminar Film Condensation on the Underside of Horizontal and Inclined Surfaces" *Int. J. Heat Mass Transfer*. Vol. 10, pp. 567–580, 1967.
8. Oosthuizen, P.H.; and Naylor, D.: *An Introduction to Convective Heat Transfer Analysis*, McGraw-Hill, NY, 1999.
9. Goldstein, R.J.; Sparrow, E.M.; and Jones, D.C.: "Natural Convection Mass Transfer Adjacent to Horizontal Plates," *Int. J. Heat Mass Transfer*, Vol. 16, Issue 5, pp. 1025–1035, 1973.
10. Rich, B.R.: "An Investigation of Heat Transfer from an Inclined Flat Plate in Free Convection," *Trans. ASME*, Vol. 75, pp. 489–499, 1953.
11. В.А. Григорьев, Ю. М. Павлов, Е. Б. Аметистов, «Кипение криогенных жидкостей», Энергия, Москва, 1977 (in Russian). (Grigoryev, V.A.; Pavlov, Yu. M.; and Ametistov, E.V.: "Boiling of Cryogenic Liquids," Energiya, Moskva, 1977.)
12. NIST Standard Reference Data 23, "Reference Fluid Thermodynamic and Transport Properties–REFPROP," Version 9.0, 2010.
13. Miller, R.W.: "Flow Measurement Engineering Handbook," 3rd ed., McGraw-Hill, NY, 1996.

14. Spalding, D.B.; and Cole, E.H.: *Engineering Thermodynamics*, 3rd ed., SI Units, Edward Arnold Ltd, London, 1973.
15. Ward-Smith, A.J.: "Critical Flowmetering: The Characteristics of Cylindrical Nozzles With Sharp Upstream eEdges," *Int. J. Heat & Fluid Flow*, Vol. 1, No. 3, pp. 123–132, 1979.
16. Simmons, F.S.: "Analytical Determination of the Discharge Coefficient of Flow Nozzles," NACA TN 3447, April 1955.
17. Cole, R.; and Rohsenow, W.M.: "Correlation of bubble departure diameters for boiling of saturated liquids," *Chem. Eng. Prog. Symp. Ser.*, Vol. 65, No. 92, pp. 211–213, 1968.
18. Levich, V.G.: *Physicochemical Hydrodynamics*, Prentice-Hall Inc., Englewood Cliffs, NJ, 1962.
19. Lockhart, R.W.; and Martinelli, R.C.: "Proposed Correlation of Data for Isothermal Two-Phase, Two-Component Flow in Pipes," *Chem. Eng. Progress*, Vol. 45, Issue 1, pp. 39–48, 1949.
20. Martinelli, R.C.; and Nelson, D.B.: "Prediction of Pressure Drop During Forced-Circulation Boiling of Water," *Trans. ASME*, Vol. 70, pp. 695–702, 1948.
21. Changhong, P.; Yun, G.; Suizheng, Q.; et al.: "Two-phase low and boiling heat transfer in two vertical narrow annuli," *Nuclear Engineering and Design*, Vol. 235, pp. 1737–1747, 2005.
22. Carey, V.P.: *Liquid Vapor Phase Change Phenomena*, Taylor & Francis, Hebron, KY, 1992.
23. Ghabari, A.; Farshad, F.F.; and Rieke, H.H.: "Newly developed friction factor correlation for pipe flow," *J. Chem. Eng. Mater. Sci.*, Vol. 2, Issue 6, pp. 83–86, 2011.
24. Chen, J.C.: "Correlation for boiling heat transfer to saturated fluids in convective flow," *Ind. Eng. Chem. Proc. Design and Dev.*, Vol. 5, No. 5, pp. 322–339, 1996.
25. Collier, J.G.: "Forced convective boiling," *Two-Phase Flow and Heat Transfer in the Power and Process Industries*, A.E. Bergles, J.G. Collier, J.M. Delhaye, G.F. Hewitt, and F. Mainger, eds., Hemisphere, NY, 1981.
26. Idelchik, I.E.: *Handbook of Hydraulic Resistance*, 3rd ed., Jaico Publishing House, Mumbai, 2008.
27. Pappel, S.S.; Saiyed, N.H.; and Nyland, T.W.: "Acquisition and Correlation of Cryogenic Nitrogen Mass Flow Data through a Multiple Orifice Joule-Thomson Device," NASA TM-103121, 1990.
28. Pappel, S.S.; Nyland, T.W.; and Saiyed, N.H.: "Liquid Hydrogen Mass Flow Through a Multiple Orifice Joule-Thomson Device," NASA TM-105583, AIAA-92-2881, 1992.

29. Jurns, J.M.: “Visco Jet Joule-Thomson Device Characterization Tests in Liquid Methane,” NASA/CR—2009–215497, NASA Glenn Research Center, Cleveland, OH, March 2009.
30. The Lee Company, *Technical Hydraulic Handbook*, 11th ed., 2009.
31. А.С. Лышевский, «Процессы распыливания топлива дизельными форсунками», Машгиз, Москва, 1963 (In Russian). (Lyshevskiy, A.S.: “Fuel atomization by diesel injectors,” Mashgiz, Moskva, 1963.)
32. Ranz, W.E.; and Marshall, Jr., W.R.: “Evaporation From Drops,” *Chemical Engineering Progress*, Vol. 48, No. 3, pp. 141–146, pp. 173–180, 1952.
33. Pasandideh-Fard, M.; Aziz, S.D.; Chandra, S.; and Mostaghimi, J.: “Cooling Effectiveness of a Water Drop Impinging on a Hot Surface,” *Int. J. Heat and Fluid Flow*, Vol. 22, Issue 2, pp. 201–210, 2001.
34. Castanet, G.; Liénart, T.; and Lemoine, F.: “Dynamics and temperature of droplets impacting onto a heated wall,” *Int. J. Heat and Mass Transfer*, Vol. 52, Issues 3–4, pp. 670–679, 2009.
35. Baumeister, K.J.; and Simon, F.F.: “Leidenfrost Temperature—Its Correlation for Liquid Metals, Cryogenes, Hydrocarbons, and Water,” *ASME J. Heat Trans.*, Vol. 96, No. 2, pp. 166–173, 1973.
36. Chun, K.R.; and Seban, R.A.: “Heat Transfer to Evaporating Liquid Films,” *J. Heat Transfer*, Vol. 93, No. 4, pp. 391–396, 1971.
37. Sonin, A.A.; Shimko, M.A.; and Chun, J.H.: “Vapor Condensation onto a Turbulent Liquid-I. The Steady State Condensation Rate as a Function of Liquid-Side Turbulence,” *Int. J. Heat Mass Trans.*, Vol. 29, No. 9, pp. 1319–1332, 1986.
38. Thomas, R.M.: “Condensation of Steam on Water in Turbulent Motion,” *Int. J. Multiphase Flow*, Vol. 5, No. 1, pp. 1–15, 1979.
39. Brown, J.S.; Khoo, B.C.; and Sonin, A.A.: “Rate Correlation for Condensation of Pure Vapor on Turbulent, Subcooled Liquid,” *Int. J. Heat Mass Trans.*, Vol. 33, No. 9, pp. 2001–2018, 1990.
40. Lin, C.S.; and Hasan, M.M.: “Effect of Liquid Surface Turbulent Motion on the Vapor Condensation in a Mixing Tank,” *Proceedings of the 4th International Symposium on Transport Phenomena in Heat and Mass Transfer*, Sidney, Australia, July 14–19, 1991, Transport Phenomena in Heat and Mass Transfer, J.A. Reizes, ed., pp. 1526–1537, 1992.
41. Chen, Y.; Schaeffer, B.M.; and Weislogel, M.M.: “Surface Evolver - Fluid Interface Tool, Version 1.060. User’s Manual,” Department of Mechanical and Materials Engineering, Portland State University, May 20, 2011.

42. Teertstra, P.; Yovanovich, M.M.; and Culham, J.R.: "Conduction Shape Factor Models for Three-Dimensional Enclosures," *J. Thermophysics and Heat Transfer*, Vol. 19, No. 4, October–December, 2005.
43. Panton, R.L.: *Incompressible Flow*, 4th ed., John Wiley & Sons, NY, 2013.
44. Elenbaas, W.: "The Dissipation of Heat by Free Convection. The Inner Surface of Vertical Tubes of Different Shapes of Gross-Section," *Physica IX*, No. 8, pp. 865–874, September 1942.
45. Schmidt, E.; and Beckmann, W.: "Das Temperatur- und Geschwindigkeitfeld vor einer Wärme abgebenden senkrechten Plate bei natürlicher Konvektion," *Tech. Mech. und Thermodynamik*, Bd.1, Nr. 10, Okt.1930, pp. 341–349 and Bd. 1, Nr.11, pp. 391–406 (in German), November 1930.
46. Incropera, F.P.; and DeWitt, D.P.: *Fundamental of Heat and Mass Transfer*, 4th ed., John Wiley & Sons, NY, 1996.
47. Rohsenow, W.M.: "Heat Transfer and Temperature Distribution in Laminar Film Condensation," *Trans. ASME*, Vol. 78, pp. 1645–1648, 1956.
48. Tollmien, W.: "Calculation of Turbulent Expansion Processes," NACA TM–1085, Langley, 1945.
49. Dominick, S.M.: "Mixing Induced Condensation Inside Propellant Tanks," AIAA-84-0514, 22nd Aerospace Sciences Meeting, Aerospace Sciences Meetings, Reno, NV, doi.org/10.2514/6.1984-514 1984.
50. Patil, R.K.; Shende, B.W.; and Ghosh, P.K.: "Designing a Helical-Coil Heat Exchanger," *Chemical Engineering*, pp. 85–88, December 13, 1982.

REPORT DOCUMENTATION PAGE

Form Approved
OMB No. 0704-0188

The public reporting burden for this collection of information is estimated to average 1 hour per response, including the time for reviewing instructions, searching existing data sources, gathering and maintaining the data needed, and completing and reviewing the collection of information. Send comments regarding this burden estimate or any other aspect of this collection of information, including suggestions for reducing this burden, to Department of Defense, Washington Headquarters Services, Directorate for Information Operation and Reports (0704-0188), 1215 Jefferson Davis Highway, Suite 1204, Arlington, VA 22202-4302. Respondents should be aware that notwithstanding any other provision of law, no person shall be subject to any penalty for failing to comply with a collection of information if it does not display a currently valid OMB control number.

PLEASE DO NOT RETURN YOUR FORM TO THE ABOVE ADDRESS.

1. REPORT DATE (DD-MM-YYYY) 01-04-2017			2. REPORT TYPE Technical Memorandum			3. DATES COVERED (From - To)		
4. TITLE AND SUBTITLE Tank System Integrated Model: A Cryogenic Tank Performance Prediction Program						5a. CONTRACT NUMBER		
						5b. GRANT NUMBER		
						5c. PROGRAM ELEMENT NUMBER		
6. AUTHOR(S) L.G. Bolshinskiy,* A. Hedayat, L.J. Hastings (retired), S.G. Sutherlin, A.R. Schnell, and J.P. Moder**						5d. PROJECT NUMBER		
						5e. TASK NUMBER		
						5f. WORK UNIT NUMBER		
7. PERFORMING ORGANIZATION NAME(S) AND ADDRESS(ES) George C. Marshall Space Flight Center Huntsville, AL 35812						8. PERFORMING ORGANIZATION REPORT NUMBER M-1431		
9. SPONSORING/MONITORING AGENCY NAME(S) AND ADDRESS(ES) National Aeronautics and Space Administration Washington, DC 20546-0001						10. SPONSORING/MONITOR'S ACRONYM(S) NASA		
						11. SPONSORING/MONITORING REPORT NUMBER NASA/TM-2017-218239		
12. DISTRIBUTION/AVAILABILITY STATEMENT Unclassified-Unlimited Subject Category 20 Availability: NASA STI Information Desk (757-864-9658)								
13. SUPPLEMENTARY NOTES Prepared by the Propulsion Systems Department, Engineering Directorate, *Jacobs ESSSA Group (contract NNM12AA41C), Huntsville, AL, **NASA Glenn Research Center, Cleveland, OH								
14. ABSTRACT Accurate predictions of the thermodynamic state of the cryogenic propellants, pressurization rate, and performance of pressure control techniques in cryogenic tanks are required for development of cryogenic fluid long-duration storage technology and planning for future space exploration missions. This Technical Memorandum (TM) presents the analytical tool, Tank System Integrated Model (TankSIM), which can be used for modeling pressure control and predicting the behavior of cryogenic propellant for long-term storage for future space missions. Utilizing TankSIM, the following processes can be modeled: tank self-pressurization, boiloff, ullage venting, mixing, and condensation on the tank wall. This TM also includes comparisons of TankSIM program predictions with the test data and examples of multiphase mission calculations.								
15. SUBJECT TERMS modeling on-orbit liquid cryogen storage and pressure control, cryogenic propellants, in-space cryogenic propulsion, heat and mass transfer in cryogenic liquids								
16. SECURITY CLASSIFICATION OF:			17. LIMITATION OF ABSTRACT		18. NUMBER OF PAGES		19a. NAME OF RESPONSIBLE PERSON	
a. REPORT	b. ABSTRACT	c. THIS PAGE	UU		144		STI Help Desk at email: help@sti.nasa.gov	
U	U	U					19b. TELEPHONE NUMBER (Include area code) STI Help Desk at: 757-864-9658	

National Aeronautics and
Space Administration
IS02
George C. Marshall Space Flight Center
Huntsville, Alabama 35812